DEPARTMENT OF MATERIAL SCIENCE

UNIVERSITY OF MILAN-BICOCCA

Doctoral Dissertation of

VINEET KUMAR

Enrollment No. **745173**
(Industrial Curriculum)

XXVI Cycle

Few Layer Graphene Reinforced Rubber Compounds for Tires

Thesis Tutor (s): **Prof. Maurizio Stefano Galimberti**, **Prof. Ulrich Giese**

Thesis co-Tutor (s): **Dr. Luca Castellani / Dr. Luca Giannini**

Thesis Supervisor: **Prof. Roberto Scotti**

2011 – 2014

Abstract

In last decade, "*Nanofillers*" have been explored extensively in rubber compounds to improve dynamic-mechanical properties. Three classes of nanofillers: Clay minerals, Carbon nanoTubes and Graphitic nanofillers have been often used. Most recently, an attention towards "*graphene*" as nanofiller was reported due to its exceptional mechanical, thermal and electrical properties. In present Ph.D. thesis, different types of commercially available "*few layer graphene*" were explored in both apolar and polar diene rubbers. These nanofillers were dispersed with melt mixing technique which is most suitable technology for industrial applications, such as for tires.

Structural-morphological characteristics of the nanofillers were made with SEM, TEM, XRD and static adsorption isotherms. Features such as shape anisotropy, number of graphene layers in a stack, BET surface area, surface activity and porosity of nanofillers were obtained. Optical microscopy was employed to obtain filler dispersion index and estimation of filler's aggregates, agglomerates. Dynamic mechanical properties of the rubber compounds were made with rheometric curves for scorch and curing time, rheological properties through RPA (strain sweep and frequency sweep) for viscoelastic properties and filler networking, stress-strain for tensile strength and multi-hysteresis cycles for energy dissipation, dynamic mechanical thermal analysis for high and low temperature properties, hardness of compound for processing features and tear strength tests for compound durability. The electrical properties of rubber compounds were investigated via dielectric AC conductivity and permittivity tests.

Epoxidation of diene rubbers (low rate, <**10**%) was obtained to investigate the effects of presence of epoxy functional groups along polymer chains on filler networking, polymer-filler interactions, filler dispersion and dynamic mechanical properties of rubber compounds. Quantitative analysis of epoxidation, rate of epoxidation and its influence on rubber matrix (such as change in glass transition temperature) was investigated through ^{1}NMR and DSC tests. Under multi-hysteresis stress-strain cycles, it was found that a stable filler networking can reduce hysteresis losses.

Fillers-

CNTs - **Carbon nanoTubes**

FLG - **Few Layer Graphene**

GNP - **Graphite nanoPlatelets**

xGnP – ***exfoliated*-Graphene nanoPlatelets**

EG – **Expanded Graphite**

nanoG – **nanoGraphite**

OC – **Organo Clay Minerals**

CB – **Carbon Black**

Ingredients

ZnO – **Zinc Oxide**

CBS - **Cyclohexyl Benzothiazol-2-Sulfenamide**

Rubbers

SBR - **Styrene Butadiene Rubber**

IR – **Synthetic Poly(1,4-*cis*-isoprene) Rubber**

EIR – ***epoxidized* -Synthetic Poly(1,4-*cis*-isoprene) Rubber**

epoxy- SBR – ***epoxidized*- Styrene Butadiene Rubber**

NR – **Natural Rubber**

xNBR – **Carboxylated Acrylonitrile Butadiene Rubber**

Techniques and related abbreviations

SEM - **Scanning Electron Microscope**

TEM – **Transmission Electron Microscope**

XRD – **X-Ray Diffraction**

WAXD – **Wide angle X-Ray Diffraction**

FWHM – **Width at Half Height**

HCP – **Hexagonal Close Packing**

^{1}NMR – ***protonated*-Nuclear Magnetic Resonance**

RPA – **Rubber Process Analyzer**

DMTA – **Dynamic Mechanical Thermal Analysis**

DSC - **Dynamic Scanning Calorimetry**

Other technical abbreviations

FPT – **Filler Percolation Threshold**

EPT – **Electric Filler Percolation Threshold**

SIC – **Strain Induced Crystallization**

$(E-E_0)/E_0$ – **Excess of Initial Modulus**

phr – **Per Hundred Parts of Rubber/Filler**

~ - **approximately**

sp^2 – **sp^2 carbon hybridization**

sp^3 – **sp^3 carbon hybridization**

0-D – **zero dimensional**

1-D – **one dimensional**

2-D – **two dimensional**

3-D – **three dimensional**

$hk\ell$ - **miller indices for crystalline materials**

$D_{\perp}$ - **correlation length $D_{00\ell}$, that means out-of-plane correlation length**

$D_{\parallel}$ - **correlation length D_{hk0}, that means in-plane correlation length**

λ – **wavelength**

$\beta_{00\ell}$ - **FWHM of 00ℓ peak**

θ – **diffraction angle**

Ω – **Ohm**

dB – **decibel**

M.U. – **mooney units**

rpm – **rounds per minute**

ϕ_F – **filler's volume fraction**

σ – **stress**

σ_F – **stress of filled rubber compound**

σ_0 – **stress of unfilled rubber compound**

γ – **strain**

M_L – **lowest torque value in rheometric curves**

M_H – **highest torque value in rhemoetric curves**

t'_{90} – **curing time**

G' – **storage modulus**

G'' – **loss modulus**

tanδ – **loss tangent**

G* - **complex modulus**

η' – **dynamic viscosity**

D_I – **filler dispersion index**

Q – **swelling**

T_g – **glass transition temperature**

H_2O_2 – **peroxide**

HCOOH – **formic acid**

X% - **rate of epoxidation**

A_{epoxy} – **sum of integral protons area by appearance of epoxy functional groups**

V/V_m – **surface coverage**

V_m – **monolayer volume**

p/p_0 – **relative pressure**

p_0 – **saturated pressure at 77 K**

Chapter 1

Introduction

A pneumatic tire is a toroidal, high performance rubber compound exhibiting characteristics of a flexible-membrane pressure container with load carrying, cushioning, and road handling capabilities. More than half of the total natural rubber and synthetic rubbers and > **85**% of the worldwide produced carbon black are presently consumed by tire industries.

Due to increasing concerns on global warming for reducing green house gases, tire companies are consistently addressed to make fuel efficient tires. Now-a-days, the concept of "*Green tires*" is implemented which are characterized by low rolling resistance, high abrasion resistance and low skidding.

1.1. Requirements of Green tires

1.1.1. EU Tire Labeling Legislation (*Regulation EC Nr. 1222/2009*)

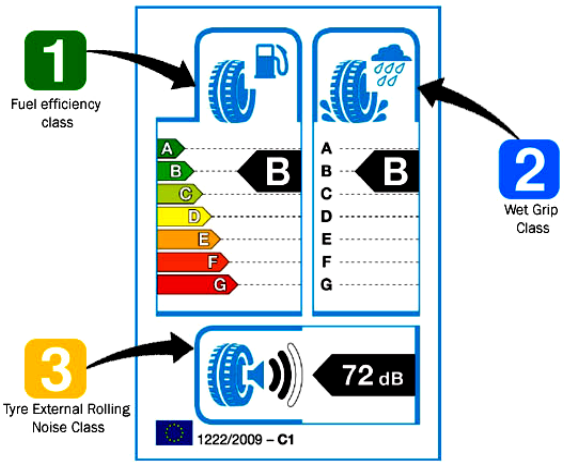

Figure 1.1: Concept of green tires [taken directly from *Regulation EC Nr. 1222/2009*]

Since **2009** onwards, a new EU tire labeling legislation enforces tire companies to meet new requirements. The **1**st label in **figure 1.1** presents fuel efficiency class/rolling resistance for the modern tires. A rolling tire deforms and dissipates energy actively. Such energy that's lost is known as rolling resistance and directly affects fuel consumption of the vehicle. The **2**nd label presents the needfulness of tires to improve wet grip and according to regulation *EC 1222/2009*. Wet grip is defined as the capacity of a

tire to brake on a wet road. In **3**rd requirement, the exterior noise levels are measured in decibel (dB) and shown as one, two or three sound waves on the label. One wave is the best performance, three is the worst.

It is well known that "fillers" influences the hysteresis loss in rubber compounds. In the last **2** decades, a significant improvement in properties (such as rolling resistance reduced by ~**18**%) was achieved through various innovative methodologies, techniques such as "silica technology". However, further improvement from present levels is needed. Recently, "*Nanofillers*" as new class filler materials are extensively explored to improve dynamic mechanical properties of rubber compounds.

1.2. Nanofillers for green tires

New improved rubber compounds used for "*green tires*" are needed to balance among important parameters such as low rolling resistance, high abrasion resistance and good wet traction. Fuel efficiency, life-span and safety on wet roads are considered as main requirements for high performance tires. [1-6] Nanofillers are recently adopted as a viable option to improve performance in rubber compounds in so-called "*green tires*". Most frequently used nanofillers are clay minerals [7-10], carbon fillers such as carbon nanotubes (CNTs) [7-9,11,12] and graphitic nanofillers [9, 13-20]. These nanofillers are made by primary particles, with at least one dimension **<1-100** nm that can be individually dispersed in the rubber matrix. Their features such as high surface area, high aspect ratio promotes higher dynamic-mechanical properties of rubber compounds. These characteristic features of nanofillers require low content (less than **10**% by weight) in a rubber matrix to form filler networks, provided that they are uniformly dispersed as individual particles in the rubber matrix. [7-20].

A significant aspect of achieving homogenous nanofiller dispersion can be obtained through exploring different filler dispersing mixing techniques or improving filler-polymer compatibility by using these nanofillers in pristine and modified forms. For example, clay minerals are functionalized with liphofilic ions [10] and graphitic nanofillers are modified through the various functional groups [21-22]. SBR is widely synthetic rubber

[23] in tire industry due to its higher dynamic-mechanical properties, and durability of compounds. Use of graphitic nanofillers in SBR is available in scientific literature [19-20].

However, in order to improve dynamic-mechanical properties of rubber compounds based on these new class fillers, there are open problems such as to promote uniform filler dispersion, improving filler networking and to improve polymer-filler compatibility. This thesis focuses on part of these challenges via exploring **low** and **high** surface area "*few layer graphene* (FLG)" as new class nanofillers into both **apolar** and **polar** diene rubbers.

1.3. Objectives of the present thesis

Main objectives of the present thesis can be summarized as follows

1. To study elastomeric compounds based on diene rubber and carbon nanofillers made by few layers of graphene (**FLG**) stacked in crystalline aggregates. Such carbon nanofillers are characterized, commonly indicated in the thesis as "few layers graphene or FLG". Both **apolar** and **polar** diene rubbers are used for compound preparation: *poly*(1,4-*cis*-isoprene) (IR) and styrene butadiene rubber (SBR) as apolar diene rubber and nitrile butadiene rubber (NBR) and epoxidized IR and SBR as polar diene rubbers.

2. To characterize FLG as nanofillers for determining their surface area, surface activity and porosity. To prepare the rubber compounds without any treatment of the pristine nanofillers prior to their mixing, in order to maintain the sp^2 nature of the graphitic carbon atoms. The nanofillers must be dispersed with a technology suitable for industrial development, such as melt mixing.

3. To study dispersion of FLG in polymer matrices through TEM or optical microscopy. To utilize optical microscopy for calculating filler dispersion index, and analysis of aggregates, agglomerates. Use of diene rubber with different polarity, as an aim to enhance homogenous filler dispersion, improving filler networking and ultimate mechanical properties.

4. To study filler networking, assessing the content of nanofiller required to have percolation, performing such determination through mechanical and electrical measurements. To study ultimate properties of the elastomeric compounds, determining in particular elongation, stress and elongation at break.

5. To identify the carbon nanofillers features that mostly affect their behavior in the elastomeric rubber compounds and thus, the compound properties

1.4. Structure of the thesis

Introduction to the thesis is reported in the present Chapter (Chapter **1**). Chapter **2** presents description on carbon allotropes, few layers graphene and rubber compounds based on these graphitic nanofillers. Four chapters are then presented (Chapters **3-6**), dedicated to elastomeric compounds. Their content is summarized in Table **1**.

Table-1: Description for chapters containing rubber compounds

S.No.	**Chapter**	**Type of Rubber**	**Nature of Rubber**	**Type of *Few Layer Graphene***	**Surface area[a]**
1.	Chapter 3	SBR, IR	APOLAR	SFG6, KS4. EXG 9840	Low
2.	Chapter 4	SBR, IR	APOLAR	xg C750, xg M5, nanoG, CB-N234	High
3.	Chapter 5	NBR	POLAR	xg C750, xg M5, UF1 C98, CB-N339	High
4.	Chapter 6	Epoxidized-IR, Epoxidized-SBR	POLAR	xg C750, CB-N234	High

[a] Surface area (m^2/g: are **13.8** for SFG6, **23.8** for KS4 and **39.5** for EXG **9840**, **817.3** for xg C**750**, higher **168.3** for xg M**5**, **114.3** for CB-N**234**, **330.3** for nano**G**, **91.8** for CB-N**339**).

Finally, **Chapter-7** describes the experimental part of thesis. More detailed explanation of Chapters is reported as follows.

Chapter 2 focused on introduction to graphitic nanofillers in rubber compounds. It describes structural and morphological features of graphite, its polymorphic forms, concept of shape anisotropy and its uses as nanofillers. Dynamic-mechanical properties of rubber compounds based on them are presented.

Chapter 3 describes the rubber compounds based on **apolar** IR, SBR polymer matrix, with long-range filler-networking of a FLG (**low** surface area) as nanofiller formed at lower filler concentration, without any treatment of the pristine graphite prior to its mixing with the polymer. The structural and morphological characteristics of nanofillers were shown and dynamic mechanical characteristics properties of rubber compounds based on these nanofillers were reported.

Chapter 4 presents FLG (**high** surface area) reinforced rubber compounds in **apolar** IR, SBR polymer matrix without any treatment of the pristine nanofiller prior to its melt mixing with the polymer in small Haake **600**®. The structural and morphological characteristics of FLG as nanofiller were presented and their dynamic mechanical characteristics, dielectric properties are described.

Chapter-5 shows FLG (**high** surface area) as nanofiller in **polar** NBR baased rubber compounds with pristine state of nanofiller before its melt mixing with the polymer in Big Haake **3000**®. The characteristic features of FLG and other nanofillers are described. The dynamic mechanical characteristics of FLG reinforced NBR compounds are investigated.

Chapter-6 demonstrates improved polymer-filler interaction, filler dispersion of pristine FLG (**high** surface area) as nanofiller in **polar** epoxidized-IR and SBR matrices. The compounding was performed by melt mixing in Small Haake **600**®. The characteristic features of epoxidized rubber were presented. The dynamic mechanical characteristics of few layer graphene reinforced NBR compounds were presented.

Chapter-7 presents details on materials, chemicals, preparation procedures and characterizations techniques used in present research activity of the thesis.

1.5. References

[1] A. R. Payne, *Reinforcement of Elastomers*, G. Kraus Ed., Interscience Publishers, New York, Ch. **3 (**1965).

[2] J.B. Donnet, E. Custodero, in *The Science and Technology of Rubber Third Ed*.; J.E. Mark, B. Erman, F.R. Eirich, Eds. Elsevier Academic Press, Chapter **8**, 367 (2005).

[3] J. L. Leblanc, *Prog. Polym. Sci*., **27(4)** 627 (2002).

[4] M.L. Studebaker, *Rubber Chem Technol*, **30(5)** 1400 (1957).

[5] S. Wolff, *Rubber Chem Technol*., **69(3)** 325 (1996).

[6] A. R. Payne and R. E. Whittaker, *Rubber Chem Technol.*, **44**, 440 (1971).

[7] M. Maiti, M. Bhattacharya, A.K. Bhowmick, *Rubber Chem. Technol*., **81(3)** 384 (2008).

[8] S. Thomas, R Stephen, *Rubber Nanocomposites: Preparation, Properties and Applications*, ISBN 978-0-470-82345-3, Wiley, (2010).

[9] M. Galimberti, V. Cipolletti, V. Kumar, *Natural Rubber Based Composites And Nanocomposites*, S. Thomas, C. H. Chan, L. A. Pothan, Ramanan, J. Maria Eds., *Royal Society of Chemistry*, Chapter **2**, 34 (2014).
DOI: 10.1039/9781849737654-00034

[10] M. Galimberti, *Rubber Clay Nanocomposites: Science, Technology, Applications*, John Wiley and Sons, First Edition 601 (2011).

[11] L. Bokobza, *Polymer*, ***40***, 4907 (2007).

[12] M. Galimberti, M. Coombs, P. Riccio, T. Ricco`, S. Passera, S. Pandini, L. Conzatti, A. Ravasio, I. Tritto, *Macromol. Mater. Eng*., **298**, 241 (2012).

[13] K. S. Novoselov, A. K. Geim, S. V. Morozov, D. Jiang, Y. Zhang, S. V. Dubonos, I.V. Grigorieva, A.A. Firsov, *Science*, **306**, 666 (2004).

[14] R. Sengupta, M. Bhattacharya, S. Bandyopadhyay, A. K. Bhowmick, *Prog. Polym. Sci.*, **36**, 638 (2011)

[15] M. Galimberti, V. Kumar, M. Coombs, V. Cipolletti, S. Agnelli, S. Pandini, L. Conzatti, *Rubber Chem. Technol.*, (2013) –in press
DOI: http://dx.doi.org/10.5254/rct.13.87903.

[17] V. Kumar, U. Giese, T. Hanel, L. Giannini, M. Galimberti, *Kautschuk Gummi Kunstoffe* (2014) (**accepted**) -in press.

[18] S. Agnelli, V. Cipolletti, S. Musto, M. Coombs, L. Conzatti, S. Pandini, T. Riccò, M. Galimberti, *eXPRESS Polym. Lett.*, **8(6)** 436 (2014).

[19] M. Bhattacharya, M. Maiti, A. K. Bhowmick, *Polym. Engg. & Sci.*, **49(1)** 81(2009).

[20] S. Araby, Q. Meng, L. Zhang, H. Kang, P. Majewski, Y. Tang, J. Ma, *Polymer*, **55**, 201 (2014).

[21] P. Singh, S. Campidelli, S. Giordani, D. Bonifazi, A. Bianco, M. Prato, *Chem. Soc. Rev.*, **38**, 2214, (2009).

[22] T. Kuilla, S. Bhadra, D. Yaoa, N. H. Kim, S. Bose, J. H. Le, *Prog. Polym. Sci*., **35(11)** 1350 (2010).

[23] J.E. Puskas. *Diene based Elastomers Handbook of Elastomers*. Chapter **33**: 817, A. K. Bhowmick, H.L. Stephens Eds., CRC Press, (2000).

Chapter 2

Graphitic Nanofillers in rubber compounds

Carbon (with atomic number-**6** and electronic configuration**1**s^2**2**s^2**2**p^2) is well-known for its allotropic nature. It exists in three main families that are diamond, graphite and fullerenes. Diamond (sp^3 (tetrahedral) hybridization) and Graphite (sp^2 (trigonal) hybridization) are naturally occurring form of carbon and are well known since centuries. Fullerene (also known as Buckminsterfullerene or Bucky Balls) was first generated in **1985** [1].

2.1. Graphite

Graphite, made up of sp^2 hybridized carbon atoms, arranged in a honey-comb like structure, consists of carbon layers bonded with covalent and metallic bonding within each layer. These layers are stacked in a *hexagonal close packed* (HCP) crystal structure, held together by weak van der Walls forces (**figure 2.1**). The single **2**-d layer in graphite is also called as "*graphene*".

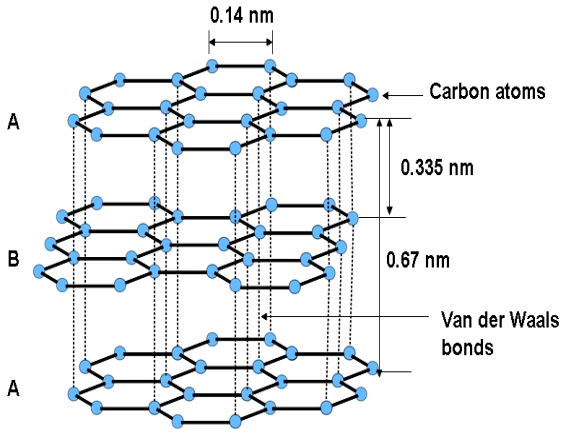

Figure 2.1: Crystal structure of hexagonal graphite

2.1.1. Graphene – mother of all graphitic forms

Graphene is defined as "a form of carbon allotrope, consisting of planar sheets, which are one atom thick (**2**-D), with the carbon atoms (sp^2 hybridized) arranged in a honeycomb-shaped lattice". It can be wrapped up into **0**-D fullerenes, rolled into **1**-D

nanotubes or stacked into **3**-D graphite and therefore regarded as "*mother of all graphitic forms*" as represented in **figure 2.2**. [2]

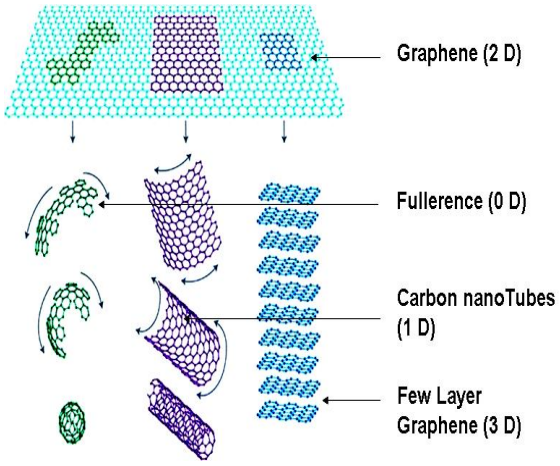

Figure 2.2: Graphene as mother of all graphitic forms; [adopted from reference] [3]

2.2. Description of Graphitic structure features and concept of shape anisotropy

2.2.1. Graphitic structure

X-ray diffraction (XRD) technique is often employed to investigate the crystalline order of materials such as graphite. In general, XRD patterns of hexagonal graphite shows three main reflections: *00ℓ*, *hk0* and *hkℓ*. As it is shown in **figure 2.3**, XRD patterns of pencil graphite reveal **002** reflections at **25.80**° as 2θ value, corresponding to a d_{002} distance of **0.339** nm, and **004** reflections at **54.3**° as 2θ value. The d_{002} distance corresponds to the distance between adjacent planes**. 002** reflection of pencil graphite appear quite narrow. The **100** and **110** reflections at **42.9**° and **77.3**° as **2**θ values respectively indicate the crystalline order in the structural layer**.** From wide angle X-ray diffraction (WAXD) data, the dimension of crystallites, in directions orthogonal and parallel to structural layers, can be estimated, by calculating the correlation length $D_{00\ell}$, that means the out-of-plane correlation lengths ($D\perp$), and the correlation length D_{hk0}, that means the in-plane correlation length ($D_{\parallel}$). The $D\perp$ was calculated from **002** and **004** reflections by using the Scherrer equation:

$$D_{hk\ell} = \mathbf{0.9}\lambda / \beta_{hk\ell}\, cos\theta_{hk\ell}$$

where 0.9 is shape factor (scherrer's constant), λ is the wavelength of incident beam, β is the width at half height (FWHM) and $\theta_{hk\ell}$ is the diffraction angle. Taking into account that the d_{002} interlayer distance is **0.339** nm, a number of about **3000** regularly stacked layers in crystalline domain can be estimated for pencil graphite.

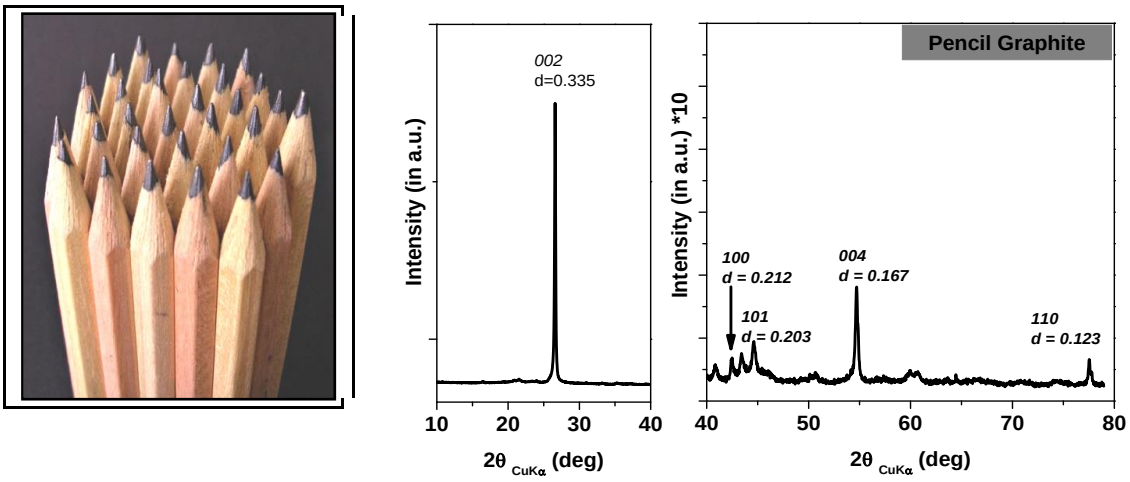

Figure2.3: (**a**) Stack of pencils; (**b**) XRD pattern in **10**° to **80**° **2**θ range of crystalline graphite obtained from pencil.

2.2.2. Concept of shape anisotropy

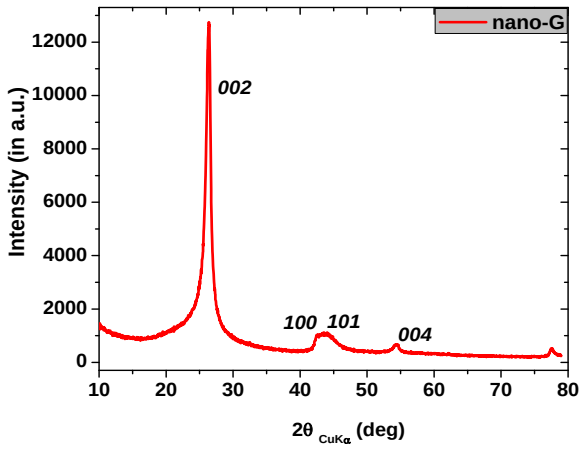

Figure 2.4: XRD pattern in **10**° to **80**° **2θ** range of nanoGraphite (nanoG) obtained from nano-G filler.

The shape anisotropy is defined as the ratio ($D_{\parallel}$ / $D_{\perp}$) between the crystallites dimensions in directions orthogonal ($D_{\perp}$) and parallel ($D_{\parallel}$) to structural layers. [3] From WAXD pattern of nanoGraphite (nano-G) as shown in **figure 2.4**, $D_{\perp}$ can be obtained from **002** and **004** reflections, whereas the $D_{\parallel}$ was determined from the **100** reflections.

The shape anisotropy of nanoGraphite (nano-G) is described in **table 2.1** below –

Material	d_{002} (in nm)	$D_{\perp}$ (in nm)	Number of staked layers estimated	$D_{\parallel}$ (in nm)	Shape anisotropy ($D_{\parallel}$ / $D_{\perp}$)
nanoGraphite (nano-G)	**0.337**	**9.8**	**~ 30**	**30.2**	**3.1**

2.3. Graphitic nanofillers in rubber compounds

Conventional fillers such as carbon black and silica are well-known source of reinforcement and used in various rubber products such as tires [4, 5]. Recently, carbon nanofillers based rubber compounds are investigated to improve their dynamic and mechanical properties. Apart from graphite and carbon nanotubes, an increasing interest is for graphene, a two-dimensional (**2**D) sheet made of sp^2-hybridized carbon atoms in an extended honeycomb network. [6] It is due to its wonderful thermal, electrical, and mechanical properties. Due to **2**-d nature of Graphene and its high lateral dimension that is a very high aspect ratio, make it an ideal candidate for use as filler in rubber or polymer matrix. Its theoretical elastic modulus of **1** TPa, and the Young modulus of **1060** MPa, is many times higher than other nanofillers such as clay minerals. [7-9] Therefore, remarkable efforts are made to prepare graphene or graphitic nanofillers made by few layers of graphene to achieve such wonderful dynamic and mechanical properties in rubber compounds.

Detailed reviews are available on different aspects of graphite nanoparticles (GNP), describing their synthesis, modification and processing. GNPs are defined as a type of graphitic nanofillers made up of stacked 2D graphene sheets. GNP are characterized by a high surface area (theoretical value up to **2630**–**2965** m^2/g) [10-14] and provide a high aspect ratio, when GNP aggregates are formed by a low number of

graphene sheets. To achieve high aspect ratio, the reduction number of stacked layers in GNP stack is attempted various techniques such as oxidation followed with chemical or thermal reduction, intercalation or ultrasonic treatment in different solvents. GNPs are reportedly used in variety of applications [15-23] and as reinforcing filler in various polymer and rubber matrixes. GNPs uses as nanofillers for polymers is recently reported and reviews are already available on processing and mechanical and electrical properties [24-42] of the ensuing polymer nanocomposites. GNP is used for thermoplastics [26-41] and for thermosets, such as epoxy resins. [42] An improved dynamic-mechanical, thermal and electric properties in these GNPs reinforced polymer matrix were reported.

Papers are available on GNPs reinforced elastomers [43-46, 48, 49, 51, 52,53, 55-59] and an improved dynamo-mechanical, thermal and electric property was reported. GNPs were used in both pristine and modified state to achieve a higher level of exfoliation. For example, pristine GNP with a thickness of **10** nm was used to prepare electrically conductive NBR-based composites [56]. In other case, EG (prepared by microwave irradiation of graphite oxide) was used and subsequently suspended in an aqueous medium as graphite nanosheets with the help of a surfactant and microwave irradiation. [54]. Rubber compounds were finally prepared by adding suspended EG in NBR latex under vigorous stirring and improved tensile and dynamic mechanical properties were observed.[50] To introduce more acid and hydroxyl groups onto the graphene layers, commercially available EG was oxidized with acids. [47] It was also reported that a master batch based on EG and epoxidized NR was prepared by solution mixing and finally compounding was carried out by melt blending. An improved mechanical, thermal, and dynamic-mechanical property for EG reinforced epoxy-NR was obtained.

2.3.1. Dispersion of Graphitic nanofillers in rubber

As compared with carbon black, silica, clay minerals or CNTs; graphitic nanofillers have not been explored extensively in field of rubber reinforcement. Very less data are available in which GNP and nanoGraphite were used as nanofillers. To obtain graphene, GNP which has few layer graphene has been sonicated in many different solvents and, in most cases, coating layers have been prepared, but no data appeared in with isoprene rubbers is explored as the matrix. In some cases, melt mixing has been

reported as a filler dispersing technique in IR as the rubber matrix:[61,62] a homogenous nanoG dispersion was reported, though it was not possible to identify in the final composite single graphene layer.

2.3.2. Polymer filler interactions

The reinforcement exerted by nanofillers depends essentially on polymer-filler interaction. The investigation dealing with polymer-filler interaction is performed at different *ranges*: (i) short range in which the nanofiller-polymer interface is investigated, (ii) medium range dealing with the tests performed under strain of the composite up to about **25**% (iii) long range, performing a strain of the composite higher than **25**%, for example Tensile tests in which we strain the sample upto elongation at break. **Table 2.1** summarizes the characterization techniques adopted, as a function of the investigation range, and the subjects of the investigation.

Table 2.1. Investigation of nanofiller-rubber interaction [63]

Range of the investigation	**Characterization technique**	**Subject of the investigation**
Short range	TEM, SEM, solid state NMR, Raman, bound rubber	interface
Medium range	Dynamic-mechanical tests	break up of nanofiller network
Long range	Tensile, quasi static tests Raman	strength of nanofiller-rubber interaction

2.3.2.1. Interactions of Graphitic nanofillers with Isoprene rubber matrix

Graphitic nanofiller-rubber interaction has not explored yet. No data is available for nano-graphitic fillers. Alternatively, investigations are dedicated to CNTs and Clay minerals as nanofillers in which Polymer-filler interactions studies are explored. [60,64]

2.4. Properties of Graphitic rubber compounds

2.4.1. Graphitic nanofillers based Isoprene rubber compounds

As of now, very few data are available for rubber compounds based on isoprene rubber and nanoGraphite (nanoG).[61,62] These findings provides first preliminary information on the reinforcing ability of nanoG in IR matrix. The tensile tests were performed on compounds based on IR with an increasing amount of nano-G, from **1** to **60** phr. The filler percolation threshold (**FPT**) of nanoG was also described in these studies which were calculated using Huber-Vilgis model. In this model, double logarithmic plot of the excess of initial modulus $(E - E_0)/E_0$ on nanoG content was taken where two straight lines were identified, with slope **0.9** and **3.5**, below and above the percolation threshold, The FPT was found to be at **21.2** phr. The network formation occurs at a level not much lower than one typical observe for traditional fillers such as CB (about **30** phr). But, it was shown that nanoG promotes higher reinforcement with respect to CB. An interesting feature of nanoG is the ability to allow high elongations at break for the rubber compounds, appreciably higher than for CB based composites at lower loadings.

Recently, hybrid nanoG/CB filler systems prepared in IR as the rubber matrix were also reported. In samples containing **60** phr of CB, a discontinuity was observed for the dependence of the excess of modulus on nanoG content, at about **6** phr as nanoG content, as if nano-G was able to establish a continuous network in the polymer matrix.

2.4.2. Rheometric curves of Graphene filled NBR compounds

Rheometric curves for graphene filled NBR matrix, at an increasing loading from **0** to **20** vol%, **160** ^{o}C is shown in **figure 2.5**. It can be noticed that with addition of graphene in the NBR matrix, the torque increases from ~**11** dNm (at **0** vol%) to ~ **24** dNm. The increase of torque could be due to influence of filler networking of graphene and its interaction with rubber. At higher filler concentration (>**10** vol%), rheological behavior of filled compounds became more pronounced. It is due to the formation of long-range filler-networks that consists of interconnected filler flocs. At higher oscillatory pre-shear amplitude, these network linkages are disrupted and lead to the formation of isolated flocs. The large number of isolated flocks also results in enhancing torque as observed in rheometric curve.

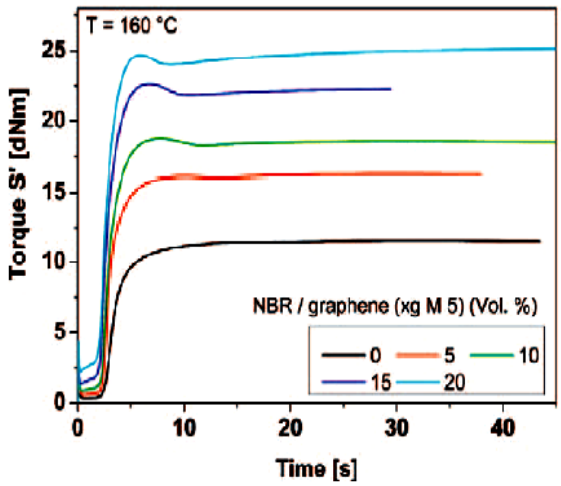

Figure 2.5: Rheometric curves for NBR based compounds with xg M5 concentration from **0** to **20** vol% [taken directly from reference]. [65]

2.4.3. Expanded graphite effect on mechanical properties in xNBR rubber compounds

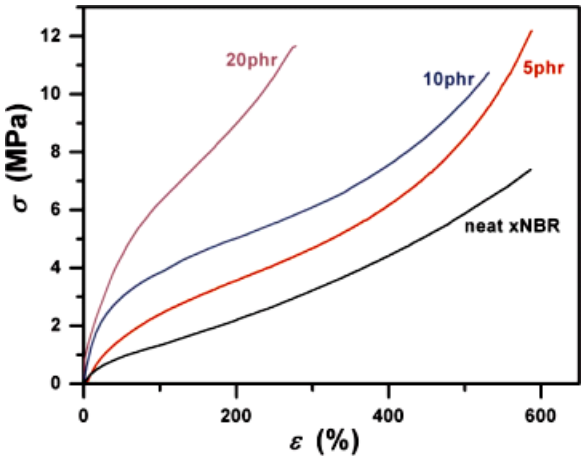

Figure 2.6: Stress-Strain behaviour of EG in xNBR matrix, with content increasing from **0** to **20** phr. [taken directly from reference]. [66]

Stress-Strain curves for expanded graphite (**EG**) filled carboxylated NBR (xNBR), with increasing filler loading from **0** to **20** phr, is shown in **figure 2.6.** It was found that the mechanical behavior of the rubber compounds was greatly improved with the increase of EG loading, and this resulted from the large aspect ratio of the layered structure and the uniform dispersion of EG. A sharp improvement in stress was observed

after **10** phr loading of EG that was due to attainment of filler percolation threshold. It was also found that the elongation at break decreases after **5** phr loading of EG in xNBR rubber compounds.

2.4.4. Electrical resistivity of Graphite nanoPlatelets filler NBR compounds

Electric resistivity of Graphite nanoPlatelets (GNP) filled NBR matrix, with increasing filler concentration from **0** to **5** phr, is shown in **figure 2.8**. It was observed that the resistivity of NBR complounds faals sharply from unfilled (~ 10^7 Ω cm) to (~10^3 Ω cm) and attains equilibrium after **2** phr loading. It is due to attainment of filler percolation threshold of the GNP after **1** phr loading in NBR matrix.

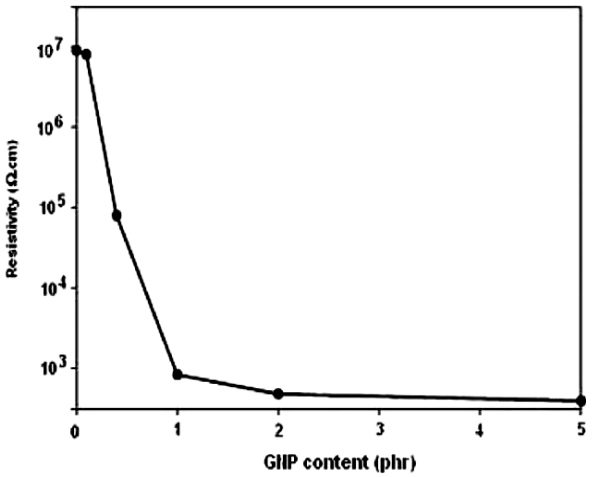

Figure 2.6: Resistivity of GNP in NBR matrix, with loading increasing from **0** to **5** phr. [taken directly from reference]. [67]

2.5. References

[**1**] H. W. Kroto, J. R. Heath, S. C. O'Brien, R. F. Curl, R. E Smalley, *Nature*, **318 (6042)**, 162 (1985)

[**2**] A. K. Geim and K. S. Novoselov, *Nat. Mater.*, **6**, 183 (2007).

[**3**] M. Mauro, V. Cipolletti, M. Galimberti, P. Longo, G. Guerra. *J. Phys. Chem.:C*, **116**, 24809 (2012).

[4] M.L. Studebaker, *Rubber Chem. Technol.*, **30(5)** 1400, (1957).

[5] J.B. Donnet, E. Custodero, "*The Science and Technology of Rubber Third Ed*.", J.E. Mark, B. Erman, F.R. Eirich, Eds. Elsevier Academic Press, Chapter **8**, 367-400, (2005).

[6] K. S. Novoselov, A. K. Geim, S. V. Morozov, D. Jiang, Y. Zhang, S. V. Dubonos, I. V. Grigorieva, and A. A. Firsov, *Science* **306**, 666 (2004).

[7] A. K. Geim and A. H. MacDonald, *Phys. Today* **60**, 35 (2007).

[8] E. T. Thostenson, C. Y. Li, and T. W. Chou, *Comp. Sci. Technol*. **65**, 491 (2005).

[9] S. Stankovich, D. A. Dikin, G. H. B. Dommett, K. M. Kohlhaas, E. J. Zimney, E. A. Stach, R. D. Piner, S. T. Nguyen, and R. S. Ruoff, *Nature*, **442**, 282 (2006).

[10] S. Park and R. S. Ruoff, *Nat. Nanotech*., **4**, 217 (2009).

[11] B. Z. Jang and A. Zhamu, *J. Mater. Sci*. **43**, 5092 (2008).

[12] T. Ramanathan, S. Stankovich, D. A. Dikin, H. Liu, H. Shen, S. T. Nguyen, and L. C. Brinson, *J. Polym. Sci. B, Polym. Phys*. **45**, 2097 (2007).

[13] B. Li and W.-H. Zhong, *J. Mater. Sci*. **46**, 5595 (2011).

[14] L. M. Viculis, J. J. Mack, O. M. Mayer, H. T. Hahn, and R. B. Kaner, *J. Mater. Chem.* **15**, 974 (2005).

[15] A. V. Yakovlev, A. I. Finaenov, S. L. Zabud'kov, and E. V. Yakoleva, *J. Appl. Chem.* **79**, 1741 (2006).

[16] J. Li, H. Lin, W. Zhao, and G. Chen, *J. Appl. Polym. Sci*. **109**, 1377 (2008).

[17] H. Fan, L. Wang, K. Zhao, N. Li, Z. Shi, Z. Ge, and Z. Jin, *Biomacromol.* **11**, 2345 (2010).

[18] T. Ramanathan, S. Stankovich, D. A. Dikin, H. Liu, H. Shen, S. T. Nguyen, and L. C. Brinson, *J. Polym. Sci. B* **45**, 2097 (2007).

[19] F. Schedin, A. K. Geim, S. V. Morozov, E. W. Hill, P. Blake, M. I. Katsnelson, and K. S. Novoselov, *Nat. Mater*. **6**, 652 (2007).

[20] J. S. Bunch, A. M. van der Zande, S. S. Verbridge, I. W. Frank, D. M. Tanenbaum, J. M. Parpia, H. G. Craighead, and P. L.McEuen, *Science*, **315**, 490 (2007).

[21] X. Li and G. H. Chen, *Mater. Lett*. **63**, 930 (2009).

[22] M. Toyoda, *Carbon* **46**, 1627 (2008).

[23] F. Vieira, I. Cisneros, N. G. Rosa, G. M. Trindade, and N. D. S. Mohallem, *Carbon* **44**, 2590 (2006).

[24] J. R. Potts, D. R. Dreyer, C. W. Bielawski, and R. S. Ruoff, *Polymer* **52**, 5 (2011).

[25] R. Sengupta, M. Bhattacharya, S. Bandyopadhyay, and A. K. Bhowmicka, *Prog. Polym. Sci.* **36**, 638 (2011).

[26] X. Jiang and L. T. Drzal, *Polym. Comp*. **31**, 1091 (2010).

[27] A. Delgado, F. Addiego, S. Ahzi, S. Patlazhan, V. Toniazzo, and D. Ruch, *IOP Conf. Ser. Mater. Sci. Eng*., **31** 012009 (2012).

[28] F. Li, J. H. Zhu, S. Y. Wei, J. Ryu, L. Y. Sun, and Z. H. Guo, *Macromol. Chem. Phys.* **212**, 1951 (2011).

[29] K. Kalaitzidou, H. Fukushima, P. Askeland, and L. T. Drzal, *J. Mater. Sci*. **43**, 2895 (2008).

[30] D. Wang, X. Zhang, J.-W. Zha, J. Zhao, Z.-M. Dang, and G.-H. Hub, *Polymer*, **54**, 1916 (2013).

[31] J. U. Roh, S. W. Mab, W. Lee, H. T. Hahn, and D. W. Lee, *Compos. Part B* **45**, 1548 (2013).

[32] Y. Han, Y. Wu, M. Shen, X. Huang, J. Zhu, and X. Zhang, *J. Mater. Sci*. **48**, 4214 (2013).

[33] G. Filippone, M. S. de Luna, D. Acierno, and P. Russo, *Polymer* **53**, 2699 (2012).

[34] A. Al-Jabareen, H. Al-Bustami, H. Harel, and G. Marom, *J. Appl. Polym. Sci*. **128**, 1534 (2013).

[35] L. Zhang, J. Q. Zhu, W. B. Zhou, J. Wang, and Y. Wang, *Energy* **39**, 294 (2012).

[36] M. Singhi and M. Fahim, *Polym. Comp.,* **33**, 675 (2012).

[37] H. Quan, B.-Q. Zhang, Q. Zhao, R. K. K. Yuen, and R. K. Y. Li, *Composites Part A* **40**, 1506 (2009).

[38] M. D. Via, J. A. King, J. M. Keith, I. Miskioglu, M. J. Cieslinski, J. J. Anderson, and G. R. Bogucki, *J. Appl. Polym. Sci.,***124**, 2269 (2012).

[39] F. He, S. Lau, H. L. Chan, and J. Fan, *Adv. Mater.*, **21**, 710 (2009).

[40] S. Kumar, L. L. Sun, S. Caceres, B. Li, W. Wood, A. Perugini, R. G. Maguire, and W. H. Zhong, *Nanotechnology,* **21**, 105702 (2010).

[41] E. Narimissa, R. Gupta, M. Bhaskaran, and S. Sriramb, *Polym. Degrad. Stab.,* **97**, 829 (2012).

[42] A. P. Yu, P. Ramesh, X. B. Sun, E. Bekyarova, M. E. Itkis, and R. C. Haddon, *Adv. Mater.,* **20**, 4740 (2008).

[43] N. Yan, H. Xia, J. Wu, Y. Zhan, G. Fei, and C. Chen, *J. Appl. Polym. Sci.,* **127**, 933 (2013).

[44] C. Li, C. Feng, Z. Peng, W. Gong, and L. Kong, *Polym. Comp.,* **34**, 88 (2013).

[45] J. R. Potts, O. Shankar, S. Murali, L. Du, and R. S. Ruoff, *Comp. Sci. Technol.,* **74**, 166 (2013).

[46] J. R. Potts, O. Shankar, L. R.Du, and S. Ruoff, *Macromolecules*, **45**, 6045 (2012).

[47] A. Malas, C. K. Das, A. Das, and G. Heinrich, *Mater. Design*, **39**, 410 (2012).

[48] M. M. del Herna`ındez, Mar Bernal, R. Verdejo, T. A. Ezquerra, and M. A. Lo`ıpez-Manchado, *Comp. Sci. Technol.*, **73**, 40(2012).

[49] J. Yang, M. Tian, Q.-X. Jia, J.-H. Shi, L.-Q. Zhang, S.-H. Lim, Z.-Z. Yu, and Y.-W. Mai, *Acta Mater.*, **55**, 6372 (2007).

[50] M. Bhattacharya, M. Maiti, and A. K. Bhowmick, *Polym. Eng. Sci.*, **49**, 81 (2009).

[51] S.H. Song, H. K. Jeong, and Y. G. Kang, *J. Industrial Eng. Chem.*, **16**, 1059 (2010).

[52] S. H. Song, H. K. Jeong, Y. G. Kang, and C. T. Cho, *Korean J. Chem. Eng.*, **27**, 1296 (2010).

[53] L. L. Wang, L. Q. Zhang, and M. Tian, *Mater. Design*, **39**, 450 (2012).

[54] L. Wang, L. Zhang, and M. Tian, *Wear*, **276–277**, 85 (2012).

[55] J. Yang, M. Tian, Q.-X. Jia, L.-Q. Zhang, and X.-L. Li, *J. Appl. Polym. Sci.*, **102**, 4007 (2006).

[56] F. R. Al-Solamya, A. A. Al-Ghamdib, and W. E. Mahmoud, *Polym. Adv. Technol.* **23**, 478, (2012).

[57] J. Yang, L.-Q. Zhang, J.-H. Shi, Y.-N. Quan, L.-L. Wang, and M. Tian, *J. Appl. Polym. Sci.* **116**, 2706 (2010).

[58] V. Sridhar, D. Xu, T. T. Pham, S. P. Mahapatra, and J. K. Kim, *Polym. Comp.* **30**, 334 (2009).

[59] Q. H. Mu and S. Y. Feng, *Thermochim. Acta* **462**, 70 (2007).

[**60**] Z. P. Sun, D. Popa, T. Hasan, F. Torrisi, F. Q. Wang, E. J. R. Kelleher, J. C. Travers, V. Nicolosi, and A. C. Ferrari, *Nano Res.*, 653 (2010).

[**61**] M. Galimberti, M. Coombs, V. Cipolletti, L. Giannini, L. Conzatti, T. Riccò, M. Mauro, G. Guerra, in *ACS Rubber Division - Proceedings of the Fall 179th Technical Meeting*, Cleveland (OH), Oct. 11-13, 2011.

[**62**] M. Galimberti, V. Kumar, M. Coombs, V. Cipolletti, S. Agnelli, S. Pandini, L. Conzatti, *Rubber Chem. Technol.*, (2013) –in press

DOI: http://dx.doi.org/10.5254/rct.13.87903.

[**63**] M. Galimberti, V. Cipolletti, V. Kumar, *Natural Rubber Based Composites And Nanocomposites*, S. Thomas, C. H. Chan, L. A. Pothan, Ramanan, J. Maria Eds., *Royal Society of Chemistry*, Chapter **2**, 34 (2014). DOI: 10.1039/9781849737654-00034.

[**64**] Z. Peng, C. Feng, Y. Luo, Y. Li, L. X. Kong, *Carbon*, **48**, 4497 (2010).

[**65**] M. M. Moewes, F. Fleck, M. Klueppel, *Rubber Chem. Technol.*, - *in press*. (2013)

DOI: http://dx.doi.org/10.5254/rct.13.87930.

[**66**] J. Yang, L-Q. Zhang, J.-H. Shi, Y.-N. Quan, L.-L. Wang, M. Tian, *J. Appl. Polym. Sci*., **116**, 2706 (2010).

[**67**] F. R. Al-solamya, A. A. Al-Ghamdi, W. E. Mahmoud, *Polym. Adv. Technol*., **23**, 478 (2012).

Chapter 3

*Compounds based on **low** surface area few layer graphene and **apolar** diene rubbers*

3.1. Introduction

Over the last few years, nanofillers have been employed to improve reinforcing properties of rubber compounds for industrial applications such as tires. [1-15] In present chapter, the main objective of the research activity was to investigate compounds based on **low** surface area few layer graphene (FLG) and **apolar** diene rubbers (SBR and IR), their filler networking and dynamic-mechanical properties. FLG as nanofiller promotes long range filler-filler interaction that is attainment of filler percolation threshold (FPT) at lower filler loading in rubber matrix. Strain sweep tests were performed in torsion mode on raw compounds to obtain dynamic-mechanical characteristics such as storage modulus -G' (in kPa). Tensile strength tests were performed through stress-strain measurements. The dependence of excess modulus $(G\gamma_{min}'-G'_o)/G'_o$ at lower deformation (~**0.56**%) were investigated to obtain FPT. This work demonstrates the correlation of surface area, number of graphene layers on filler percolation threshold, filler-networking and over-all mechanical properties for FLG as nanofillers.

3.2. Results and discussion

3.2.1. Morphological characterization of FLG as nanofillers by Scanning Electron Microscopy (SEM)

SEM micrographs of EXG **9840**, KS**4**, SFG**6** as FLG nanofillers are presented in **figures 3.1** at lower and higher magnifications. EXG **9840** shows "*worm-like*" or "*accordion-like*" morphology presenting highly corrugated or exfoliated graphene like layers which are stacked loosely to each other (**figure 3.1(a,b)**). Such corrugated nature of EXG **9840** (expanded FLG) could be due to their preparation under acidic or thermal treatments. It is interesting to observe the SEMs micrographs of KS**4** (**figure 3.1(c,d)**) and SFG**6** (**figure 3.1(e,f)**). Both FLG nanofillers show "*platelet*" morphology. SFG**6** shows denser particles distribution than KS**4** with a distorted arrangement of the graphene sheets.

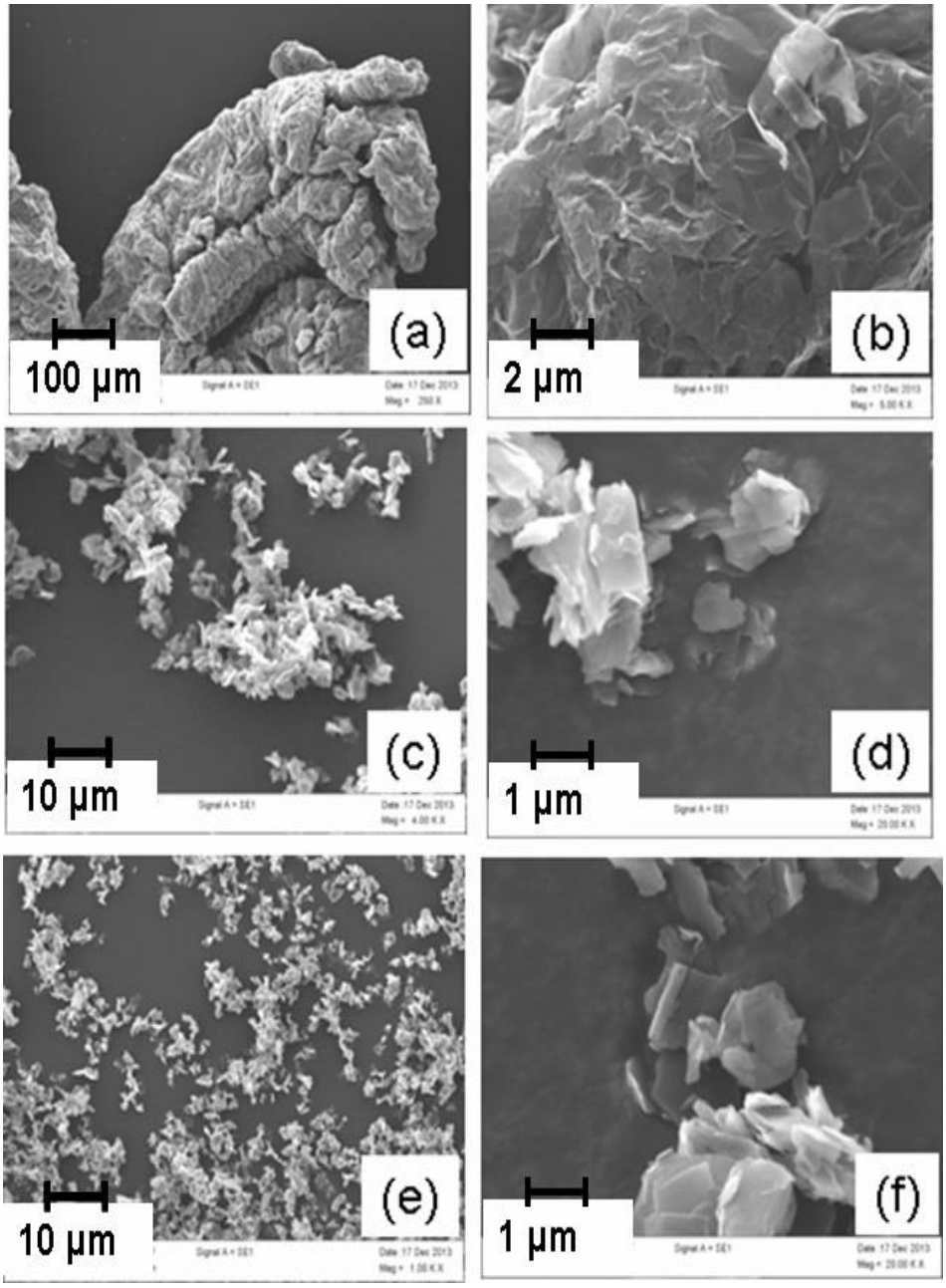

Figure 3.1: SEM micrographs at lower and higher magnification respectively: EXG **9840** (**a**,**b**); KS**4** (**c,d**); SFG**6** (**e,f**).

3.2.2. Wide angle X-Ray Diffraction (WAXD) of FLG as nanofillers

The crystalline order of SFG**6**, KS**4**, EXG **9840** as FLG nanofillers were investigated through WAXD analysis (presented in **figure 3.2**). WAXD patterns of **FLG**

as nanofillers reveals **002** reflections at **26.20°** as **2θ** value, that refers to a d_{002} distance of **0.339** nm, and **004** reflections at **54.3°** as **2θ** value. The width of **002** peaks of all three FLG as nanofiller (SFG**6**, KS**4** and EXG **9840**) was relatively similar and the presence of amorphous carbon is revealed by the pattern. The **100** and **110** reflections at **42.5°** and **77.6°** as **2θ** values respectively indicate the crystalline order in the structural layer [11, 21].

Considering the interlayer distance of d_{002} peak, number of about **45** regularly stacked layers can be calculated for SFG**6**, **45** for KS**4** and **48** for EXG **9840** respectively. The shape anisotropy is defined as the ratio between the crystallites dimensions in directions orthogonal and parallel to structural layers. [11] The shape anisotropy of SFG**6** was **1.7**, KS4 was **1.6** and **1.0** for EXG **9840** was estimated. The features of higher shape anisotropy of these FLG as nanofillers, in particular of SFG**6** and KS**4**, would favour the formation of filler percolation threshold into rubber matrix at lower filler concentration. The method for calculating number of layer and shape anisotropy is described in section **2.2.1** and **2.2.2** of chapter **2**.

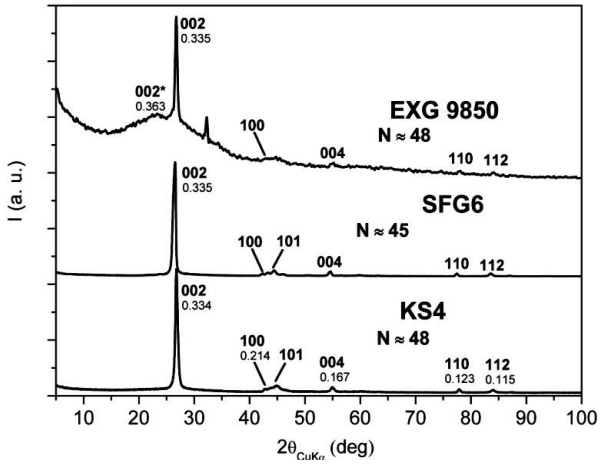

Figure 3.2: XRD pattern in **10°** to **100°** 2θ range of crystalline FLG as nanofillers **(**EXG **9840**, SFG**6** and KS**4**).

3.2.3. Nitrogen adsorption isotherms of FLG as nanofillers

Surface features of SFG**6**, KS**4** and EXG **9840** were obtained from static adsorption isotherms measurements (**figure 3.3**). The surface coverage ($\mathbf{V/V_m}$ where $\mathbf{V_m}$ is the monolayer volume) was performed in nitrogen as a function of relative pressure

p/p_o (**p_o** is saturation pressure at **77** K). The procedure for calculating BET surface area using adsorption isotherms on similar filler systems was adopted from literature [22]**.** BET surface area calculated at a relative pressure range (p/p_0) =**10^{-1} - 10^0**. The values are **13.8** m^2/g for SFG**6**, **23.8** m^2/g for KS**4** and **39.5** m^2/g for EXG **9840**.

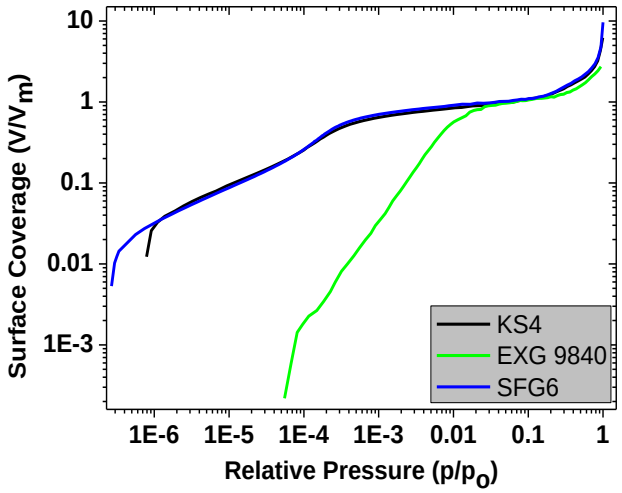

Figure 3.3: Nitrogen adsorption isotherms of nanographitic fillers – KS**4**, SFG**6**, EXG **9840**: plot of surface coverage versus relative pressure.

3.3. Compounds based on **styrene butadiene rubber** as **apolar** diene rubber

3.3.1. Rheometric curves

The rheometric curves for SFG**6** filled SBR matrix with an increasing filler concentration from **2** phr to **40** phr, is presented in **figure 3.4a**. KS**4** and EXG **9840** rheometric curves showed a similar trend as SFG**6** filler.

Three regions are observed in rheometric curves. The first region is the scorch delay or induction period where the torque of filled rubber compounds decreases. The second region is where the curing reaction occurs. The cross-linking network structure was formed in this period, and an increment of the torque was observed. In third region, it was observed that the curing curves reached to a plateau and networking features matured to equilibrium.

M_L is the lowest torque and **M_H** is the highest torque at curing curves. M_H-M_L (increase in torque) represents the crosslink density of vulcanization; curing time (**t'_{90}**) is defined as the time where **90**% of the maximum torque is reached.M_H-M_L (increase of

torque) increases after increasing loading of SFG**6**, KS**4** and EXG **9840** (**figure 3.4b**). This indicates that the addition of filler affects crosslink density of rubber vulcanization, in agreement with literature that increasing filler concentration increases the torque. [11, 21, 22, 26, 30] On other hand, curing time decreases (**figure 3.4c**). The curing time **t'$_{90}$** was found **~32** minutes at lower loadings (upto **20** phr) and decreased to **~28** minutes at higher loadings (after **20** phr). It was further observed that EXG **9840** (acid treated) shows sharp fall in curing time compared to SFG**6** and KS**4**. It could be due to presence of acidic functional groups that facilitate sharp acceleration of curing reaction.

S.H. Song et al already reported that the curing time of rubber compounds using acid-graphite platelets are faster than that of rubber composites with natural-graphite platelets.[26] We have observed similar behavior for EXG **9840** (acid treated), SFG**6** and KS**4**. It was described that the reason for the shorter cure time of the rubber compounds using acid treated (similar to EXG **9840**) is probably due to the improvement of thermal transition of SBR in the presence of acid centers which could promote curing reaction either by improving polymer-filler interaction or other unknown reasons. [26]

S.H. Song et al recently reported that the cure time of SBR composite can be influenced by using acid-graphite and coupling agent (A/C) which improves than other rubber composites. [27] Many recent studies on rubber-clay compounds emphasize the importance of understanding the curing mechanism [17-20]. The study of curing kinetics and processing behavior through rheometric curves as described below provides a clear insight into the actual mechanisms of curing and its effect on the final properties of the end products. [16]

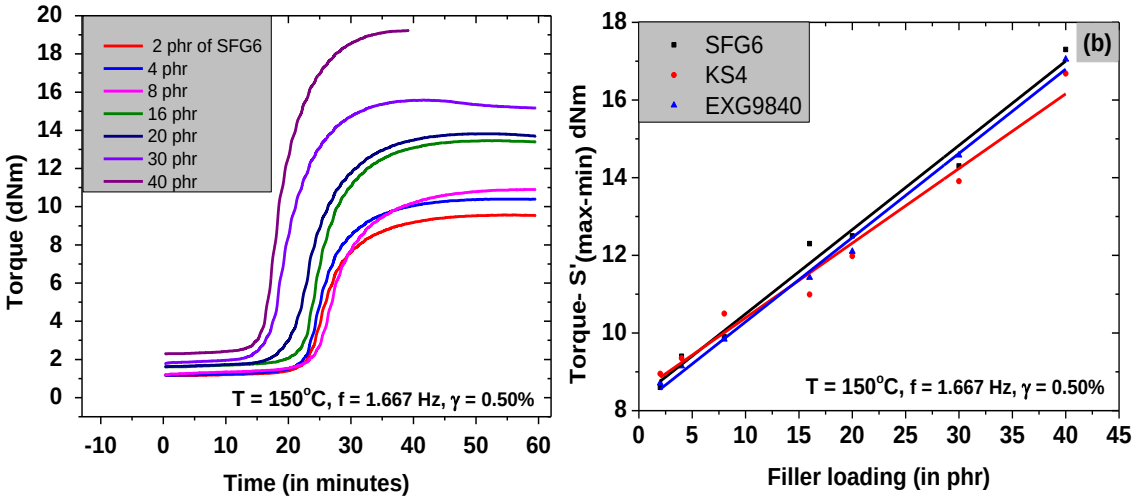

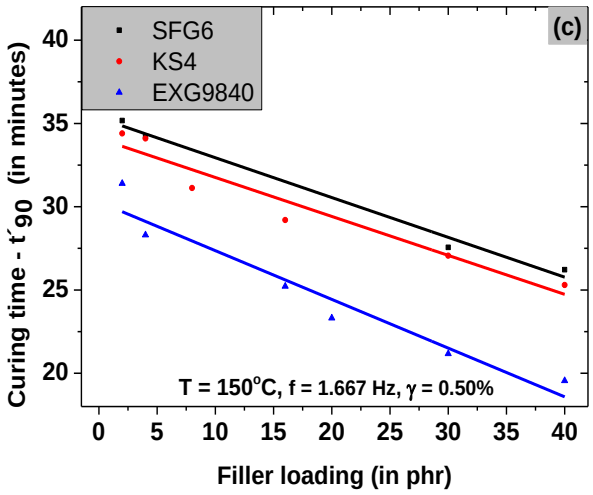

Figure 3.4: Rheometric curves for SBR based compounds: **(a)** containing SFG**6** concentration from **2** to **40** phr; (**b**) torque versus fillers loading with different concenrtration of SFG**6**, KS**4**, EXG **9840**; (**c**) the t'_{90} (curing time) decreasing behavior with increasing filler loading of SFG**6**, KS**4**, EXG **9840** nanofillers.

3.3.2. "*Exfoliation-polymer intercalation-shear*" model

The surface energy or surface activity of filler determines intermolecular interactions at the interfaces of a filler and polymer chains in a compound. It could be suggested that due to reactivity of graphene sheets arranged in stack, free surface energy or higher surface activity of acidic graphite filler such as EXG **9840**, polymer chains adsorption on filler's surface and within the graphitic interlayer galleries occurs. This physical adsorption of filler with rubber matrix could be caused by intermolecular interactions at interfaces, i.e., London dispersive force, Debye inductive force, Keesom orientation forces or hydrogen bonding etc. The shear forces would create randomness in regular graphitic structure (as shown in **Scheme 3.1**) thereby providing the intercalation for more individual polymer chains within the filler's galleries. Once a sufficient interlayer gap is created in graphitic galleries, the polymer chains intercalate into the interlayer spacing. In next stages, they push away the single graphite layers apart (as shown in **Scheme 3.1**). Such process is accelerated by the mechanical shear forces during

melt mixing. The phenomena of intercalation of graphite by a polymer chains contributes in filler's exfoliation which enhance reinforcing characteristic of filler.

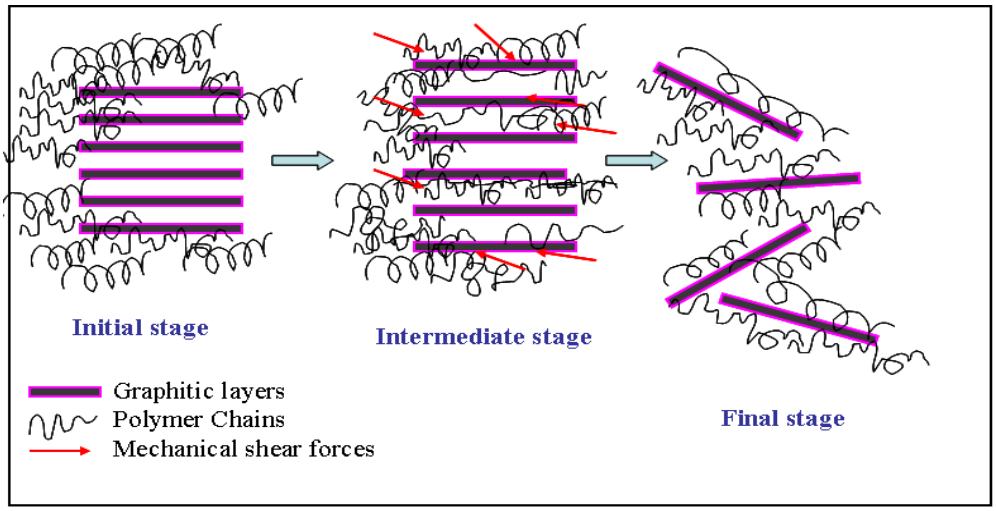

Scheme 3.1:''*Exfoliated-Polymer intercalation-Shear*'' model for polymer intercalation into graphite gallery. It presents that shear forces that exerts during Haake mixing or other mechanical forces during dynamo-mechanical tests contributes in exfoliation of filler with platelet morphologies such as Graphite and in the end led to filler intercalation with polymer chains or filler exfoliation due to shear energy.

3.3.3. Rheological Properties through RPA studies

Rubber processing analyzer (RPA) was used to characterize the filler network and interaction between filler and rubber as a function of strain sweep (from **0.28**% to **400**%). Storage modulus- G' (in kPa) as a function of strain amplitude for SFG**6**/SBR compounds with increasing filler content from **2** to **40** phr is presented in **figure 3.5a**. It was observed that the storage modulus increases with increasing filler content. Such effect could be due to the increase in the degree of compaction of the filler in rubber matrix due to filler networking. A higher degree of compaction is expected to increase the stiffness and reduce the deformation that is responsible for viscous behavior.[23] A sharp fall in modulus was observed after **100**% strain amplitude. It could be due to rupture of filler networking at higher strain amplitude. It was reported that due to the *accordion-like* microstructure of exfoliated graphite and the preferred in-plane orientation of the graphite layers in flexible graphite [24], an in-plane compression is expected in such systems that cause more sliding among the graphite layers that make up a cell wall of

exfoliated graphite than out-of-plane compression and therefore results into filler's exfoliation or polymer intercalation in filler's gallery.

The sliding behavior in graphitic filled system causes interface-related energy loss that is stored in the system. The storage modulus (G', in kPa) and dynamic viscosity (η' in MPa-s) of SFG**6**, KS**4** and EXG **9840** filled SBR rubber compounds as a function of filler loading are comparatively presented in **figure 3.5b and 3.5c**. It can be noticed that G' and η' values of all filled rubber compounds were found increasing with increasing filler loading. It was recently reported that the rheological behavior (such as complex viscosity, storage, and loss modulus) of rubber composites strongly depends on the formation and evolution of the filler networking structures in rubber with strain, time, and temperature. [25] The increasing loading of GNPs in a melt polymer could gradually lead to a phase transformation, due to formation of mechanically stable networking by GNPs interacting with polymer chains. To be more specific at low loading, the G' and η' values of the compound melt is frequency dependent at low frequencies, the same as pure polymer melt. As the loading goes up, the network of GNPs will form step by step, and the frequency dependence of storage modulus at low frequency, indicating a typical solid-like behavior. [25] We had same hypothesis for our filler system presented in **figure 3.5b** and **3.5c**. Another reason for enhancement of G' and η' values could be due to "*Exfoliation-polymer intercalation-shear*" model as described above. In general, when filler is added for reinforcing a polymer matrix, the degrees of freedom of the rubber chains are decreased due to the interaction and adsorption of non deformable filler's surface onto the rubber. This adsorption reduces the mobility of the rubber chains and results in formation of a "rubber-shell" on the filler surface. The reduced mobility and the rubber shell increase the viscosity of rubber composite.

The filler networking can be investigated by determining the dependence of storage modulus- G' values at minimum deformation G'(γ min) against the filler volume fraction. Filler percolation threshold (**FPT**) was calculated from excess modulus by adopting Huber-Vilgis double logarithmic plot (**figure 3.5d**). From the plot, it was found that FPT obtained from double log plot for FLG as nanofillers are: SFG6 **(~29.5 phr**), KS4 (**~31.1 phr**), EXG 9840 **(~28.2 phr**).

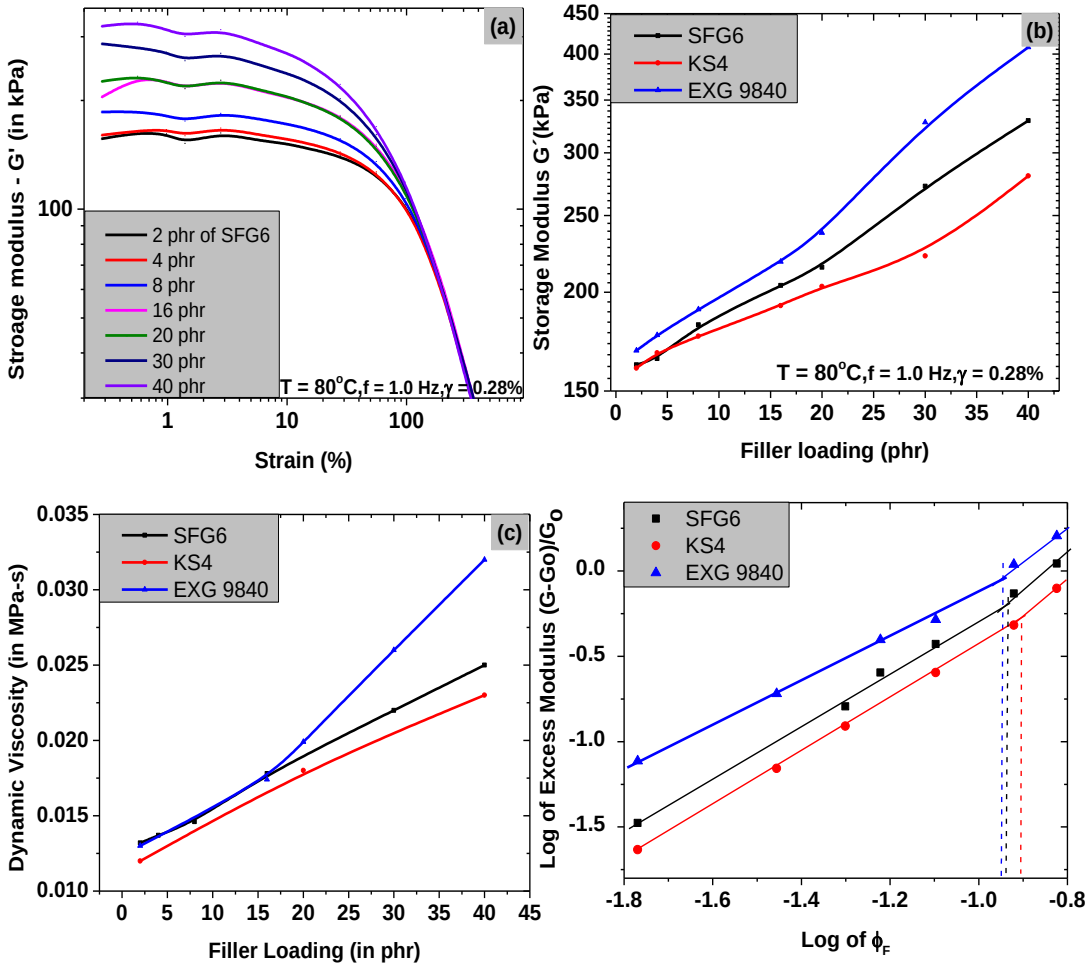

Figure 3.6: Rheological Properties of SBR compounds through RPA studies: (**a**) Storage modulus (G', kPa) as a function of different strains (increasing from 0.28% to 300%) for SFG**6** filler; (**b**) Storage modulus at minimum strain for compounds based on SFG6, KS4, EXG 9840 fillers; (**c**) Dynamic Viscosity at minimum strain on SFG**6**, KS**4**, EXG **9840** fillers; (**d**) Filler Percolation Threshold: Double logarithmic plot of the excess modulus, with respect to neat rubber, as a function of the filler volume fraction / (Huber–Vilgis plot).

3.3.4. Stress-strain behavior for Tensile strength

The stress-strain behavior of vulcanized SFG**6** filled SBR compounds are displayed in **figure 3.6a**. It can be clearly seen that with the increase in the SFG**6** content from unfilled system to **40** phr, the slope of curve at initial stage increased significantly, and the compound improves in stiffness than compared with softer unfilled SBR

compounds. As already reported in literature for similar filler in carboxylated NBR that such high reinforcement by graphite nanosheets could be attributed due to the nanoscale uniform dispersion of graphite as well as the large aspect ratio of the layered structure, which was similar to nanoclay filler. [28]

It was found that that with increasing SFG**6** concentration in SBR matrix, the tensile strength of rubber compound is found to be superior leading to higher tensile stress and elongation, indicating that nano-size dispersed SFG**6** can be dispersed more uniformly and reinforce rubber more effectively. It could be proposed that with increasing graphite content, higher dispersion and exfoliation of graphite higher effective filler volume fraction, better graphite-rubber interface adhesion and better rubber reinforcement. Recently, *L. Wang* et al reported that nano-sized graphitic flake filled NBR shows higher tensile strength than micro-sized flakes. Micro-dispersion of graphite leads to thick sheets, poor interfacial adhesion, interfacial stress concentration, and fracture at low tensile stress and low elongation rate. In our case, we used SFG**6** and we obtained higher reinforcement, better adhesion and relatively higher elongation at break. [29] A comparative reinforcing factor that means the ratio between the stress at a particular strain between filled and unfilled composites (σ_f/σ_0), studies at **50**%, **100**% and **200**% elongation respectively shows that SFG**6**/SBR compounds show higher reinforcing factor than all other comparative fillers (**figure 3.6b-d**) at all respective elongations.

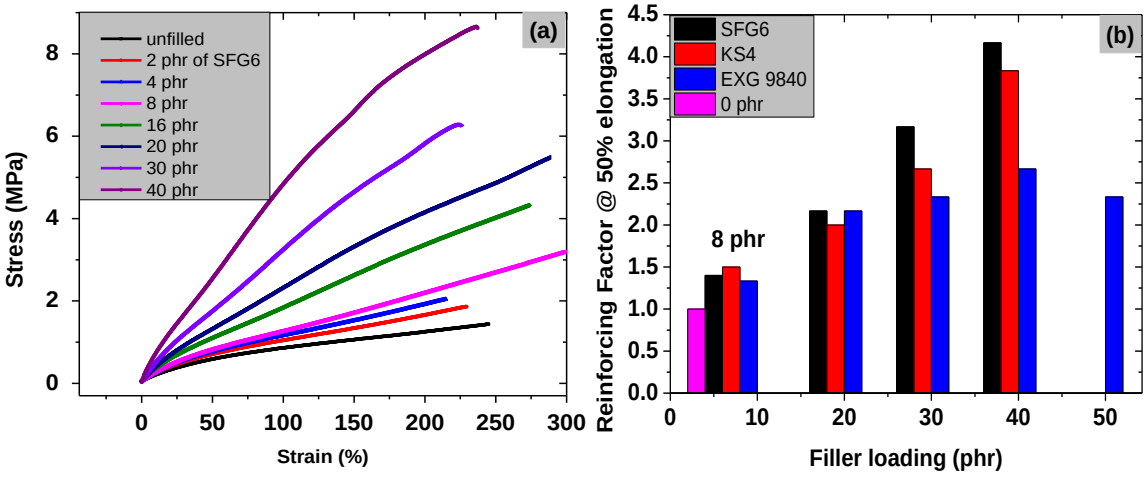

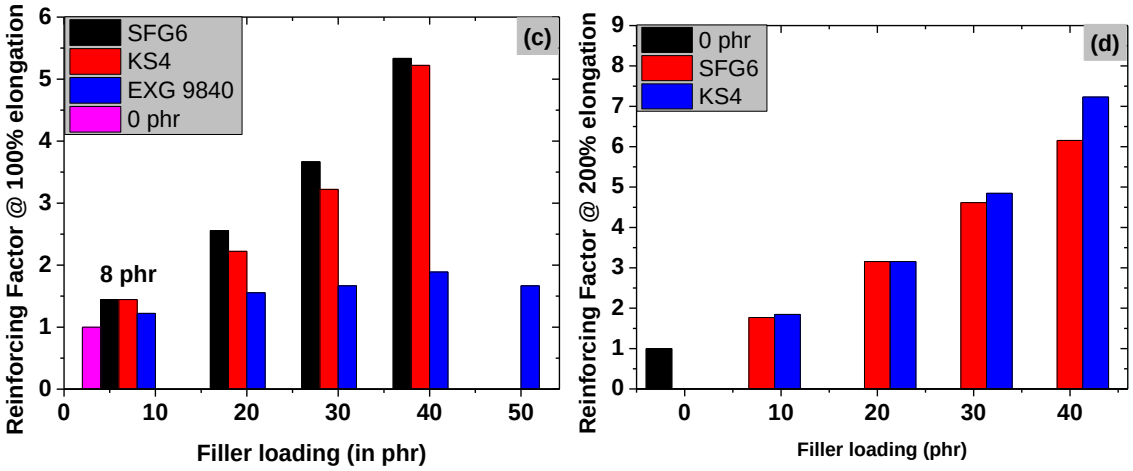

Figure 3.6: Stress-Strain behaviour of SBR compounds: **(a)** for SFG6 content increasing from 0 to 40 phr; Reinforcing factor (σ_F/σ_0) on SFG**6**, KS**4**, EXG **9840** fillers: **(b)** at **50**% elongation; (**c**) at **100**% ; and (**d**) at **200**%.

3.4. Compounds based on **synthetic isoprene rubber** as **apolar** diene rubber

3.4.1. Rheometric curves

The rheometric curves for EXG **9840**/IR compounds, with an increasing filler concentration (from **0** to **30** phr), are presented in **figure 3.7a.** The behavior of rheometric curves, their curing and scorch time were found not to deviate largely. The increasing concentration of EXG **9840** in IR improves the increased torque, **ΔS** ($S'_{max-min.}$) and decreases the scorch time.

It is well known that reversion process experienced in natural or isoprene rubber would led the vulcanized rubber to revert back to the gum state. It involves three types of crosslinks in the vulcanizate such as - polysulfidic, disulfidic and monosulfidic. Lyubchanskaya et al. demonstrated that the thermal decomposition of polysulfidic bonds proceeds at one order of magnitude faster than the oxidation of the polymer chain for a vulcanizate not containing antiozonants. [31] Blackman et al. suggested that crosslink degradation processes might contribute to the deterioration in physical properties of the vulcanizate. [32] Nasir et al. found that for NR, polysulfidic crosslinks gave rise to improved mechanical properties, except tear strength, than either mono or disulfidic crosslinks. [33] A little higher **ΔS** and lower scorch time was seen for acidic EXG **9840**

filled IR at similar loading which could be due to better filler-polymer interaction. The torque changes (**ΔS**) and curing time (t'_{90}) for KS**4** and EXG **9840**/IR were presented as a function of filler loading (**figure 3.7b,c**) where it was found to be relatively similar at smaller loading level (upto **12** phr) which indicate that they were cured to similar crosslinking degree. It was however seen that **ΔS** increases with further increase of filler loading (after **12** phr loading) which was higher in EXG **9840** than KS**4**. It can be due to improved polymer-filler interface in EXG **9840** (acidic) as described above. Therefore, it could be concluded that filler dispersion and the magnitude of interfacial interaction between filler particles and rubber matrix could be dominant factors results an improved **ΔS** of filled rubber compounds. Similar interfacial interaction hypothesis is presented by Yang et al. [34]

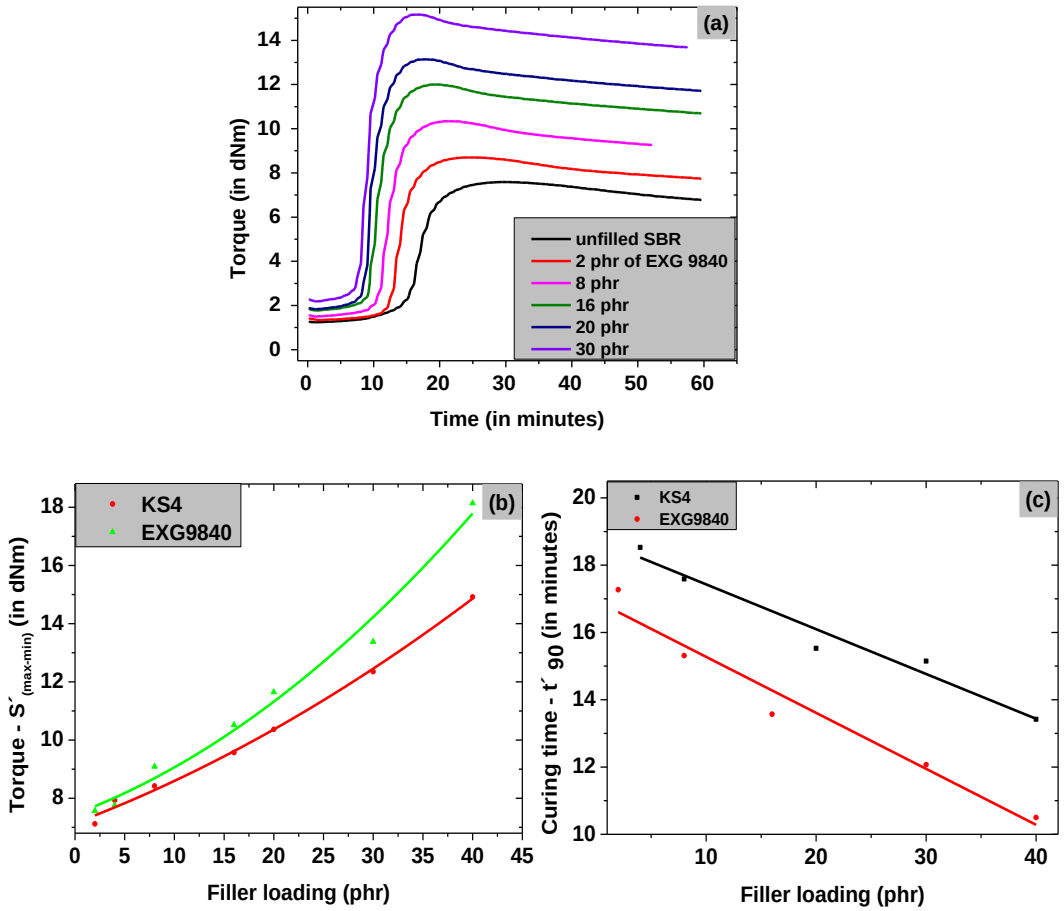

Figure 3.7: Rheometric curves for IR based compounds (**a**) with EXG **9840** concentration from **0** to **40** phr; (**b**) The increased torque (**ΔS**) torque change as a function of filler loading with different concentration of EXG 9840 and KS4; and (**c**) t'_{05} (curing time) for SFG**6** and KS**4** filler.

3.4.2. Rheological Properties through RPA studies

It was observed from **figure 3.8a** that the curing time decreases with increasing filler loading. EXG **9840**/IR rubber compounds shows lower curing time than KS**4** filled IR compounds. Similar behavior of EXG **9840**/IR was observed with SBR matrix as described in section **3.3.3** of this chapter. It could be due to improved filler-polymer interaction in EXG **9840** as described above. The shape and surface activity of the filler play huge roles in the polymer-filler interaction and thus for reinforcement. The role of the physicochemical nature of the filler's surface in reinforcement offered to rubber matrix is however not fully understood yet. [35] The storage modulus comparative (G', in kPa) of KS**4** and EXG **9840**/IR filled rubber compounds were described with increasing filler concentration and are presented in **figure 3.8a**. It can be noticed that G' values for EXG **9840** and KS**4**/IR filled rubber compounds were found increased with increasing filler concentration.

For spherical fillers such as carbon black, high modulus produced by the high structure blacks was not because the carbon black agglomerates restricted the crosslinked network. It is because these aggregates when broken down during methods like dry mixing for filler's dispersion that produces active free radicals. These radicals are capable of reacting with rubber thereby promoting polymer-filler interactions.[36] EXG **9840**/IR compounds shows higher values of G' after **20** phr loading which could be also be due to improved polymer-filler interaction due to acidic nature and reactive functional groups of EXG **9840** in IR than KS**4** filler. At higher filler concentration, increase in filler flocs would also led the higher increase of G' values after **20** phr concentrations of both EXG **9840** and KS**4** filled compounds. It was reported that such flocculation depends on filler's concentration, filler's chemistry, polarity of rubber matrix etc. [37] The flocculated filler's aggregates particles provide sites for high stress concentration because they act like flaws that initiate failure. In order to achieve a high degree of reinforcement the particulate must be well dispersed and uniformly distributed within the rubber matrix.

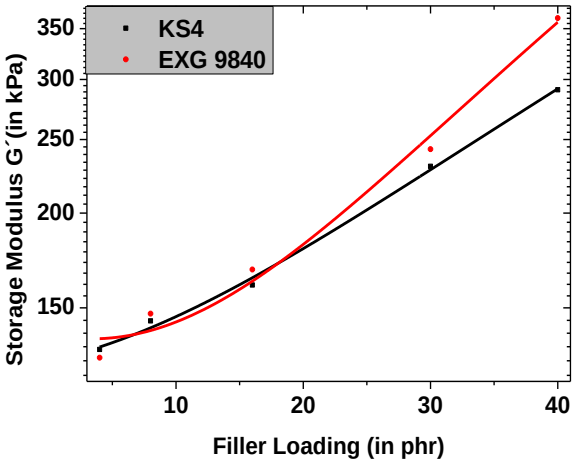

Figure 3.8: Rheological Properties of IR compounds through RPA studies: Storage modulus at minimum strain for compounds based on KS4, EXG 9840 fillers.

3.4.3. Stress-strain behavior for Tensile strength

The reinforcing factor that means the ratio between the stress at a particular strain between filled and unfilled composites (σ_f/σ_0) comparatives of KS**4** and EXG **9840**/IR rubber composites at **50**%, **100**% and **200**% are presented in **figure 3.8a-c**. It can be noticed that KS**4** shows higher reinforcement than EXG **9840**/IR for all filler loadings at **50**% elongation, **100**% elongation and **200**% elongations. The reinforcement magnitude increases progressively with increasing filler concentration in the polymer matrix. It was observed **in figure 3.8c** that at **200**%, the extent of reinforcement increases sharply as compared to reinforcement at **100**% as shown in **figure 3.8b**. It could be due to a good extent of favorable molecular orientation of isoprene rubber chains which takes place during extension and led to the rise in degree of crystallization due to strain is known as "Strain induced crystallization (SIC)" resulting an enhanced reinforcement at **200**% strain. The crystallites in SIC consist of many chains aligned closely together and provide some form of reinforcement. The stress is such cases transferred to the crystals which are made up of lumps of chains. It is similar as if the stress is transferred to hundreds of chains that are knitted together closely. The chain segments are of different dimensions (short and long) which are distributed randomly in the network. Under strain, the shortest chain will break first and the stress will be transferred to surrounding chains. Its worth to

know that in crystallizing rubbers such as natural rubber, hystersis occurs mainly from crystallization at high strain and is relatively unaffected by changes in temperature or frequency, while the hystersis of SBR is due to internal viscosity which is continually varying.

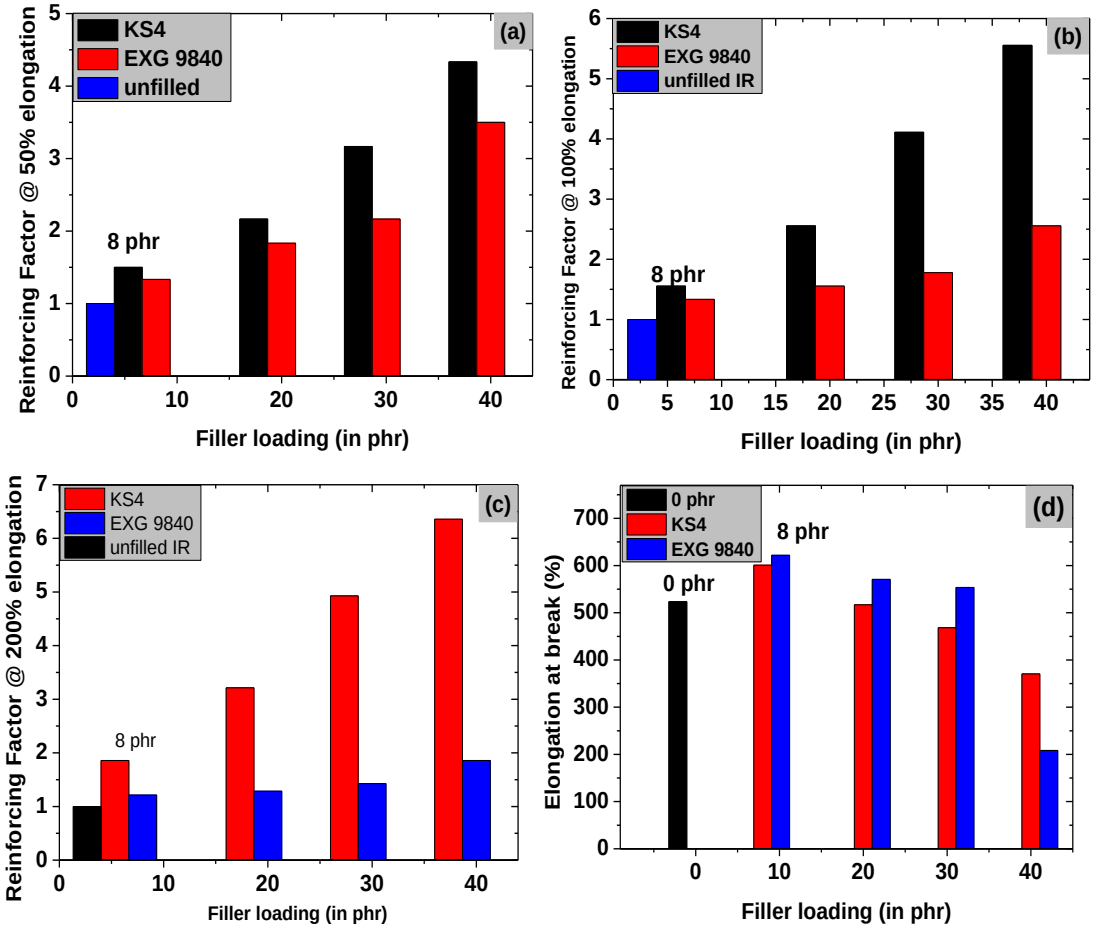

Figure 3.8: Stress-Strain behaviour of IR compounds: Reinforcing factor (σ_F/σ_0) on KS**4**, EXG **9840** fillers: **(a)** at **50**% elongation; **(b)** at **100**%; **(c)** at **200**%; and (**d**) Elongation at break.

3.5. Conclusions

It has been demonstrated from the study that the use of few layer graphene characterized with "low" surface area (EXG **9840**, SFG**6** and KS**4**) brings a significant improvement in dynamic mechanical properties of compounds. SEM micrographs show "*worm-like*" morphology of EXG **9840** presenting highly corrugated or exfoliated

graphene like layers which are stacked loosely to each other. It is interesting to observe the SEMs micrographs of KS**4** and SFG**6** a typical platelet-like morphology. From WAXD, a number of about **45** regularly stacked layers were calculated for SFG6, **45** for KS4 and **48** for EXG **9840** respectively. The shape anisotropy of SFG6 was **1.7**, KS4 was **1.6** and **1.0** for EXG **9840** was estimated. Surface characteristics of the nanofillers studied through adsorption isotherms. BET surface area calculated at a relative pressure range from $p/p_0 = 10^{-1}$ to 10^{0} was calculated as **13.8** m^2/g for SFG**6**, **23.8** m^2/g for KS**4** and **39.5** m^2/g for EXG **9840**.

The compounds were successfully prepared using small Haake **600**® by dry melt mixing method. Rheometric curves show that the scorch time (t'_{05}) decreases with increasing filler concentration in the rubber matrix. Acid treated EXG **9840** shows sharp fall in curing time with increasing filler loading in SBR matrix than SFG**6** and KS**4** filled compounds. Strain sweep measurements shows that the characteristic plateau of G' at low strain increases with an increase of filler concentration in rubber matrix. Filler percolation threshold was obtained using Huber–Vilgis double logarithmic plot in both neat and filled rubber matrix from tensile tests; it was observed that the stresses increase with filler content in the rubber matrix.

Stress-Strain measurements in SBR compounds demonstrate that SFG**6**/SBR has dominant tensile strength against KS**4** and EXG **9840** filled compounds. In other side, Strain curves of Ir compounds shows that KS**4**/IR has higher reinforcing factor and elongation at break than EXG **9840** filler.

3.6. References

[**1**] M. Maiti, M. Bhattacharya, A. K. Bhowmick, *Rubber Chem. Technol*., **81**, 384 (2008).

[**2**] M. Galimberti, V. Cipolletti, V. Kumar, *Natural Rubber Based Composites And Nanocomposites*, S. Thomas, C. H. Chan, L. A. Pothan, Ramanan, J. Maria Eds., *Royal Society of Chemistry*, Chapter **2**, (2014).

[**3**] Vocabulary – Nanoparticles, ***PAS 71 BSI*** (2005).

[**4**] S. S. Ray, M. Okamoto, *Prog. Polym. Sci.*, **28**, 1539 (2003).

[**5**] Chen B., Evans J. R. G., Greenwell H. C., Boulet P., Coveney P. V., Bowden A. A., Whiting A., *Chem. Soc. Rev.*, **37**, 568 (2008).

[**6**] D. R. Paul, L. M. Robeson, *Polym. Nanotech.: Nanocomp. Polym*., **49**, 3187 (2008).

[**7**] M. Galimberti, *Rubber Clay Nanocomposites: Science, Technology, Applications*, 1st edition, John Wiley and Sons, 601(2011).

[**8**] M. Galimberti, *Advanced Elastomers - Technology, Properties and Applications*, edited by Anna Boczkowska, Chapter **4**, (2012).

[**9**] M. Galimberti, V. Cipolletti, M. Coombs, *Handbook of Clay Science, Bergaya and Lagaly Eds.*, Chapter **4**, (2013) in press.

[**10**] L. Bokobza, *Polymer*, **48**, 4907 (2007).

[**11**] M. Galimberti, V. Kumar, M. Coombs, V. Cipolletti, S. Agnelli, S. Pandini, L. Conzatti, *Rubber Chemistry and Technology*, (2013) – in press.

DOI: http://dx.doi.org/10.5254/rct.13.87903

[**12**] F. R. Al-Solamya, A. A. Al-Ghamdib, W. E. Mahmoud, *Polym. Adv. Technol.,* **23**, 478, (2012).

[**13**] A. K. Bhowmick, M. Bhattacharya, S. Mitra S., *J. Elastom. Plast*., **42**, 517 (2010).

[**14**] Bhattacharya M., Maiti M., Bhowmick A. K., *Polym. Eng. Sci*., **49**, 81 (2009).

[**15**] Sridhar V., Xu D., Pham T. T., Mahapatra S. P., Kim J. K., *Polym. Comp.,* **30**, 334 (2009).

[**16**] D. Choi, M. A. Kader, B. H. Cho, Y.-I. Huh and C. Nah, *J. Appl. Polym. Sci*. **98**, 1688 (2005).

[17] Q. Liu, W. T. Ren, Y. Zhang and Y. Zhang, *J. Appl. Polym. Sci*. **123**, 3128 (2012).

[**18**] A. Usuki, A. Tukigase and M. Kato, *Polymer*, **43**, 2185 (2002).

[19] K. G. Gatos, N. S. Sawanis, A. A. Apostolov, R. Thomann and J. Karger-Kocsis, *Macromol. Mater. Eng*. **289**, 1079 (2004).

[**20**] C. Albano, M. Hernandez, M. N. Ichazo, J. Gonzalez and W. De Sousa, *Polym. Bull*. **67**, 653 (2011).

[**21**] V. Kumar, U. Giese, T. Hanel, L. Giannini, M. Galimberti, *Kautsch. Gummi Kunstst.*, (2014) (accepted)- in press.

[**22**] M. M. Moewes, F. Fleck, M. Klueppel, *Rubber Chem. Technol.,* (2013)- *in press*. DOI: http://dx.doi.org/10.5254/rct.13.87930.

[**23**] P.-Hsiu Chen, D.D.L. Chung, Carbon, **50**, 283 (2012).

[**24**] A. Celzard, J.F. Mareche, G. Furdin, *Prog Mater Sci*, **50(1)**, 93 (2005).

[**25**] Bin Li, Wei-Hong Zhong, *J Mater Sci*, **46**, 5595 (2011).

[**26**] S.H. Song, H.K. Jeong, Y. G. Kang, *J. Indus. Eng. Chem*., **16**, 1059 (2010).

[**27**] S. H. Song, H. K. Jeong, Y. G. Kang, C. T. Cho, *Korean J. Chem. Eng.*, **27(4)**, 1296 (2010).

[**28**] J. Yang, L-Q. Zhang, J.-H. Shi, Y.-N. Quan, L.-L. Wang, M. Tian, *J. App. Polym. Sci.*, **116**, 2706 (2010).

[**29**] L. Wang, L. Zhang, M. Tiana, *Wear*, **276– 277**, 85 (2012).

[**30**] V. Kumar, U. Giese, T. Hanel, M. Galimberti, L. Giannini, *Kautsch. Gummi Kunstst.*, (2014) (accepted)- in press.

[**31**] Huang C., Fan R., Zhang Y., Zhang Y. "*Effet of Aging on NR Vulcanizates*," H- C. Xiang, J. G. Ye: China Synthetic Rubber Industry, **23(5)** 288 (2000).

[32] Blackman E.J., McCall E.B. *Rubber Chem. Technol.*, 651 (1969).

[**33**] Nasir M., The G.K, *Eur. Polym. J.*, **24(8)** 733 (1988).

[**34**] J. Yang, M. Tian, Q.-X. Jia, L.-Q. Zhang, X.-L. Li, *J. Appl. Polym. Sci.*, **102**, 4007, (2006).

[35] J. B. Donnet, E*lastomeric matrix and carbon black interactions in rubber compounds*, in Proceedings International Rubber Conference, Rubber Research Institute of Malaysia, Kuala Lumpur, 323 (1977).

[**36**] J. B. Horn, *Rubber Technol. Manufacture*, 174 (1971).

[**37**] S. R. Raghavan, S. A. Khan, *J. Rheol.* **39(6)** 1311, (1995).

Chapter-4

*Compounds based on **high** surface area few layer graphene and **apolar** diene rubbers*

4.1. Introduction

In present work, few layer graphene (FLG) with **high** surface area were explored as nanofillers for improving reinforcing and dielectric properties of **apolar** diene rubber compounds. Exfoliated graphene nanoplatlets (xGnPs), nano-graphite with high shape anisotropy (nano**G**) and furnace carbon black (N**234**) were selected as the carbon nanofillers. The shape anisotropy is defined as the ratio between the crystallites dimensions in directions orthogonal and parallel to structural layers. [1] Nanofillers were characterized with adsorption isotherms to obtain surface characteristics such as BET surface area, surface activity and porosity. [2] Dynamic-mechanical measurements were performed in the torsion mode, with strain sweep and frequency sweep experiments. Guth-Gold Smallwood equation was used to correlate initial modulus values with the filler volume fraction. Mechanical properties were assessed by means of stress-strain and multi-hysteresis tests. Electrical properties were investigated through dielectric AC conductivity measurements. This work describes the correlation of FLG with high surface area, shape anisotropy, number of graphene layers on filler networking, filler dispersion, dynamic mechanical and dielectric properties of rubber compounds.

4.2. Results and discussion

4.2.1. Morphological characterization of FLG as nanofillers by Scanning Electron Microscopy (SEM)

The xGnPs consists of a FLG arranged parallel to each other in form of a stack. These graphene stacks are a few nanometers thick and have large lateral dimensions. The structural morphology of xGnPs were investigated by SEM. **figures 4.1 (a) and 4.1 (b)** show SEM of xg M**5** filler grade. High in-plane lateral dimension (from **0.5** to **>2** μm) of xg M**5** was observed at low resolution. The high resolution image (**figure 4.1 (b)**) shows a typical platelet-like morphology and random arrangement of graphene sheets in a stack was observed. **figures 4.1 (c) and 4.1 (d)** show SEM of xg C**750** at lower and higher magnification respectively. The high resolution image shows a damaged (ruptured)

platelet morphology which could be due to several vigorous treatments (acidic or thermal) during preparation to achieve high surface area. A discontinuous arrangement of these graphene sheets was also noticed. The aggregates and agglomerates were found to be in the range of a few nanometers to a sub-µm in lateral dimension.

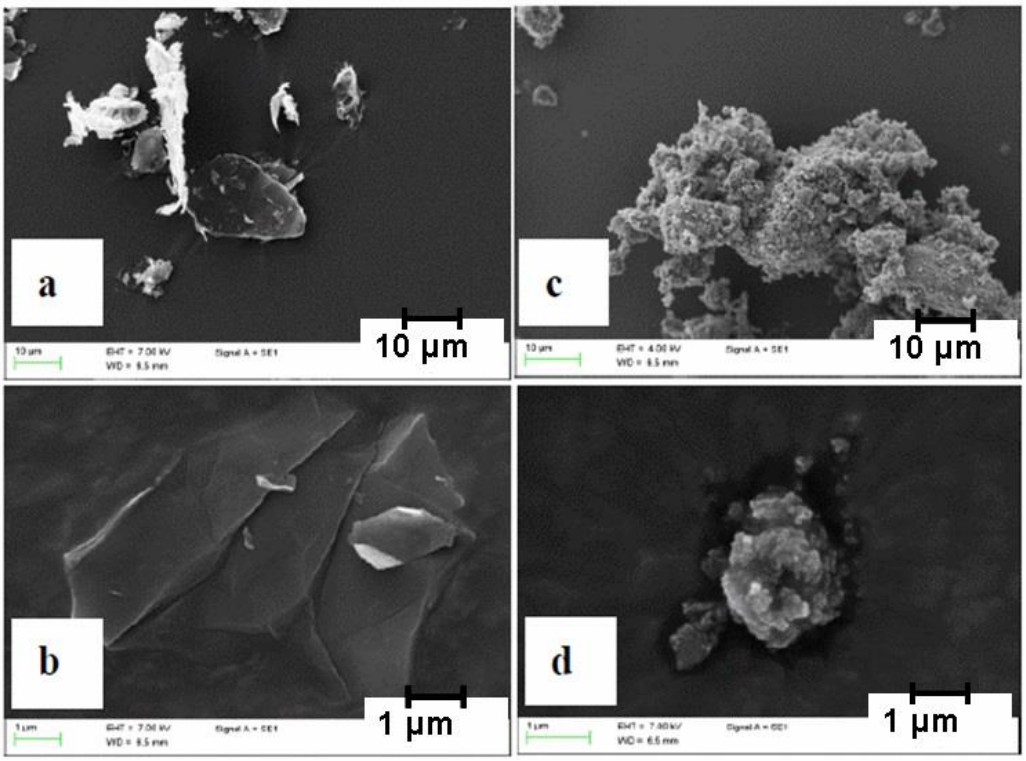

Figure 4.1: SEM micrographs at different magnifications of xg M**5** (**a,b**); and xg C**750** (**c,d**) graphene filler grades**.**

4.2.2. Wide angle X-Ray Diffraction (WAXD) of FLG nanofillers

The crystalline order of both xGnPs samples were studied by means of WAXD analysis. As it is shown in **figure 4.2**, WAXD patterns reveal 002 reflection of xg M**5** sample appear quite narrow. The **002** peak of xg C**750** is larger and the presence of amorphous carbon is revealed by the pattern. The **100** and **110** reflections at **42.5**° and **77.6**° as **2**θ values respectively indicate the crystalline order in the structural layer [1]**.** Taking d_{002} interlayer distance into account, a number of about **26** and about **59** regularly stacked layers can be estimated for xg C**750** and xg M**5** respectively. The xg C**750** has larger shape anisotropy (**2.7**) than xg M5 (**1.7**). xg C**750** reveals thus a large in-plane correlation length. The features of xGnPs, in particular of xg C**750**, should favour the

formation of rubber compounds. The method for calculating number of layer and shape anisotropy is described in section **2.2.1** and **2.2.2** of chapter **2**.

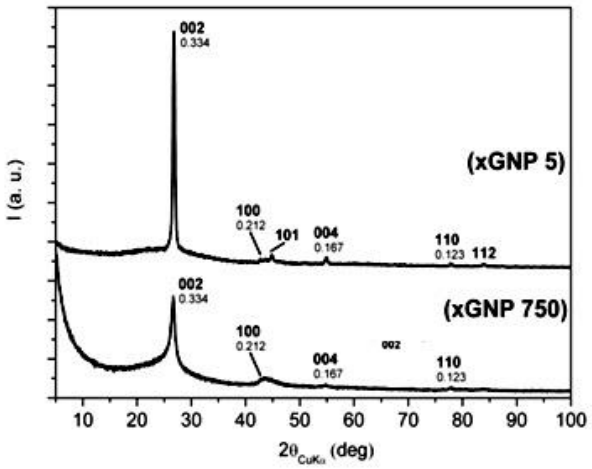

Figure 4.3: XRD pattern in **10**° to **100**° 2θ range of crystalline FLG as nanofillers **(**xg C**750** and xg M**5**).

4.2.3. Nitrogen adsorption isotherms of FLG nanofillers

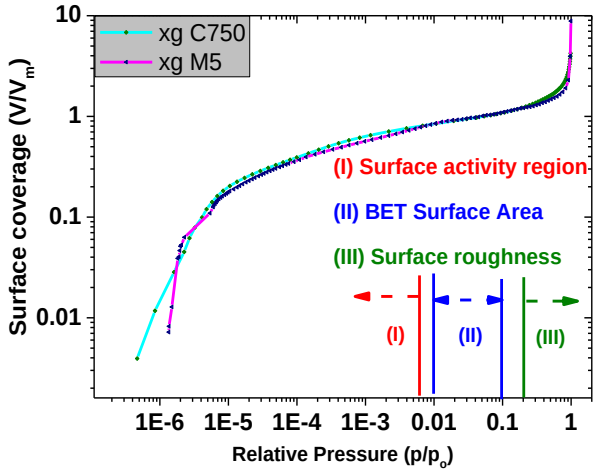

Figure 4.3: Nitrogen adsorption isotherms of xg M**5**, xg C**750** and nanoG filler: plot of surface coverage versus relative pressure.

Surface characteristics of carbon nanofillers (xg C**750**, xg M**5)** were investigated from adsorption isotherms measurements (as shown in **figure 4.3**). The surface coverage (V/V_m where V_m is the monolayer volume) was studied in nitrogen as a function of relative pressure p/p_o (p_o is saturation pressure of nitrogen at **77** K). The low pressure

regime (p/p_0 =10^{-6} to 10^{-3}) gives data on the filler's surface activity. The methodology for calculating surface activity, BET surface area and surface porosity using adsorption isotherms on similar filler systems was adopted from literature without any significant change [2]. The BET surface area of xg C**750** in N_2 calculated from isotherms was found to be **817.3** m^2/g, higher than the one of xg M**5**, equal to **168.3** m^2/g. The surface activity (%) of xg C**750** was found **7.3** at partial pressure of **3***10^{-6} and **29.1** at partial pressure of **3***10^{-5}. The surface activity (%) of xg M**5** was found **4.6** at partial pressure of **3***10^{-6} and **43.9** at partial pressure of **3***10^{-5}. The third region (p/p_0 =10^{0} to 10^{1}) at highest pressure presents porosity or surface roughness of the fillers. The roughness of xg C**750** was higher (~**2.759** nm) than xg M**5** (~ **2.676** nm). **figure 4.3** shows that the large amount of adsorbed gas in the low-pressure regime illustrates the presence of strongly adsorbing sites on surface of nanofillers like xg C**750** and xg M**5**.

4.2.4. Morphological characterizations of compounds through TEM

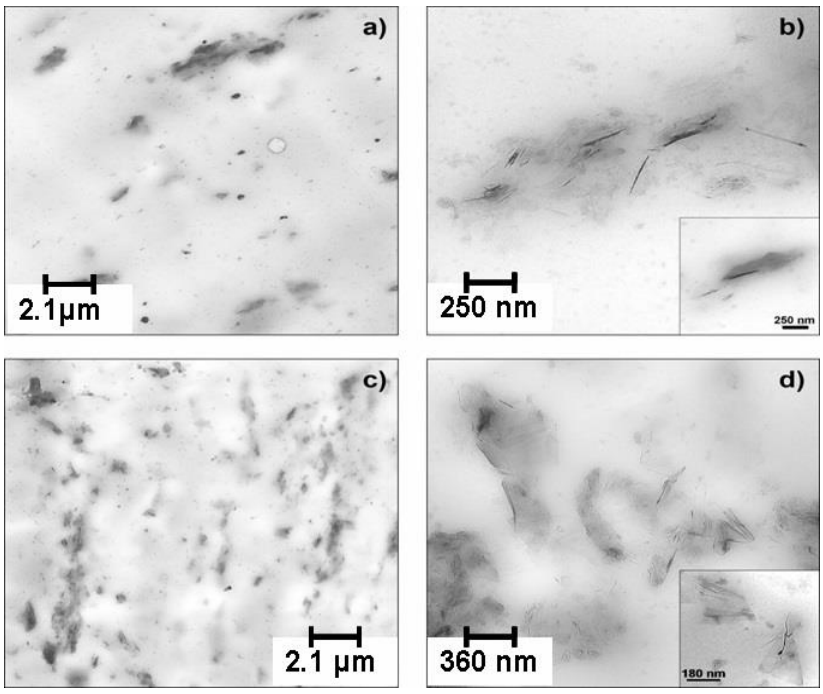

Figure 4.4: TEM micrographs at different magnifications of G-**2** (**a,b**) containing **2** phr of nanoG; and G-**12** (**c,d**) containing **12** phr of nanoG on crosslinked IR rubber compounds.

TEM analysis was performed to assess distribution and degree of dispersion of nanoG into the IR matrix. **figures 4.4a** and **4.4b** show TEM micrographs of IR rubber

compounds containing a low amount of nanoG, **2** phr. At low magnification (**figure 4.4a**), **G** appears to be evenly distributed, with a fairly fine dispersion. Most agglomerates have sub-micrometric dimensions, some are about **5** μm large and only few are about **10** μm large. At higher magnification (**figure 4.4b**) it is possible to observe a disordered placement of graphene layers inside the agglomerates and stacks of only a few graphene layers, as indicated by the stack thickness. It is thus possible to comment that nanocomposites were prepared from nanoG, being **100** nm the size threshold for having a nano-ingredient. [3] At this low content, nanoG particles do not form a long-range filler-networking in the IR matrix. **figures 4.4(c)** and **4.4(d)** show TEM micrographs of crosslinked composites containing a higher amount of nano**G**: **12** phr.

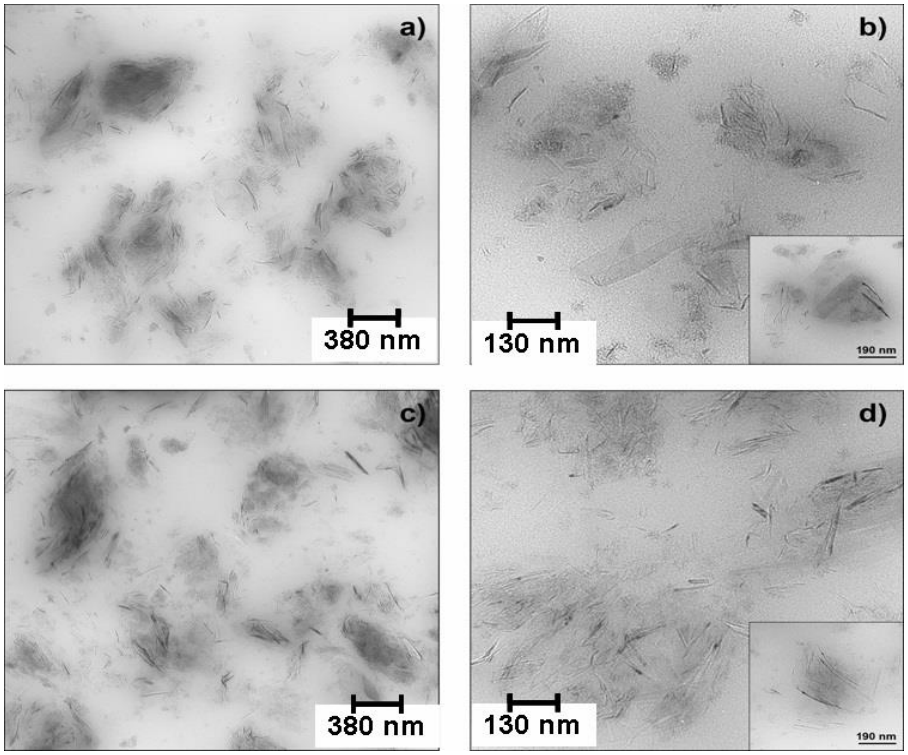

Figure 4.5: TEM micrographs of G-**20** (a,b); and G-**40** (c,d) crosslinked composites.

NanoG appears to be evenly distributed and highly delaminated (**figure 4.5c**, low magnification). Moreover, it appears to form a network, though not continuous, made by nanoG agglomerates, few of which are about **7** μm large, some are about 3 μm large and many are submicrometric sized. The agglomerates appear highly disordered. At higher magnification (**figure 4.5d** and insert), very few graphite layers appear located close to

graphene agglomerates and, in few cases, are dispersed in the IR matrix. **figure 4.5** shows TEM images of nanocomposites G-**20** and G-**40**, containing **20** phr (**figures 4.5a** and **4.5b**) and **40** phr (**figures 4.5c** and **4.5d**) of nano**G**, respectively. TEM images of both IR rubber compounds show, at low magnification, an even distribution of nanoG particles. A high level of delamination was observed: agglomerates are not larger than **10** μm and most of them are submicrometric sized and characterized by a disordered structure of the graphene layers. A very high amount of few and single graphite layers can be observed at higher magnifications, also in G-**40**, in spite of the high nanoG content. A continuous nanoG network within the IR matrix can be identified in micrographs of G-**20** and is evident in TEM images of G-**40**.

4.2.5. Wide-angle X-ray Diffraction (WAXD) studies of compounds

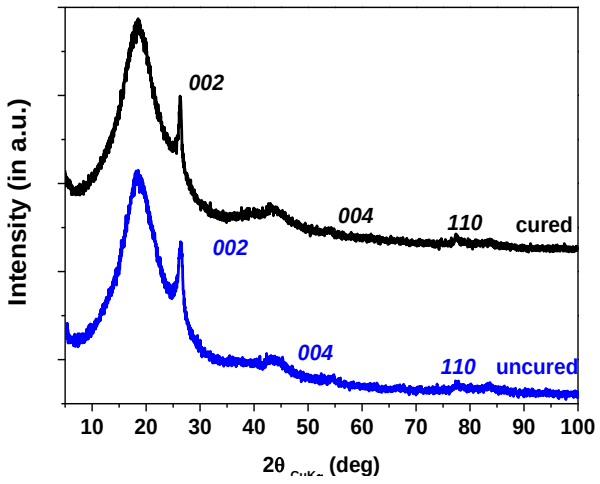

Figure 4.6: X-ray diffraction (CuK_α) pattern in the **2** range **0** - **100**° of nanoG containing **12** phr loading.

XRD analysis was performed on the IR rubber compounds containing nanoG, to investigate the crystalline order of stacked layers in the polymer matrix. **figure 4.6** shows the XRD patterns of the sample with **12** phr as nano**G** content as taken from the mixer, not crosslinked. Both patterns show a sharp peak at **26.2**° as 2□ value, corresponding to the **002** reflection of nanoG. The Williamson-Hall plot could not be applied to determine the $D_{hk\ell}$ correlation lengths, because of the low intensity (absence) of reflections other

than **002**. $D_{hk\ell}$ were thus determined by applying the Scherrer equation to the **002** reflection. $D_{hk\ell}$ values of about **11** nm for the uncrosslinked sample and of **22** nm for the crosslinked sample were calculated. Taking into account that the d_{002} interlayer distance in crystalline graphite is **0.339** nm, a number of about **32** and about **65** layers, stacked in an ordered manner, was estimated for the uncrosslinked and the crosslinked sample, respectively. Interestingly, the crosslinking step, that implies the application of a remarkable pressure (**150** bar) on the rubber nanocomposites, promotes a higher degree of order in the graphite aggregates: a higher number of sheets become regularly stacked in crystalline domains. It could be commented that the application of energy on a system makes the system moving towards a minimum of energy, such as the nanoG crystallite. Cured samples were also characterized through dynamic-mechanical measurements.

4.3. Compounds based on **styrene butadiene rubber** as **apolar** diene rubber

4.3.1. Rheometric curves

Rheometric curves for xg M**5** based SBR rubber compounds, at increasing filler loading (from **0** to **30** phr), are presented in **figure 4.7a**. It can be observed that the addition of nanofiller leads to the increase of torque and to the decrease of scorch time. The decrease in scorch time could be due to amino groups or by sulphur itself adsorbed on the filler`s surface, that accelerate the crosslinking reaction thereby favoring earlier network formation. Recently, similar behavior was reported for xg M**5**/IR nanocomposites [4, 5]. A comparative rheometric study of xg M**5**, nano**G** and N**234** filled rubber compounds were performed. Rheometric curves for composites with **2** phr as nanofiller content are presented in **figure 4.7b**, whereas the dependence of the t'_{05} (scorch) time on the amount of carbon filler is shown in **figure 4.7c**. Enhancement of torque at shortest times and more pronounced reduction of scorch time can be observed, in **figure 4.7b** and **4.7c** respectively, for the compounds based on nanoG and xg M**5** as the nanofillers. The effect of carbon fillers on torque and on the scorch time is appreciably different for the different nanofillers and appears to be more evident with the increase of the filler surface area. These findings are in line with what reported recently by Klueppel et al [2]**:** the incubation time decreased for CB and xg M**5**/NBR based compounds as the filler content increased and the incubation times for xg M**5** based composite was shorter than for the CB systems [2].

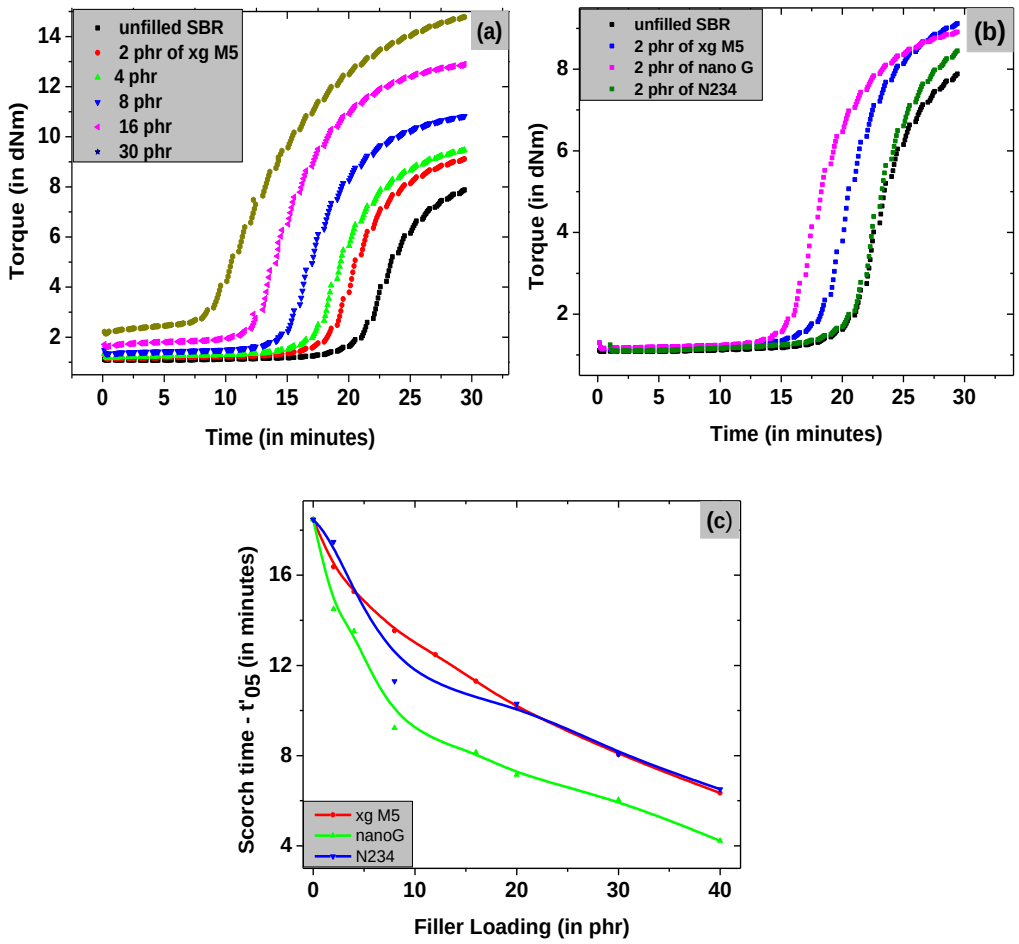

Figure 4.7: Rheometric curves for SBR based nanocomposites (**a**) containing xg M**5** concentration from 0 to 30 phr; (**b**) comparative for xg C**750**, xg M**5**, nanoG and N**234** filler grades at **2** phr loading; **(c)** The t'_{05} decreasing in SBR nanocomposites with different concentration of xg M**5**, xg C**750**, nanoG and N**234** filler grades.

4.3.2. Rheological Strain Sweep tests

The viscoelastic behavior of xGnPs, nano**G** and N**234** filled composites was investigated via strain sweep and frequency sweep measurements. The dependence of storage modulus-G' as a function of strain amplitude for xg C**750** filled nanocomposites, with nanofiller amount from **0** to **50** phr, is presented in **figure 4.8a**. It appears that the characteristic plateau of G' at low strain reaches lower strain amplitudes as the filler content increases. Particular enhancement of the G' plateau value is observed passing from **20** to **30** phr as xg C**750** content. Substantial reduction of G' value is observed only for relatively large strain amplitudes. This phenomenon is known as Payne effect that is

interpreted with two main models. The first model relates to the filler networking concept and assumes agglomeration - de-agglomeration process of the filler network above the filler percolation threshold [7, 8]. The second one refers to the filler–matrix interaction and assumes matrix-filler bonding and debonding mechanisms [9, 10].The storage modulus (G', in kPa) at lower strain (values taken at **0.56** % strain) of xg C**750**, xg M**5**, nanoG and N**234** filled composites is plotted in **figure 4.8b** as a function of filler loading. It can be noticed that higher G' values at low deformation were measured for xg C**750** filled rubber nanocomposites. The high surface area of such nanofiller is likely to favour the filler networking in the SBR matrix. A high polymer – filler interfacial area is known to provide better stress transfer from matrix to the filler. The dependence of storage modulus on the filler volume fraction was studied by adopting the Guth-Gold Smallwood model [10,11]. According to this model, the enhancement of the initial modulus for filled polymer melts and elastomers, as a consequence of the presence of spherical filler, is predicted by the following equation (**equation 4.1**): $G' = G'_o (1+0.67f\phi+ 1.62f^2\phi^2)$ - [**4.1**]

Deviations of experimental data, from the best fitting line according to **equation 4.1**, occurs when filler network is formed and filler particles jam either by direct contact or via layer of rubber shell around them. The experimental values of excess storage modulus - G' at lower strain (values taken at **0.56**% strain) and the curve (dotted line) derived from the theoretical values calculated using the Guth-Gold Smallwood equation, are reported in **figure 4.8c**. A good fitting was obtained for N**234** up to a value of Φ of about ~**0.117** (~**28** phr) and for xg C**750** up to a value of Φ of about ~**0.067** (~**15** phr). Deviations from the theoretical curves should be thus due to the filler percolation. Filler percolation threshold (FPT) was calculated adopting the Huber-Vilgis method. The double logarithmic plot of the storage modulus excess $((G'-G_o)/G_o)$ as a function of filler volume fraction is shown in **figure 4.8d** for xg C**750** and N**234** as well as for xg M5 and nanoG filled rubber composites. It appears that the lowest FPT is obtained for xg C750 (~**16.6** phr), followed by xg M5 (~**23.2** phr), nanoG (~**21.9** phr), and N234 (~**29.6** phr). From measurements in the torsion mode, dynamic viscosity (η'- in MPa-s) was measured as a function of filler loading for xg C**750**, xg M**5**, nanoG and N**234** filled uncured SBR composites. Dependence of dynamic viscosity on filler loading is presented in

figure 4.8e. xg C**750** filled nanocomposites shows higher η' values than xg M**5**, nano**G** and N**234** fillers at all filler loadings. N**234** based compounds reveal stronger enhancement of dynamic viscosity as the filler content increases, with respect to xg M**5** and nanoG based compounds. It is known that the viscosity of a rubber compound depends on the amount of occluded rubber that is expected to achieve larger values for nanostructured fillers.

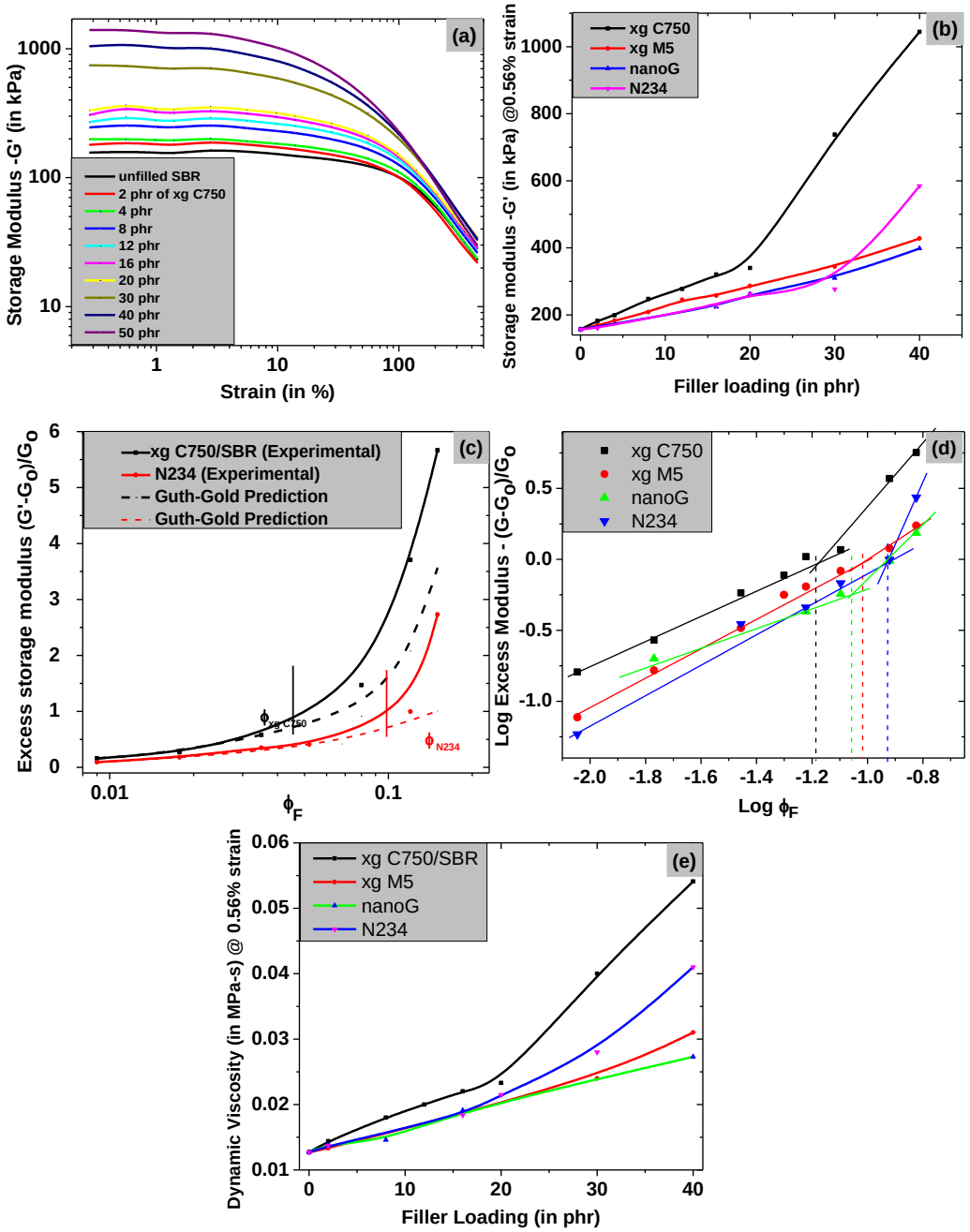

Figure 4.8: **(a)** Storage modulus -G', in kPa) as a function of different strains (increasing from **0.28**% to **300**%) for xg C**750** filler; **(b)** Comparative storage modulus (G', kPa) with different filler loading of xg C**750**, xg M**5**, nanoG and N**234**; **(c)** Dependence of excess storage modulus (G', kPa) in xg C**750**, N**234** filled SBR nanocomposites with increasing loading from **0** to **40** phr: experimental (dark dots) and Guth- Gold predicted (dotted line); **(d)** Double logarithmic plot of the excess modulus, with respect to neat rubber, as a function of the filler volume fraction / (Huber–Vilgis plot); **(e**) Comparative dynamic viscosity (η', MPa-s) with different filler loading of xg C750, xg M**5**, nano**G** and N**234** filler grades.

4.3.3. Frequency-sweep studies using RPA

Storage modulus and dynamic viscosity dependence on type and amount of fillers were studied with frequency sweep tests. Curves in **figure 4.9a** show the increase of storage G' modulus with increasing filler loading for xg C**750** filled compounds, over the whole frequency sweep range (from **0.1** to **30** Hz). It can be observed that all xg C**750** filled nanocomposites show an increase of G' at frequencies from **0.1** to **4** Hz and attain stability after **4** Hz. Storage G' modulus was then determined, with frequency sweep tests, for composites based on xg C**750**, xg M**5** and nanoG, at **20** phr nanofiller loading: curves are in **figure 4.9b.** xg C**750** shows slightly higher G' values, whereas xg M**5** and nano**G** based composites show very similar curves on the same levels.

The dynamic viscosity (η') of nanocomposites with xg C**750** as the nanofiller decreases with increasing frequency and increases with increasing filler loading from **2** to **50** phr loading, as revealed by the curves in **figure 4.9c**. At **20** phr loading (**figure 4.9d**), the comparative studies for xg C**750**, xg M**5** and nanoG filled SBR nanocomposites shows that xg C**750** and nano**G** filled compounds have comparable η' values, higher than those of xg M**5** filler grades.

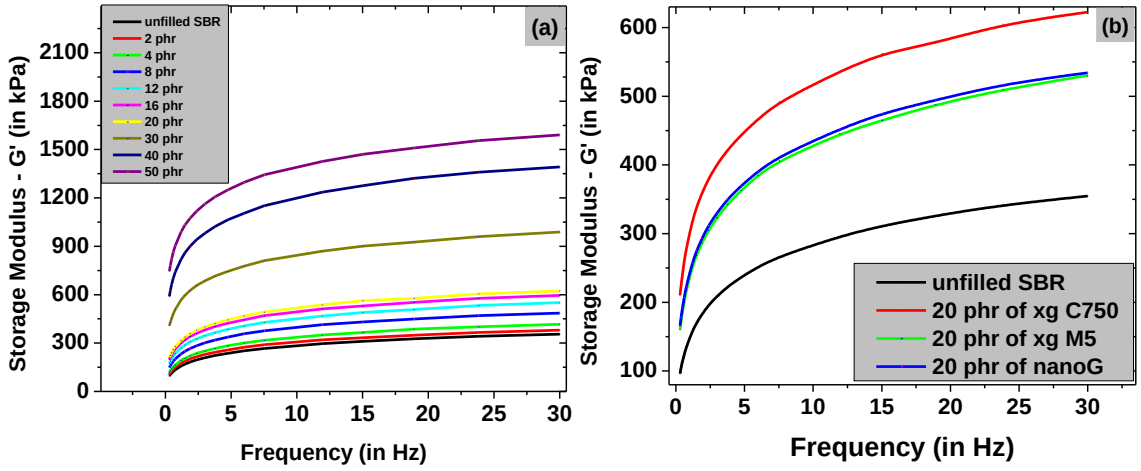

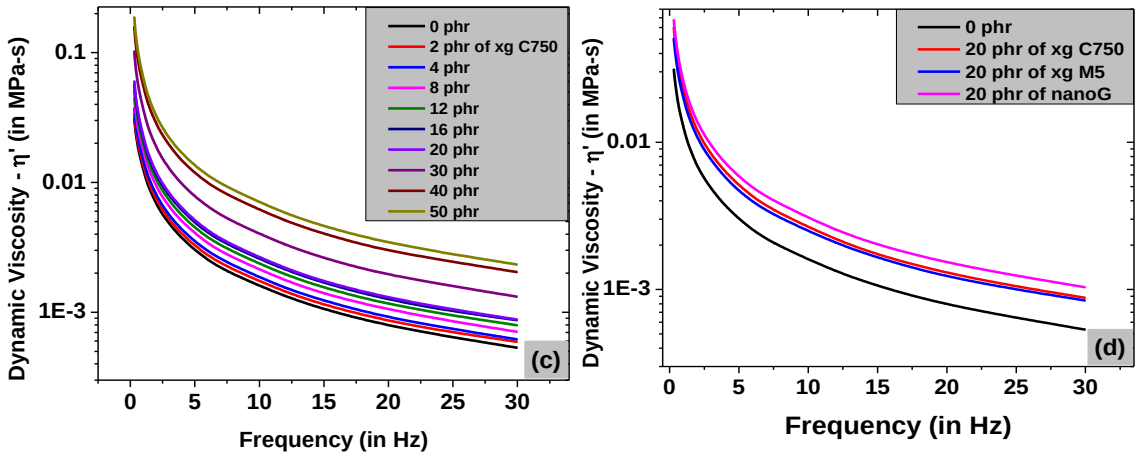

Figure 4.9: Storage modulus variation in different frequency **(a)** from increasing filler loading from **0** to **50** phr for xg C**750**; **(b)** at **20** phr for xg C**750**, xg M**5** and nanoG filled nanocompsoites; **(c)** Dynamic viscosity (η', MPa-s) plotted against frequency from **0.1** to **30** Hz from increasing filler content from **0** to **50** phr for xg C**750**; and **(d)** for xg C**750**, xg M**5** and nano**G** filled nanocompsoites at **20** phr.

4.3.4. Stress-strain behavior for Tensile strength

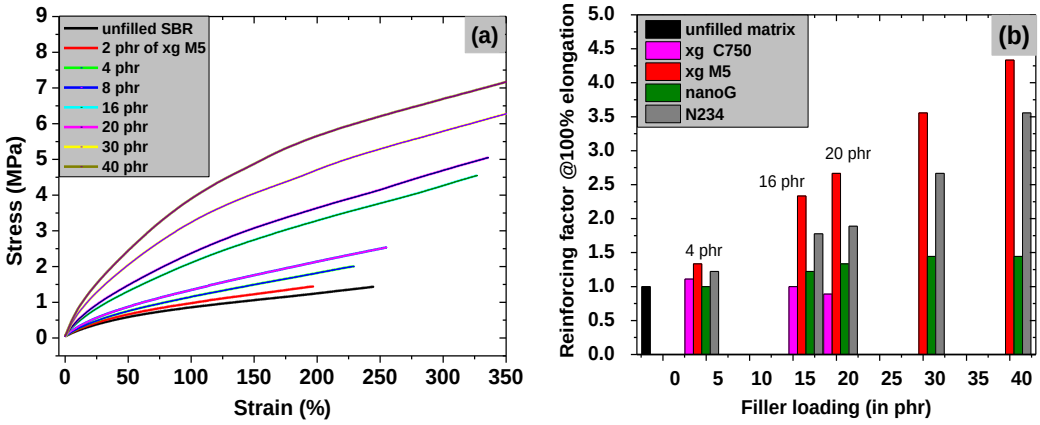

Figure 4.10: Stress-Strain behaviour of xg M**5** **(a)** content increasing from **0** to **40** phr; **(b)** Reinforcing factor at different filler loading of xg M**5**, xg C**750**, nano**G** and N**234** filled SBR compounds.

Stress-strain curves for xg M**5** filled SBR compounds are in **figure 4.10a.** Stresses at all the elongations remarkably increase with the filler content in the SBR matrix. The xg M**5** based compounds shows appreciably higher modulus at low strain with respect to

the xg C**750** and nano**G** based ones. Dominating character of fillers at low strain, beside the volume fraction, is the aspect ratio. However, for high aspect ratio filler, one must also consider the influence of processing that might orient the filler particles, as in the case of fillers with platelet morphology, such as xg C**750**, xg M**5** and nano**G**. The same behavior of xg C**750**, xg M**5** and CB systems are reported in NBR matrix recently [2]. The reinforcing effect of the carbon fillers was studied by calculating, for compounds with different filler content, the so called reinforcing factor, that means the ratio between the stress at **100**% strain between filled and unfilled composites $(\boldsymbol{\sigma_f/\sigma_0})_{100\%}$. Reinforcing factor is shown in the bar chart of **figure 4.10b**. xg M**5** shows better reinforcing ability than xg C**750**, nano**G** and N**234**, for the explored filler contents.The filled rubber nanocomposites undergo phenomena such as energy dissipation and losses beyond elastic limit during loading and unloading cycles.

The multi-hysteresis is a well-accepted technique to describe such phenomena and was carried out for N**234** and xg C**750** filled SBR compounds in present work. In **figure 4.11a**, are shown multi-hysteresis stress strain curves. For N**234** filled compounds, with increasing filler loading (from **0** to **30** phr) in SBR matrix, the hysteresis loop broadens, revealing increase in energy dissipation and increase in stress values as it is shown in **figure 4.11a**. Loading-unloading cycles are shown in **figure 4.11b** for xg C**750** filled (loading from unfilled to **20** phr) SBR nanocomposites. Lower filled composites show lower stresses at low strains and lower energy dissipation than with higher xg C**750** filled composites. It can also be noted that the first cycle exhibits higher energy dissipation than the third cycle. Higher hysteresis in the first cycle could be due to the break down, during loading cyclic strain, of more pronounced filler network, that is not completely re-established during successive cycles. Larger amount of filler leads to a larger number of filler-filler interactions. The stress-strain hysteresis may be significantly related by the filler networking because of reduction of an effective volume of the rubber and by the surface energy distribution on the filler surface (active regions). Another reason for high energy dissipation would be the release of bound rubber after breaking of filler networks when cyclic sweeps are extended to higher strains. Under stress, the filler clusters can break and become softer, leading to a decreasing strain amplification factor.

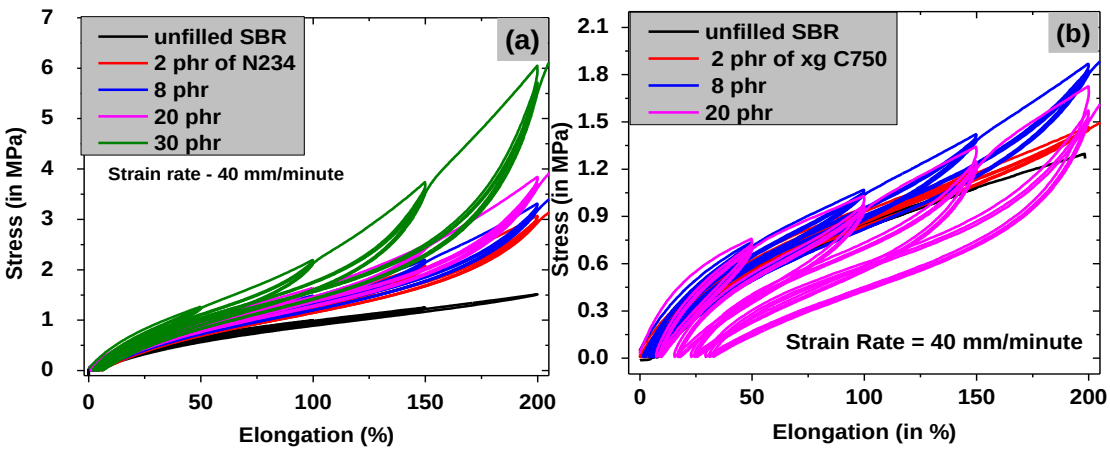

Figure 4.11: **(a)** Multi-Hysteresis Stress-Strain of xg C**750** filled SBR nanocomposites; (**b**) Multi-Hysteresis Stress-Strain of xg C**750** filled SBR nanocomposites.

4.3.5. Dielectric AC Conductivity Properties

The dielectric AC conductivity and permittivity properties were measured within frequency range from 10^{-2} to 10^{6} Hz (**figure 4.12a and 4.12b**). The conductivity was studied for filler concentration of **2** phr, **16** phr, **20** phr and **30** phr in SBR matrix for xg C**750**, and nanoG. The nanoG data is not presented since it showed very poor dielectric AC conductivity (**10^{-13}** at **40** phr). The conductivity of xg C**750** filled nanocomposites increases with increasing filler concentration into SBR matrix. At lower loadings, the dielectric conductivity shows a plateau value at small frequencies, whereas the conductivity does not appreciably change over the whole range of frequencies. The enhancement of electrical conductivity in polymer nanocomposites is strongly dependent upon the filler morphology; the formation of percolating pathways between filler particles is necessary to render an insulating polymer such as rubber [12]. Conductivity of greater than 10^{-9} (Siemens/cm) was observed at 30 phr filler loading of xg C**750**.

To obtain electrical percolation threshold (**EPT**), dielectric conductivity was taken at very low frequency (**0.1** Hz) and plotted against filler volume fraction (**figure 4.12c**). An exponential increase in dielectric conductivity was seen at all frequencies for filler loading ~**18.9** phr. This could be due to either due to the attainment of filler percolation threshold or the establishment "web-like" structure of xGnPs platelets in SBR

matrix. It was reported that reduced graphene oxide in natural rubber (RG-O/NR) nanocomposites showed maximum enhancement in conductivity not when the filler was homogeneously dispersed, but rather arranged into a connected ‘‘*web-like*’’ structure of platelets [13].

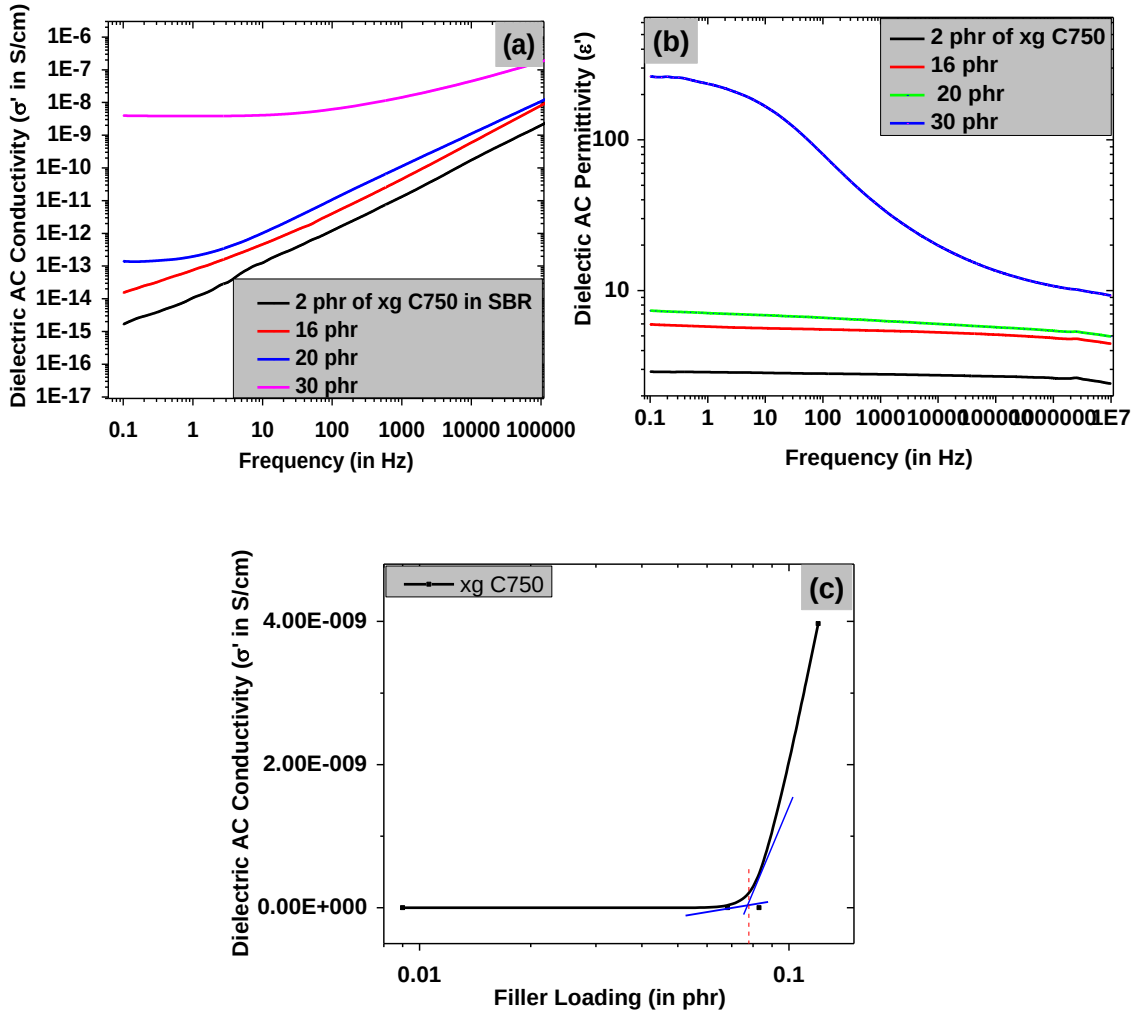

Figure 4.12: (**a**) Dielectric AC conductivity; (**b**) Dielectric AC Permittivity as a function of frequency of xg C**750** filled SBR nanocomposites; (**c**) Filler Percolation Threshold: Dielectric AC conductivity as a function of xg C**750** filled SBR nanocomposites.

4.4. Compounds based on **synthetic isoprene rubber** with **high** surface area few layer graphene

4.4.1. Rheometric curves

figure 4.13(a) shows the rheometric curves for compounds with different xg M**5** nanofiller loadings. It is evident that the increase of nanofiller content brings about the

reduction of scorch time (t'_{05}) and the increase of the maximum torque. **figure 4.13**(b) shows the reduction of scorch time as a function of increasing filler loading.

The scorch time values decrease moving from CB-N**234** to xg M**5** to xg C**750**. It seems that they are not related with the filler surface area. However, it could also be hypothesized that the surface are detected for xg M**5**, the nanofiller with larger number of stacked layers, is completely accessible to the nitrogen molecules used for the determination, but only partially interacts with the polymer chains. This assumption for nanofillers was recently reported [14], to justify the different correlation of initial modulus values with surface area for CB, CNT and nano-graphite.

Activating effects due to the interaction of fillers with activating (ZnO) or accelerating (CBS) ingredients could also play a role in such effects. The reversion of crosslinking reaction for all fillers was observed to be below **4-5**%.

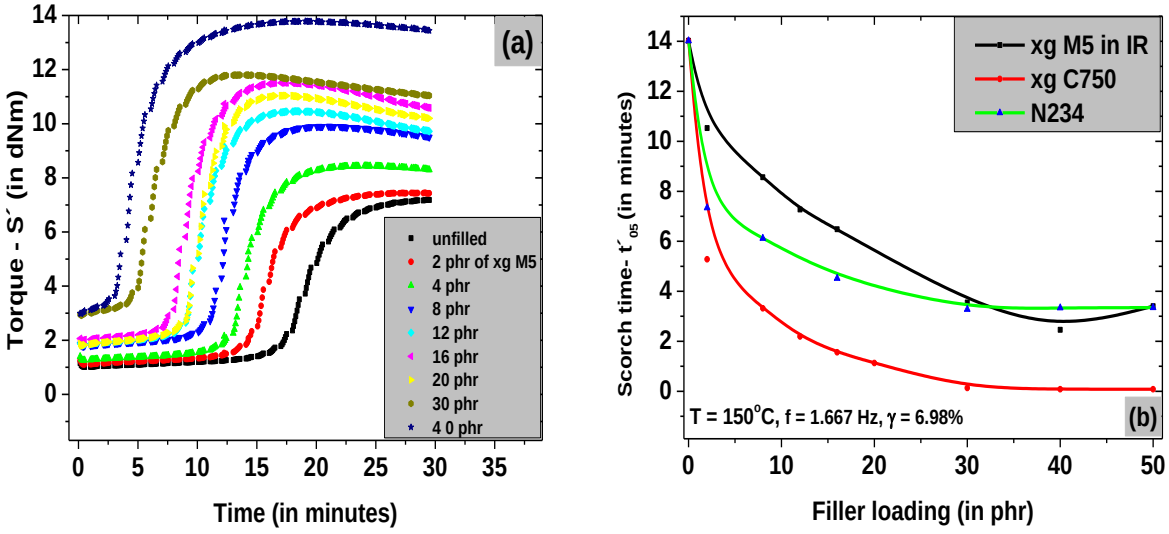

Figure 4.13: **(a)** Rheometric curves for IR based nanocomposites containing xg M**5** concentration from unfilled to **40** phr; **(b)** The t'_{05} decreasing behavior in IR nanocomposites containing xg M**5**, xg C**750** and N**234** filler grades.

4.4.2. Rheological Properties through RPA studies (strain sweep)

The dependence of storage modulus (G´, in kPa) on strain amplitudes is presented in **figure 4.14(a)** for uncured xg C**750** filled nanocomposites. The non linear behaviour, observed in the **figure 4.14(a)** is known as "*Payne effect*" and indicates the occurring of

the filler networking phenomenon. The filler network is formed by filler particles interactions either by direct contact or via interaction with polymer chains around them. G' values at low strain increase with increasing filler content, from **2** to **50** phr. A long plateau for the G' values were evidenced up to about **10**% strain. The increase of strain amplitude beyond this value leads to a decrease of G', with a sharp fall beyond **100**% strain. This severe decrease could be attributed due to disentangling of rubber macromolecular chains, rupture of secondary interactions or reorientation of filler anisotropy or polymer chains against direction of applied strain.

Experimental Storage modulus-G' as well as dynamic viscosity (η′) and theoretical points were elaborated according to the Guth-Gold Smallwood equations. [10,11] In short, actual changes in η′ and G′ by addition of filler can be directly related with filler concentration, by using Guth-Gold Smallwood equation up to a filler concentration at which filler network is established.

Excess modulus $(G'-G_o)/G_o$ at **0.56**% strain for xg M**5** and N**234** based composites is shown in **figure 4.14(b)** as a function of filler loading. Storage modulus (G') and Dynamic viscosity (η′) at **0.56**% strain for xg C**750** based composites are shown in **figure 4.14(c).** In both curves it is evident the deviation of experimental points with respect to theoretical curves at about **0.0743** as volume fraction (ϕ), that means at about **15** phr.

FPT is defined as a concentration in the rubber matrix after which long range filler-filler networs are established and measurements values deviated largely from normal pattern of the property under investigation. Here, we calculated FPT by plotting dynamic viscosity and storage modulus as a function of filler volume fraction, in **figure 4.14(d)** and **4.14(e)** respectively. It was found that the experimental values improve largely after filler percolation threshold. A lower percolation threshold was observed for xg C**750** filled nanocomposites than for xg M**5** and N**234** filled nanocomposites. The larger ability of xg C**750** to give rise to filler networking is in line with the higher surface area and surface activity of this nanofiller.

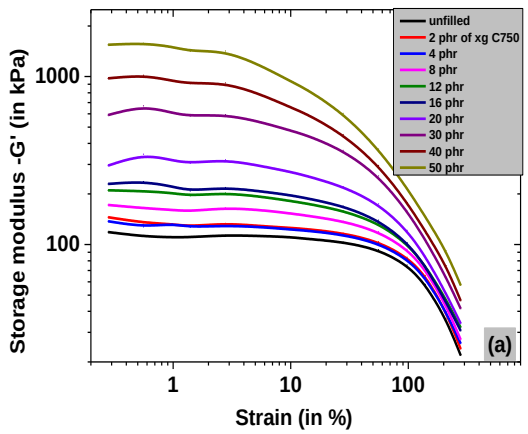
unfilled
2 phr of xg C750
4 phr
8 phr
12 phr
16 phr
20 phr
30 phr
40 phr
50 phr
Storage modulus -G' (in kPa)
1000
100
1
10
100
Strain (in %)
(a)

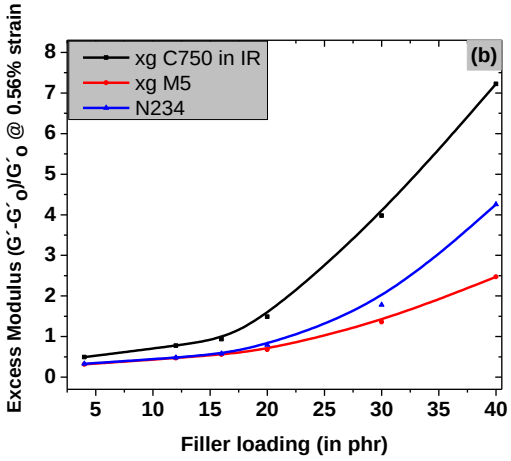
xg C750 in IR
xg M5
N234
(b)
Excess Modulus (G´-G´o)/G´o @ 0.56% strain
0
1
2
3
4
5
6
7
8
5
10
15
20
25
30
35
40
Filler loading (in phr)

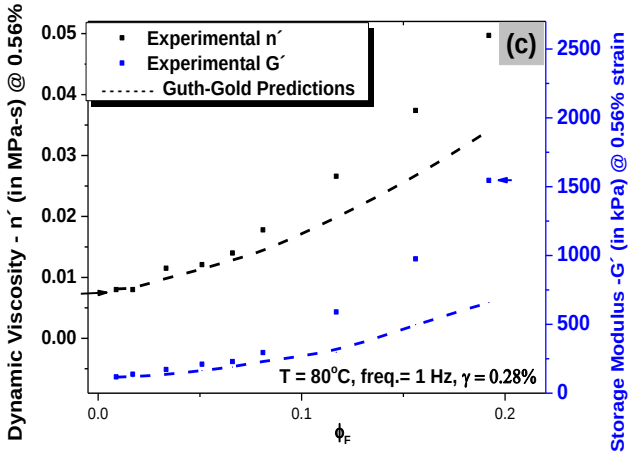
Experimental n´
Experimental G´
Guth-Gold Predictions
(c)
Dynamic Viscosity - n´ (in MPa-s) @ 0.56%
0.00
0.01
0.02
0.03
0.04
0.05
0.0
0.1
0.2
ϕF
T = 80°C, freq.= 1 Hz, γ = 0.28%
Storage Modulus -G´ (in kPa) @ 0.56% strain
0
500
1000
1500
2000
2500

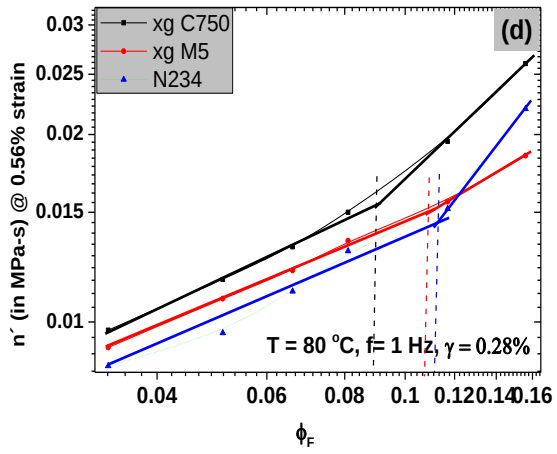
xg C750
xg M5
N234
(d)
n´ (in MPa-s) @ 0.56% strain
0.01
0.015
0.02
0.025
0.03
0.04
0.06
0.08
0.1
0.12
0.14
0.16
ϕF
T = 80 °C, f= 1 Hz, γ = 0.28%

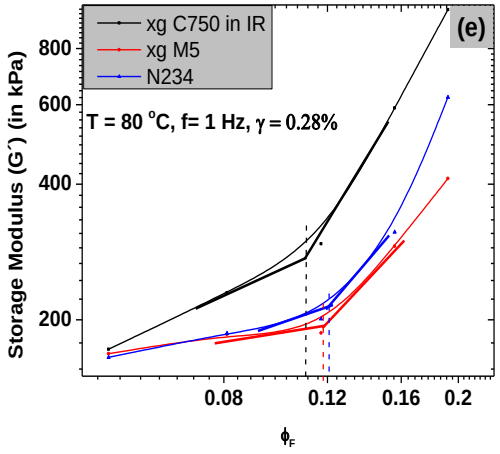
xg C750 in IR
xg M5
N234
(e)
Storage Modulus (G´) (in kPa)
200
400
600
800
0.08
0.12
0.16
0.2
ϕF
T = 80 °C, f= 1 Hz, γ = 0.28%

Figure 4.14: (a) Storage modulus (G´) as a function of different strains (increasing from 0.28 % to 300 %) for xg C750 filled uncured IR nanocomposites; **(b)** G´ with different filler loadings of xg C**750**, xg M**5** and N**234**; **(c)** Dynamic viscosity (η') and storage modulus (G´) in xg C750 filled IR nanocomposites with increasing concentration from 0 to 50 phr: experimental (dark) and Guth-Gold predicted (dotted lines); **(d)** Filler percolation threshold: Dynamic viscosity; **(e)** Storage modulus **(**G') both as function of filler volume fraction for xg C**750**, xg M**5** and N**234** filled uncured nanocomposites.

4.4.3. Rheological frequency sweep tests

Many static or dynamic experimental techniques are available to study viscoelasticity of rubber. At low frequency, the storage modulus (G') (**figure 4.15(a)**) and dynamic viscosity (η') (**figure 4.15(b)**) respectively shows a non-linear behavior as a function of frequency. G' and η' for all filled IR compounds increase with increasing filler loading.

The transient filler network does not break during frequency sweep tests as they are carried out at **0.1**^{o} strain which was too weak to break filler interactions. The compounds beyond filler percolation threshold show lower elastic responses and at low frequencies, there is sufficient time for polymer chains to relax fully.

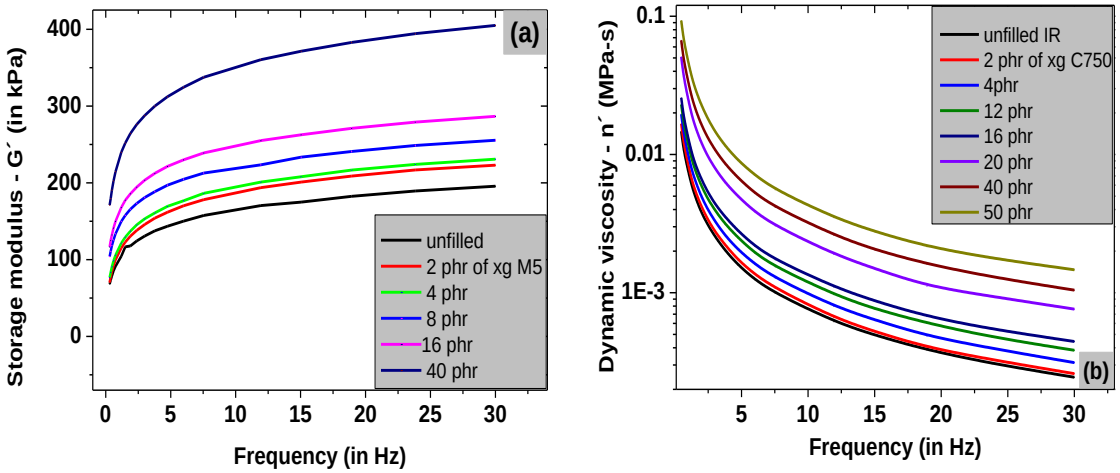

Figure 4.15: **(a)** Storage modulus (G`) variation in different ranges of frequency for xg M**5** filled nanocomposites; **(b)** Dynamic viscosity (η') plotted as a function of increasing frequency from **0.1** to **30** Hz for xg C**750** filled IR nanocomposites.

4.4.4. Stress-strain behavior for Tensile strength

The tensile strength as a function of filler loading was plotted in **figure 4.15(a).** The increased stress values at higher strain amplitudes reflect the transfer of deformed strain in the form of heat dissipated from polymer chains to interface of enclosed xGnPs aggregates. Above **16** phr, a stronger increase in stress was observed along with a decrease in the elongation at break. For high *cis*-polyisoprene, it is known to exhibit strain induced crystallization (SIC) above a certain strain value which makes a significant contribution to reinforcement at higher deformations. This effect is much lower than in the case of natural rubber because of the slightly reduced *cis*-1,4-content.

However, especially for high aspect ratio fillers, the influence of processing, orientation of filler etc. on reinforcement should also be considered. It is also very interesting to study effect on reinforcing factor as a function of filler loading (**figure 4.15(b)**). With regard to the unfilled state which displays very poor tensile strength, significant improvement in reinforcement properties was observed when nanofillers were incorporated. The tensile tests show that with an increase in the concentration of graphene into IR-based nanocomposites, there is a significant increase in reinforcement at **100**% strain and decrease in elongation at break as shown in **figure 4.15(b) and 4.15(c)**. The reinforcement by xGnPs which was compared with N**234** as traditional filler clearly shows the differences both at low and high filler loading.

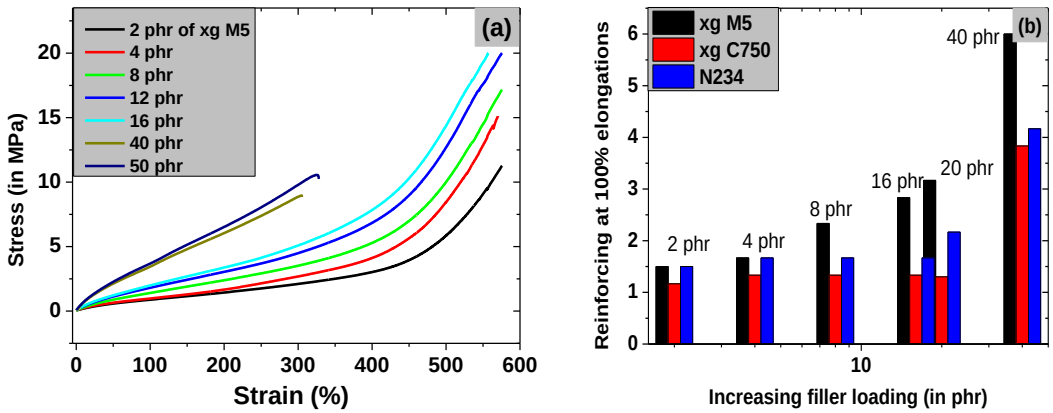

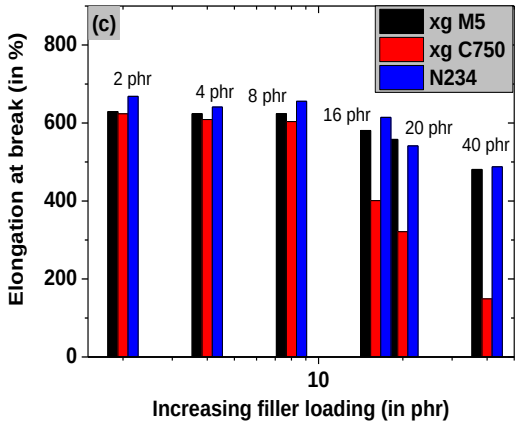

Figure 4.15: **(a)** Stress-Strain curves obtained from xg M5/IR nanocomposites with varying strain; **(b)** Reinforcing factor factor for xg M5, xg C**750** and N**234** filled IR nanocomposites with increasing filler loading from **2** to **40** phr; **(c)** Elongation at break (%) dependence against different filler concentration for xg M**5**, xg C**750** and N**234** filled IR nanocomposites.

4.4.5. Dielectric AC Conductivity Properties

The dielectric AC conductivity and electrical permittivity for xg M**5** filled rubber nanocomposites were plotted against frequency (**figure 4.16a and 4.16b**). The electrical conductivity and permittivity of xg M**5** were found very low at **2** phr as filler content and increased with the filler loading. At lower loadings, the conductivity plateau remained almost similar in a small frequency range and conductivity was not affected significantly. An exponential increase in dielectric conductivity and permittivity was seen at all frequency for filler loading above **20** phr which is due to attainment of filler percolation threshold.

To investigate electrical filler percolation threshold (**EPT**) of carbon nanofillers, conductivity S' (S/cm) was measured at low frequency (~**0.1** Hz) and plotted as a function of nanofiller loadings (**figure 4.16c**). However, a careful inspection of the curves reveals that xg C**750** filled nanocomposites exhibit percolation threshold at lower filler loadings than xg M**5** based ones. This is in line with the larger surface area of xg M**5**. Electrical conductivity equal to $\mathbf{10^{-9}}$ (S/cm) is considered sufficient for many applications such as the one for tire compounds. The xg C**750** filled nanocomposites

showed dielectric conductivity of ~**2x10**$^{-8}$ at **30** phr filler loading and can be thus considered suitable filler for antistatic tyre compounds.

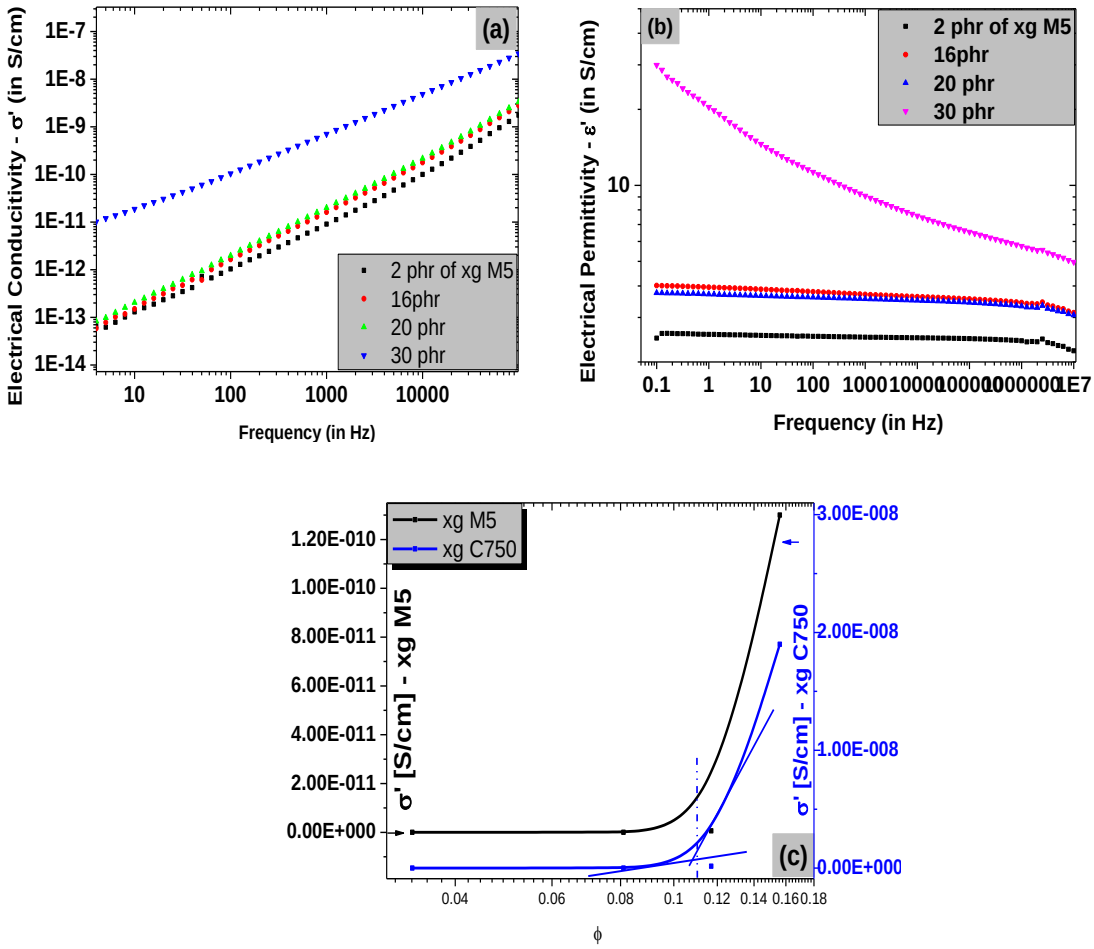

Figure 4.16: Scheme of dielectric measurements: (**a**) di-electric AC conductivity; (**b**) dielectric AC permittivity for xg M**5**/IR nanocomposites respectively at different frequency range; (**c**) The electric filler percolation threshold behavior for conductivity at **0.1** Hz with varying filler concentration of xg M**5**/IR cured nanocomposites.

4.5. Compounds based on **synthetic isoprene rubber** with **high** shape anisotropy and **high** surface area few layer graphene

4.5.1. Rheometric curves

Characterizations were performed on samples crosslinked with a typical sulphur based system. Rheometric curves are shown in **figure 4.17**. The reversion of the

crosslinking reaction was lower than **5**% and the values of both M_L and M_H increased with the nanoG content. As it can be seen in **figure 4.17**, the crosslinking reaction became faster as the nanoG content increased: t_{s1} and t_{90} values decreased from **13** to **4** min and from **19** to **10** min, respectively, passing from the neat IR matrix to the nanocomposite with **60** phr of nanoG. In the literature, the crosslinking reaction of NR was reported to be accelerated by a so called functionalized graphite, obtained by thermal reduction of GO and containing about **9**% of oxygen atoms.[15] The enhanced thermal conductivity of the nanocomposite was commented to be responsible for the faster curing reaction. Conversely, it is also reported in the literature that, with CNT as the carbon nanofiller, the curing reaction rate was lower than that of pure natural rubber (NR) [16, 17] and the scorch time was longer.

The adsorption of curatives on CNT was hypothesized to cause higher curing activation energy and lower reactivity. [16, 17] Analogously, in SBR as the polymer matrix, the curing time of the composites filled with CNTs was found to be longer than that of samples with CB.[18] The decrease of vulcanization time, scorch and optimum cure time and the increase of the maximum torque was also found [19] by adding acid treated and ball milled CNT to NR. The effect of carbon nanofillers on vulcanization behaviour seems to deserve further investigations. However, crosslinking data reported in this chapter allows concluding that polymer chains were properly crosslinked.

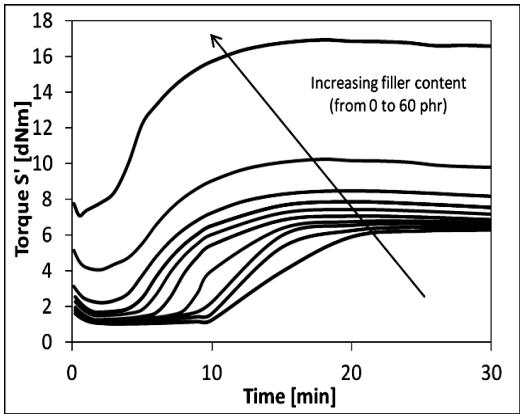

Figure 4.17: Rheometric curves for IR based composites with nano-G content from unfilled to **60** phr.

4.5.2. Rheological Properties through RPA studies

Strain sweep tests were carried out at **50**°C in the torsion mode, by applying a sinusoidal stress with a frequency of **1** Hz and strain amplitude increasing from **0.1** to **25**%. Dynamic shear storage *G'* and loss *G''* moduli were determined as a function of the strain amplitude. The filler networking phenomenon was investigated by determining the dependence of *G'* modulus at minimum deformation $G'_{(\gamma_{min})}$ on the filler content and the dependence of *G'* and *G''* moduli on nanoG content. **figures 4.18a** and **4.18b** show the dependence on the strain amplitude of the storage *G'* and loss *G''* moduli, respectively. It is known that viscoelastic moduli of polymer melts and elastomers depend on the strain amplitude, besides on frequency and temperature, in the presence of a filler network. This non linear behaviour is known as "*Payne Effect*" [20] and implies a reduction of *G'* as the strain increases and a variation of *G"*, that usually passes through a maximum. This phenomenon is due to the disruption of a secondary network formed when filler particles join together either by direct contact or *via* layer of polymer shell around them.

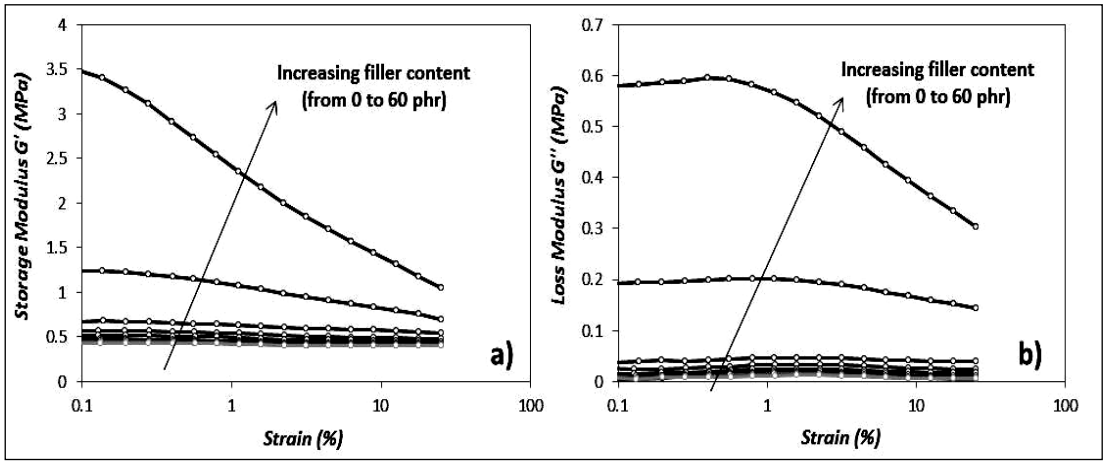

Figure 4.18: Behaviours of *G'* (**a**) and *G''* (**b**) as a function of strain for composites containing different amounts of nanoG.

4.5.3. Stress-strain behavior for tensile strength

Nominal stress – nominal strain curves are shown in **figure 4.19**. As it can be seen, the presence of nanoG leads to worsen ultimate properties of the nanocomposites, in spite of the good dispersion, the high surface area, the relatively high aspect ratio and the high

shape anisotropy of the nanofiller. However, other factors can affect the ultimate properties of filled and crosslinked elastiomeric composites, as for example the filler-matrix adhesion, the crosslink density and the strain crystallization behavior. The effect of nanoG on these factors is still unknown. The partial re-aggregation of graphite sheets, shown by XRD analysis, could somehow favour the deterioration of ultimate properties. However, it is noteworthy that nanocomposites based on nanoG still show remarkable elongation at break, higher than **700** % and **410** %, even for nanoG content of **40** and **60** phr, respectively

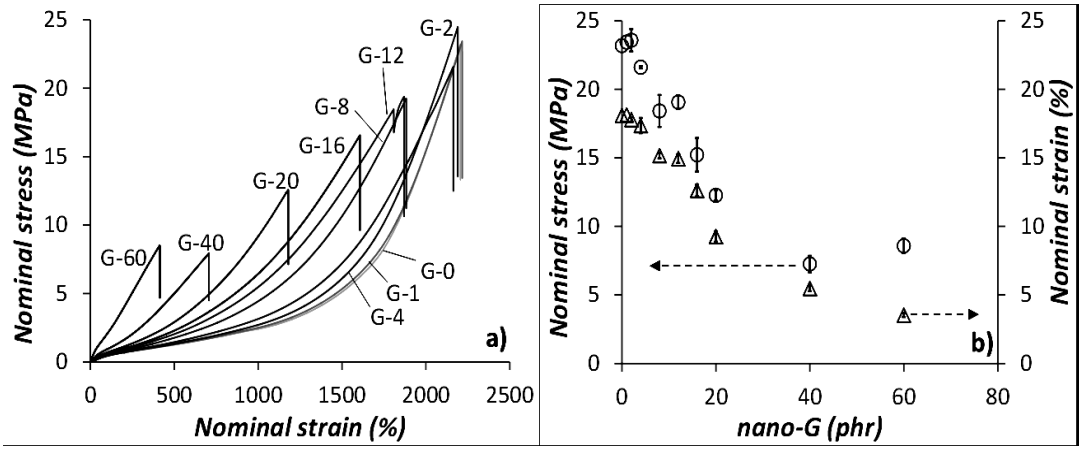

Figure 4.19: **a**) Nominal stress–nominal strain curves obtained for crosslinked IR/nano-G composites; **b**) nominal stress at break (open circles) and nominal strain at break (open triangles), with standard deviations, vs phr of nanoG

4.6. Compounds based on **synthetic isoprene rubber** with **hybrid** filler system

4.6.1. Rheometric curves

The rheometric curves for hybrid filler system at increasing filler concentration of xg C**750** (from **0** to **15** phr) are presented in **figure 4.20a** and **4.20b**. It was observed that an increasing concentration of filler results in decreasing scorch time and an increase in torque. Similar behavior of decreasing scorch time and increasing torque is reported and described in the literature both for xg C**750** based fillers or other hybrid systems (nanoG+CB) etc in IR or SBR or NBR rubber compounds [2, 5, 21, 22].

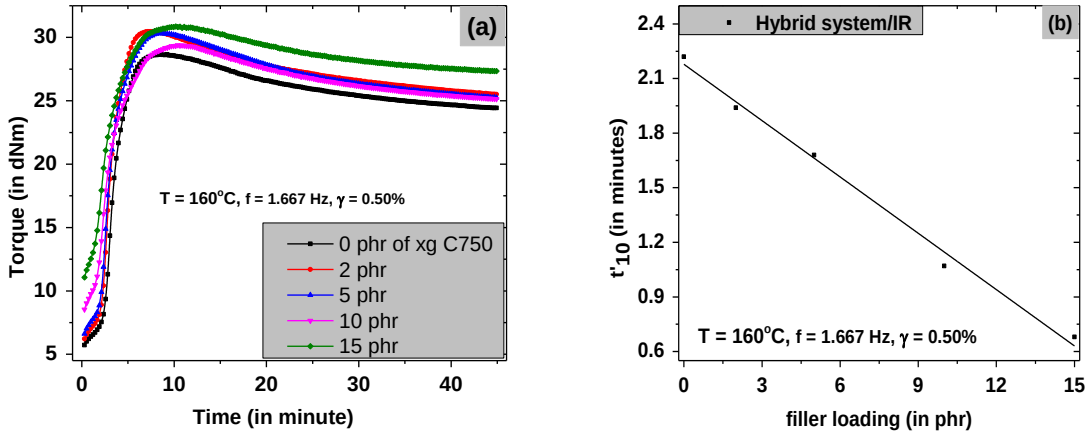

Figure 4.20: **(a)** Rheometric curves for Hybrid/IR system based nanocomposites containing xg C750 concentration from **0** to **15** phr; (**b)** The t'_{10} decreasing behaviour in Hybrid/IR nanocomposites containing different filler concentration of xg C750.

4.6.2. Rheological Properties through RPA studies

Strain sweep tests were employed to investigate the dynamic-mechanical behaviour of the compounds containing hybrid filler system. It is known that viscoelastic moduli of polymer melts and elastomers depend on the strain amplitude, besides on frequency and temperature, in the presence of a filler network. This non linear behaviour implies a reduction of G' as the strain increases. The filler networking phenomenon was investigated by determining the dependence of G' modulus at minimum deformation G'(γ_{min}) on the filler content and the dependence of G' modulus on xg C**750** content in hybrid system as presented in **figure 4.21a**. It was observed that the characteristic plateau of storage modulus (G') increases at lower strain amplification with increasing filler concentration and decreases with increasing strain.

Similar behavior is reported and described in the literature both for xg C**750** based fillers or other hybrid systems (nanoG+CB) etc in IR or SBR or NBR rubber compounds [2, 5, 21, 22]. The storage modulus (G', in kPa) of Hybrid/IR filled rubber compounds as a function of filler loading are comparatively presented in **figure 4.21b**. It can be noticed that G' values for xg C**750** filled rubber nanocomposites were found higher than other fillers investigated. It could be due to high surface area which favors improved filler

networking in IR matrix. The addition of xg C**750** brings about a shift in G' values to higher values at lower strain values (~**0.56**%). The pronounced enhancement of G' (in particular after **3** phr of xg C**750**) and the findings reported in **figure 4.21c** suggest investigating if xg C**750** is able to develop a synergism with CB+CNT. Recently, it was reported in literature that in composites based on CB/CNT [14], CB/nanoG [21] and CB/OC, CB/Nanoclay, [22] hybrid filler systems, nanofillers (OC, NC, nanoG, CNT) were found to develop a synergism with CB.

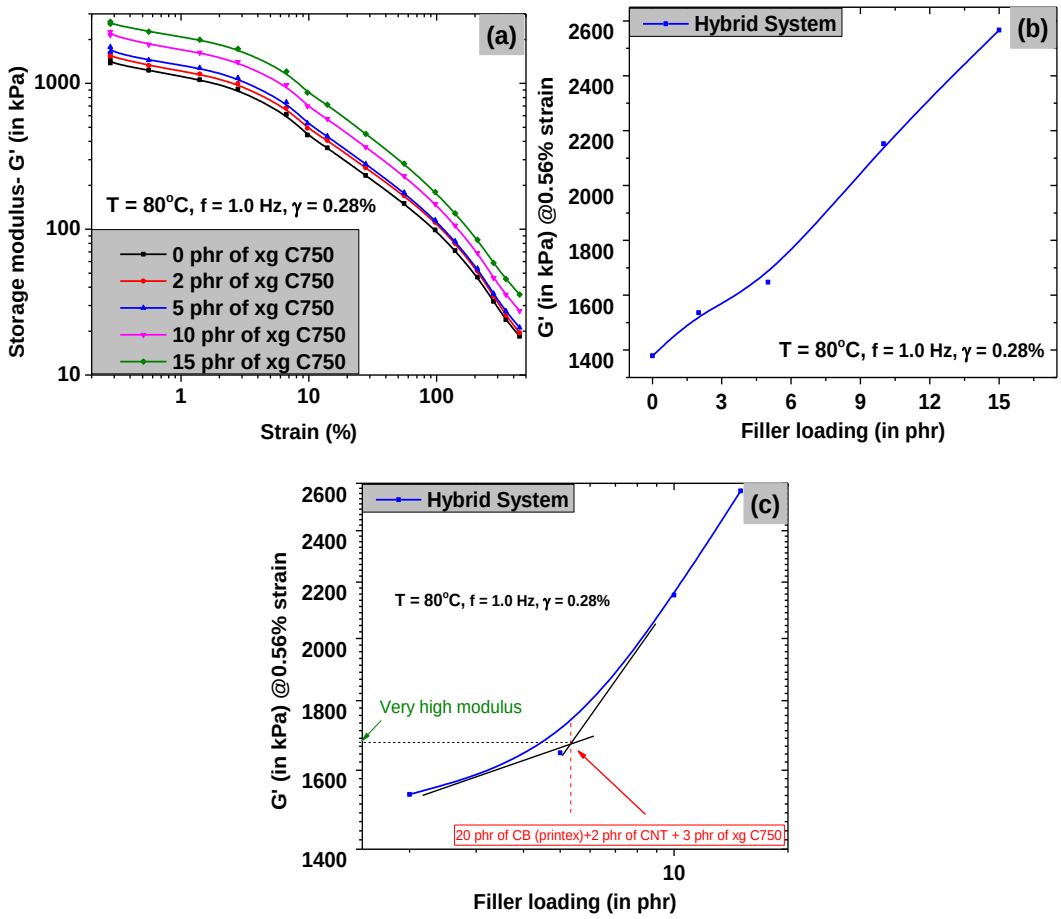

Figure 4.21: **(a)** Storage modulus (G', kPa) as a function of different strains (increasing from 0.28% to 300%) for Hybrid/IR nanocomposites; (**b)** Comparative description of storage modulus with different filler loadings of xg C**750** for Hybrid/IR nanocomposites; **(c)** Synergestic effect demonstrated from storage modulus as a function of filler loading for xg C**750** in Hybrid/IR nanocomposites.

4.6.3. Stress-strain behavior for Tensile strength

The stress-strain curves for Hybrid/IR system shows marked improvement in modulus with increasing xg C**750** concentration in rubber matrix (**figure 4.22a**). It was found that nanocomposites containing xg C**750** are able to attain remarkable elongations at break. These results are in line with similar results stress-strain published recently on CB/CNT [14], CB/nanoG [21] and CB/OC, CB/Nanoclay, [22] hybrid filler systems.

Recently, it was reported in literature that by incorporating **10** phr of nanoclay to the control SBR containing **20** phr CB shows **153**% increase in tensile strength, **157**% increase in elongation at break and **144**% stress improvement at **100**% strain, which showed synergistic effect between the fillers. [14] Similar synergistic effects in our hybrid system was noticed in which we observed increased in tensile strength, increase in stress and increase of elongation at break upto **10** phr of xg C**750** after which it decrease. These findings agree with those published in literature. We concluded that hybrid system improves properties of composites. [24]For a given polymer and cure system, the impact of the filler network, both in its strength and architecture, on the dynamic modulus and hysteresis during dynamic strain was reported in the literature [25]. The filler induced stress softening and hysteresis of highly strained elastomers are referred to the hydrodynamic reinforcement of rubber elasticity.

The multi-hysteresis stress-strain was carried out for Hybrid/IR system. In **figure 4.22b**, we have presented multi-hysteresis for hybrid system containing **0** and **2** phr of xg C**750** filler grade in IR matrix master batch containing **20** phr of CB-Printex xe2+2 phr of CNT. During multi-hysteresis cyclic strain, it can be hypothesized that a stable filler network can reduce the hysteresis of the filled rubber, the breakdown and reformation of the filler network could cause an additional energy dissipation (as can be seen especially for **1**st cycle) that resulting in higher hysteresis.

It could be due to strain amplification by stiffer filler clusters and cyclic breakdown and re-aggregation (healing) of softer, already damaged filler clusters.In simpler sense, one can hypothesize that all soft clusters are broken at the turning points of the cycle and the mechanical energy stored in these strained clusters is completely dissipated; i.e. only irreversible stress contributions result. Theorotically, the cluster mechanics of the material is complicated to be understood fully due to the fact that not all

soft clusters are broken at the turning points of a cycle. [25]. A comprehensive for **5** phr, **10** phr and **15** phr of xg C**750** filled IR master batch are shown in **figure 4.22c**. It was also reported that the filler network can substantially increase the effective volume of the filler due to rubber trapped in the agglomerates, leading to high elastic modulus. [25]

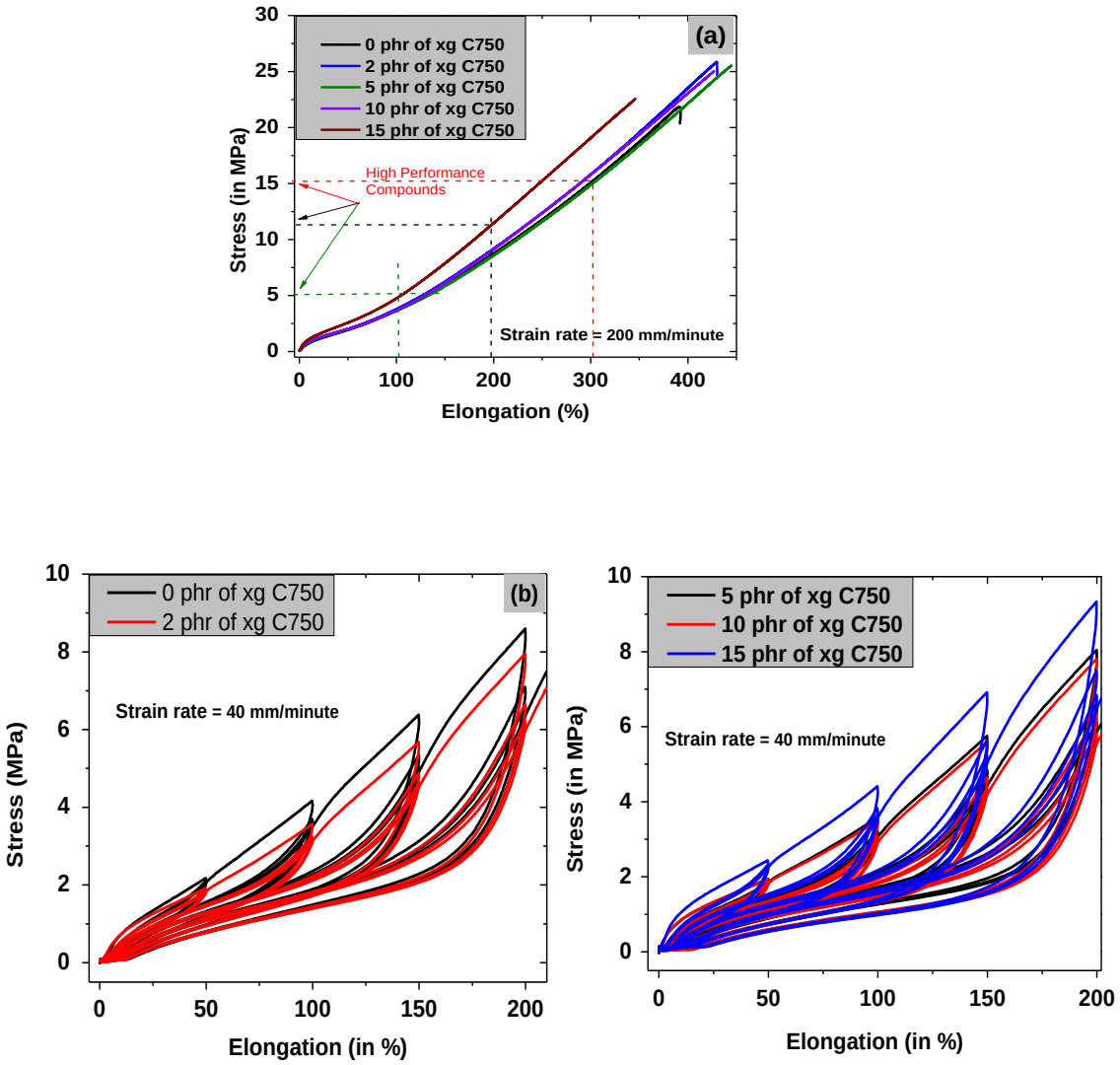

Figure 4.22: **(a)** Stress-Strain curves obtained from Hybrid/IR nanocomposites; **(b)** Multi-Hysteresis Stress-Strain curves comparatives for 0 phr and 2 phr of xg C750 in Hybrid/IR nanocomposites; **(c)** Multi-hysteresis Stress-Strain comparative for 5 phr, 10 phr and 15 phr of xg C750 in Hybrid/IR nanocomposites.

4.6.4. Dynamic mechanical temperature analysis (DMTA analysis)

The mechanical performance can be further evaluated through DMTA test. It was performed to analyze the reinforcing efficiency of the graphene and the extent of

polymer–filler interaction [26]. **figure 4.23a** and **4.23b** presents the behavior of modulus and loss tangent (tan δ). The glass transition temperature (T_g) can be obtained from the maximum peak in the tan δ curve and G*, and it can be observed that the Tg of composites containing **15** phr of xg C**750** (**-65.4** ^oC) was ~**3**^oC higher than that of composites containing no xg C**750** (**-63.6**^oC).

It could be because of the fact that the xg C**750** can enforce restriction to the polymer chain mobility due of the strong interfacial adhesion or higher polymer-filler interaction (since xg C**750** has higher surface activity) between NR and xg C**750** platelets. The area under tan **δ** curve under different temperatures indicates the total amount of energy that can be absorbed by a material. It can be concluded that the introduction of xg C**750** improves the overall stiffness of IR master batches; its elasticity is not affected significantly. Such characteristics are exciting, because most reinforcement will inevitably lead to a higher rigidity. Similar hypothesis is reported for such behavior in the literature [27].

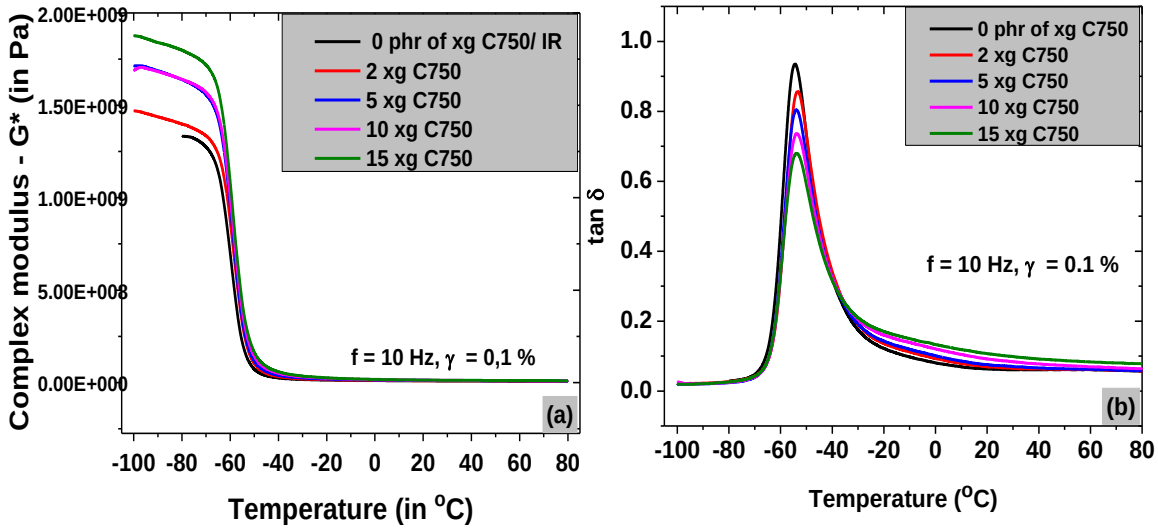

Figure 4.23: **(a)** DMTA comparative of Hybrid/IR system based nanocomposites containing xg C**750** concentration from **0** to **15** phr; **(b)** tan **δ** comparative of Hybrid/IR system based nanocomposites containing xg C750 concentration from **0** to **15** phr.

4.6.5. Dielectric AC Conductivity Properties

The dielectric AC conductivity and properties were measured within frequency range from 10^{-2} to 10^{6} Hz (**figure 4.24a and 4.24b**). The conductivity was studied for

filler concentration of **0** phr, **2** phr, **5** phr, **10** phr and **15** phr of xg C**750** in IR master batch. A very good conductivity of the Hybrid system was seen which increases with increasing concentration of xg C**750** into IR master batch. At lower loadings, the dielectric conductivity plateau remains almost similar at small frequency range and conductivity does not affected significantly. A higher conductivity of greater than **1.4***10^{-1} was observed at hybrid system containing **15** phr of xg C**750** in IR matrix. To obtain electrical synergistic effect, dielectric AC conductivity was taken at very low frequency (0.1 Hz) and plotted against filler volume fraction (**figure 4.24c**). A significant improvement of conductivity was observed after **3** phr which could be due to filler synergistic effect at this concentration. The conductivity of composites of hybrid system with varying content of xg C**750** exhibit a synergistic effect at lower values due to electron high mobility of nanoparticles in IR matrix.

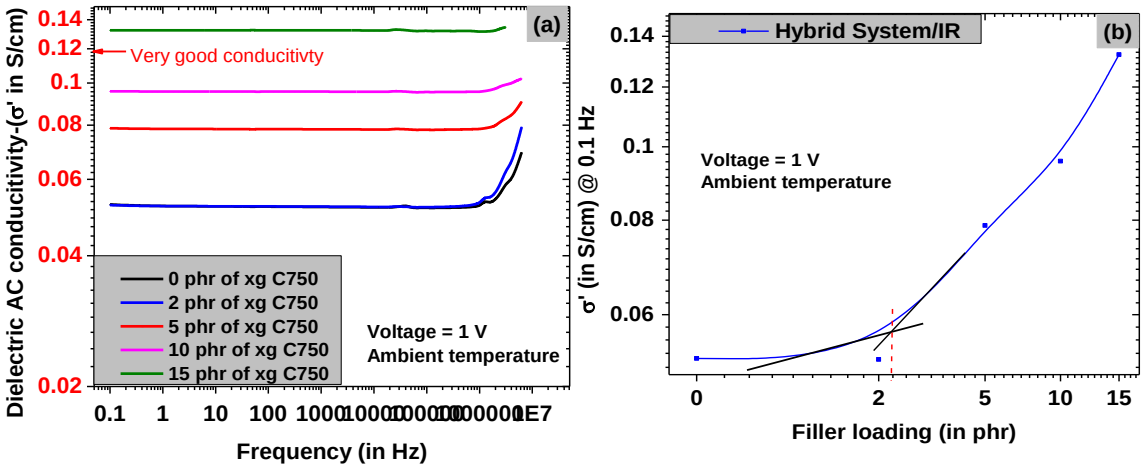

Figure 4.24: (a) Di-electric AC conductivity of Hybrid/IR composites; (**b)** Synergestic effect demonstrated from di-electric AC conductivity as a function of filler loading for xg C750 in Hybrid/IR nanocomposites.

4.7. Conclusions

It has been demonstrated from present investigations that the use of nanofillers (xg C**750**, xg M**5** and nano**G**) brings a significant improvement in over-all properties of nanocomposites as compared with traditional filler such as CB-N**234**. Adsorption isotherms show that BET surface area and surface activity of xg C**750** graphene grade was higher than xg M**5** filler grade. From SEM investigations, it was found that the

platelet-like morphology was observed to be more damaged (ruptured) in the xg C**750** filler grade than in xg M**5**. TEM analysis in compounds revealed that in all the samples, an even dispersion of nano**G** and the presence of nanometric aggregates made also by few layers of graphene. Through XRD analysis, it was observed that the $D_{\perp}$ correlation length of nano**G** aggregates remained substantially unchanged passing from pristine sample to the IR nanocomposite and increased upon performing the crosslinking reaction, thus suggesting the re-organization of nanoG in a liquid matrix such as IR, upon applying a high pressure. NanoG behaves thus differently from clays, that experience a progressive exfoliation as a consequence of the mixing energy.

The compounds were successfully prepared by dry melt mixing method and a sulphur-based crosslinking system was observed to be effective. From rheometric studies, it was found that the scorch time (t'_{05}) was found to decrease with increasing filler concentration which was more pronounced for nanoG than xg M**5** and N**234** fillers. The effect of carbon fillers on the scorch time was found to differ appreciably for the different nanofillers. From strain sweep measurements, It was found that the characteristic plateau of G' at low strain reaches lower strain amplitudes with an increase of filler concentration in rubber matrix. A particular enhancement of the G' plateau value is obtained passing from **20** phr to **30** phr loading ofnanofillers. A quantitative analysis of the percolation threshold with Huber–Vilgis double logarithmic plot was performed in the neat and filled rubber matrix through dynamic-mechanical measurements. From stress-strain measurements, it was observed that the stresses at all the elongations remarkably increase with the filler content in the SBR matrix. The xg M**5** shows dominating reinforcing properties and reinforcing factor than xg C**750**, nanoG and N**234** fillers at all loadings. Multi-hysteresis stress-strain investigations show the first cycle exhibits higher energy dissipation than the third cycle and it was demonstrated that a stable filler networking can reduce hysteresis losses.

For compounds based on **SBR** as diene rubber, during dry mixing temperature was observed to increase upon adding the nanofiller and remained however below **85** °C which was far below the curing temperature (**150** °C). A filler percolation threshold of xg C**750** (~**16.6** phr), followed by xg M5 (~**23.2** phr), nanoG (~**21.9** phr), and N234 (~**29.6** phr) was estimated.

For compounds based on **IR** as diene rubber and **high** surface area few layer graphene, it was found that the maximum temperature during dry mixing (**90** °C) was far below than vulcanization temperature of **150** °C. The filler percolation threshold of xg C**750** was achieved at lower loading (< **20** phr) than xg M5 (~**22** phr) and N**234** (~**25** phr). The xg C**750** based rubber nanocomposites had diecectric conductivity of ~$\mathbf{2x10^{-8}}$ at **30** phr filler loading which is sufficiently higher than needed for applications in the tire industry.

For compounds based on **IR** as diene rubber and **high** shape anisotropy and **high** surface area few layer graphene**,** a pristine nanoGraphite (nanoG), without any pre-treatment to reduce the number of stacked layers, was found to promote filler networking in poly (**1,4**-*cis*-isoprene), at a relatively low concentration. This work presents that shape anisotropy as an important feature of layered nanofiller such as a nanoGraphite. NanoG with high shape anisotropy was successfully dispersed in an elastomer matrix as aggregates made by few layers, thus forming a long-range filler-networking at relatively low concentration without the need of any pre-treatment and maintaining a long range crystalline order within the layer. Further investigations have to be performed in order to assess the correlation between the nanofiller shape anisotropy and the nanocomposite properties. NanoG with high shape anisotropy appears as the ideal candidate to achieve extensive exfoliation through the treatments reported in the prior art.[**28-31**]

For compounds based on **IR** as diene rubber and **hybrid** filler system**,** it has been demonstrated from experiments that the use of hybrid filler system in IR brings a significant improvement in the properties of rubber nanocomposites. A synergistic effect was observed after xg C**750** loading of **3** phr in IR master batches. The glass transition temperature (T_g) can be obtained from the maximum peak in the tan δ curve and G*, and it can be observed that the Tg of composites containing **15** phr of xg C**750** (**-65.4** ^{o}C) was ~**3** ^{o}C higher than that of composites contining **0** phr of xg C**750** (**-63.6** ^{o}C). The xg C**750** based rubber nanocomposites had diecectric conductivity of ~$\mathbf{1.4x10^{-1}}$ at **15** phr filler loading of xg C**750** in hybrid system which more than sufficient than needed for applications in the tire industry.

4.8. References

[1] M. Mauro, V. Cipolletti, M. Galimberti, P. Longo, G. Guerra. *J. Phys. Chem.:C,* **116**, 24809 (2012)

[2] M. M. Moewes, F. Fleck, M. Klueppel, *Rubber Chem. Technol*., (2013)- in press DOI: http://dx.doi.org/10.5254/rct.13.87930

[**3**] G. Ramorino, F. Bignotti, S. Pandini, T. Riccò, *Comp. Sci. Technol*. **69**, 1206 (2009).

[4] V. Kumar, U. Giese, T. Hanel, L. Giannini, Proceedings of the 1st ISN2A, 1st International Symposium on Nanoparticles/ Nanomaterials and Applications (20-22 January- 2014) Caparica - Almada, Portugal, ISBN 978-9-8998415-9-8.

[5] V. Kumar, U. Giese, T. Hanel, L. Giannini, M. Galimberti, *Kautsch. Gummi Kunstst.*, (2014) (accepted) – in press.

[**6**] M. Galimberti, M. Coombs, P. Riccio, T. Ricco`, S. Passera, S. Pandini, L.Conzatti, A. Ravasio, I. Tritto, *Macromol. Mater. Eng*., **298**, 241 (2012).

[**7]** G. Heinrich, M. Klüppel, *Adv. Polym. Sci*., **160**, 44 (2002).

[**8]** P.G. Maier, D. Goritz, *Kautschuk Gummi Kunstoffe*, **49**, 18 (1996).

[**9]** S.S. Sternstein Maier, A-J. Zhu, *Macromolecules*, **35**, 7262 (2002).

[10] E. Guth, Rubber Chem. Technol., **18 (3)** 596 (1945).

[11] E. Guth, O. Gold, *Physical Review*, **53**, 322–328 (1938).

[12] W. Bauhofer, J.Z. Kovacs , *Compos Sci Technol.*, **69(10)** 1486 (2009).

[13] J. R. Potts, O. Shankar, L. Du, R.S. Ruoff, *Macromolecules*, **45**, 6045 (2012).

[14] S. Agnelli, V. Cipolletti, S. Musto, M. Coombs, L. Conzatti, S. Pandini, T. Riccò, M. Galimberti, *eXPRESS Polym. Lett.*, **8(6)** 436 (2014).

[**15**] M. Hernandez, M. del Mar Bernal, R. Verdejo, T. A. Ezquerra, M. A. Lopez-Manchado,*Compos. Sci. Technol.*, **73**, 40 (2012).

[**16**] G. Sui, W. H. Zhong, X. P. Yang, Y. H. Yu, S. H. Zhao, *Polym. Adv. Technol.*,**19**, 1543 (2008).

[**17**] G. Sui, W. H. Zhong, X. P. Yang, Y. H. Yu, S. H. Zhao, *Mater. Sci. Eng.: A*, **485**, 524 (2008).

[**18**] L. Lu, Y. Zhai, Y. Zhang, C. Ong, S. Guo, *Appl. Surf. Sci.*, **255**, 2162 (2008).

[**19**] G. Sui, W.H. Zhong, X.P. Yang, Y. H. Yu, S.H. Zhao, *Polym. Adv. Technol.*, **19**, 1543 (2008).

[**20**] A. R. Payne, R. E. Whittaker, *Rubber Chem. Technol.*, **44**, 440 (1971).

[21] M. Galimberti, V. Kumar, M. Coombs, V. Cipolletti, S. Agnelli, S. Pandini, L. Conzatti, *Rubber Chem. Technol*., in-Press (2013).

DOI: http://dx.doi.org/10.5254/rct.13.87903

[22] V. Kumar, U. Giese, T. Hanel, M. Galimberti, L. Giannini, *Kautsch. Gummi Kunstst.*, (2014) (submitted and accepted).

[23] S. Praveen, P.K. Chattopadhyay, P. Albert, V.G. Dalvi, B.C. Chakraborty, S. Chattopadhyay, Compos. Part A: Appl. Sci. and Manufacturing, **40 (3)**, 309 (2009).

[24] V. Nigam, D. K. Setua, G. N. Mathur, J. Mater. Sci., **36(1)**, 43 (2001).

[25] H. Lorenz, M. Klüppel, *J. Mech. Phys. Solids*, **60(11)** 1842 (2012).

[26] U. Lange, T. Hirsch, V.M. Mirsky, and O.S. Wolfbeis, *Electrochim. Acta*., **56**, 3707 (2011).

[27] Z. Peng, C.F. Feng, Y.Y. Luo, Y.Z. Li, and L.X. Kong, *Carbon*, **48**, 4497 (2010).

[**28**] A. V. Yakovlev, A. I. Finaenov, S. L. Zabud'kov, E. V. Yakoleva, *Russ. J. Appl. Chem.*,**79**, 1741 (2006).

[**29**] J. Li, H. Lin, W. Zhao, G. Chen, *J. Appl. Polym. Sci.*, **109**, 1377 (2008).

[**30**] H. Fan, L. Wang, K. Zhao, N. Li, Z. Shi, Z. Ge, Z. Jin, *BioMacromol.*, **11**, 2345 (2010).

[**31**] T. Ramanathan, S. Stankovich, D. A. Dikin, H. Liu, H. Shen, S. T. Nguyen, L. C. Brinson, *J. Polym. Sci. B*, **45**, 2097 (2007).

Chapter 5

*Compounds based on **high** surface area few layer graphene and **polar** acrylonitrile butadiene rubbers*

5.1. Introduction

The nanofillers have been reported and study widely in polymer matrix and formulations based on nanofiller shows improved properties. [1-13] In this **chapter**, an overview of rubber compounds based on **high** surface area few layer graphene and nitrile butadiene rubbers are discussed. The nanofillers used are xg C**750**, xg M**5** as **high** surface few layer graphene which are compared with UF**1** C**98** nanographitic filler and traditional filler carbon black N**339**. The measurements were performed both on cured and uncured rubber compounds. Mechanical properties were assessed by stress-strain and multi-hysteresis investigations. This work demonstrates the correlation of FLG with **high** surface area on filler networking, filler dispersion, and dynamic mechanical and dielectric properties in a **polar** NBR rubber.

5.2. Results and discussion

The morphological and structural chatacertizations such as SEM, XRD of xg C**750** and xg M**5** high surface area FLG are described in section **4.2.1** and **4.2.2** of previous chapter **4**. Static adsorption features of the filler as described below.

5.2.1. Adsorption isotherms of nanofillers in nitrogen and butane

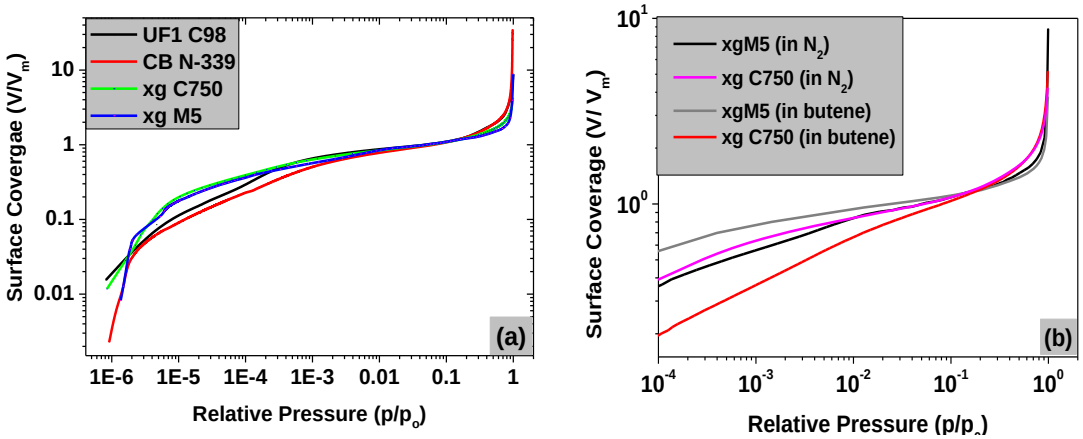

Figure 5.1 : (a) Nitrogen adsorption isotherms of xg M**5**, xg C**750**, UF**1** C**98** and CB-N**339** as nanofillers: plot of surface coverage versus relative pressure; **(b)**: BET surface area comparision of nanofllers in nitrogen and butane.

The adsorption isotherms measurements were carried out to observe surface characteristics of fillers. The adsorption isotherms were carried out for xg C**750**, xg M**5**, UF1 C**98** and CB-N**339** as shown in **figure 5.1(a)**. The differences in surface area of xg C**750**, into n-butene and N_2 are presented in **figure 5.1(b)**. It was interesting to observe the decrease in the BET surface area while changing gas from nitrogen to butane. The BET surface area in (m^2/g):

Nitrogen- **817.3** for xg C750, **168.3** for xg M5, **91.8** for CB-N339.

Butene- **534.4** for xg C750, **101.7** for xg M5, **77.9** for CB-N339.

5.2.2. Optical microscopy for studying filler dispersion

The filler dispersion of the FLG filled NBR matrix is studied by optical microscopy as presented in **figure 5.2 (a,b)** shows optical image of NBR composite containing **10** vol % of N**339** and xg C**750**. A homogenous dispersion of N**339** filler particles in NBR was observed. In xg C**750** filled compounds; filler was found to be un-evenly distributed, with appearance of larger aggregates, in a fairly fine dispersion. Most aggregates and agglomerates have sub-micrometric dimensions, some are about **5-10** μm large and only few are above **10** μm large. **figure 5.2(c)** presents the dispersion index @ **70**% grey scale (the shape of grey-scale histogram is directly related to the quality of the dispersion that is low variance represents good filler dispersion). It can be noticed that xg C**750** shows uneven dispersion (D_I of < **50**% @ **10** vol %) irrespective as compared to N339 filled NBR compounds irrespective of high surface area of xg C**750**. The lower filler dispersion of xg C**750** presents poor filler-rubber matrix compatibility that results in formation of higher aggregated xg C**750** filler particles. On the other hand, N**339** shows a very good filler dispersion index (D_I) of more than **99.5**% overall and hence good filler-rubber compatibility.

Optical images of fillers were processed in program "*analysis pro*" for getting the dimension of filler aggregates and agglomerates in rubber matrix. **figure 5.2(d,e)** describes the quantative analysis filler aggregates and agglomerates for both N**339** and xg

C**750**. It was found that in N**339**, particles of dimension upto **300** μm^2 were observed while xg C**750** shown particle aggregates of upto **700** μm^2. A large number of particles (>**1200**) were noticed into xg C**750** with range between **30-100** μm^2. as compared with N**339** which has ~**30** number of particles.

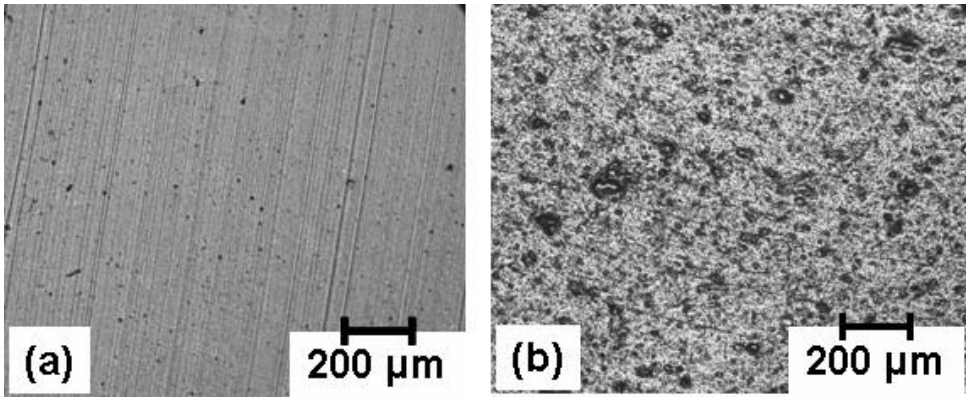

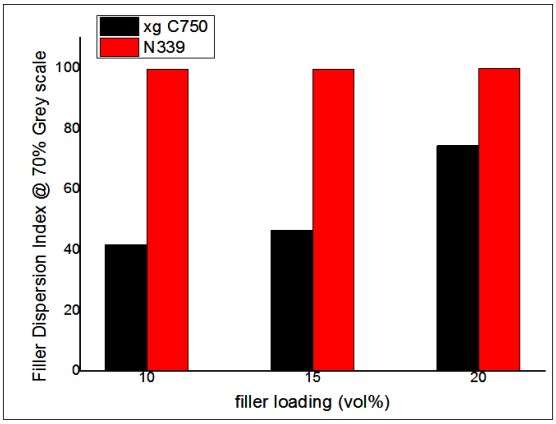

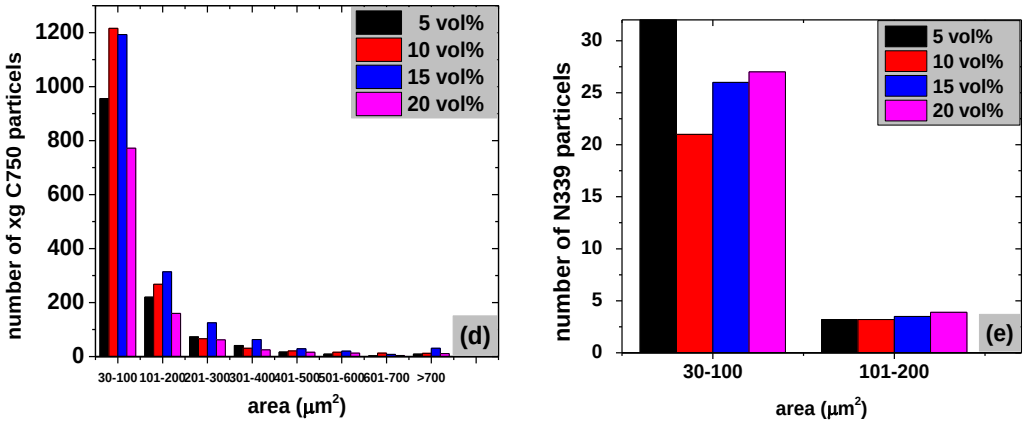

Figure 5.2: Optical micrographs in NBR rubber matrix at lower magnification: (a) **10** vol % CB-N339; **(b)** xg C750; **(c)** Filler dispersion index plot of xg C750 and xg M5 as a function of filler loading; Quantitative analysis of filler aggregates, agglomerates for **(d)** xg C**750**; and **(e)** N**339** fillers.

5.3. Compounds based on **nitrile butadiene rubber** as **polar** diene rubber

5.3.1. Rheometric curves

The sulphur based crosslinking system was adopted in present work. **figure 5.3(a)** shows Rheometric curves of N**339** filled rubber compounds. A comparative study on increase in torque change, **ΔS** (M_H-M_L) for xg C**750**, xg **M5**, UF**1** C**98** and N**339**, is presented in **figure 5.3(b)**. It was found that **ΔS** increases with increasing filler loading. The increase of torque could be due to influence of filler networking of graphene and its interaction with rubber. It was reported that filler particles has higher interaction in butyl rubber (BR) due to large number of unsaturated bonds in BR than NBR, EPDM and isoprene-co-isobutylene rubber (IIR).[16]

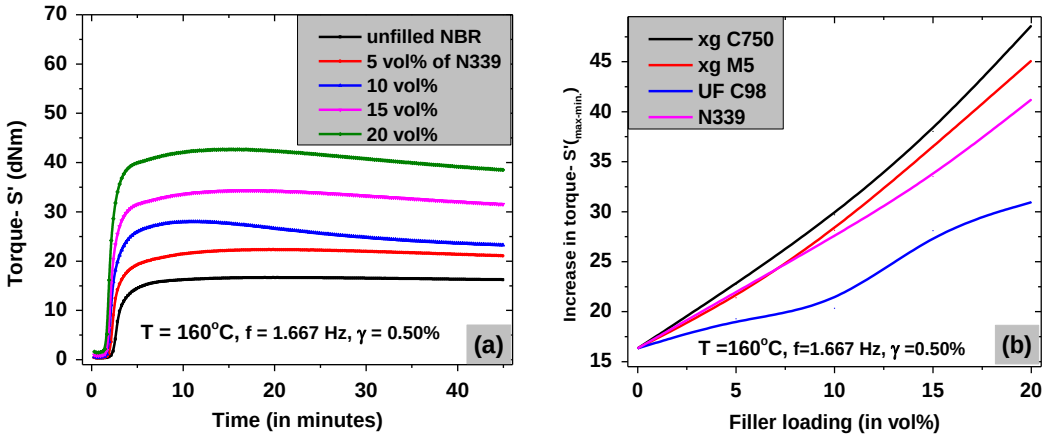

Figure 5.3: Rheometric curves for NBR based compounds **(a)** with N339 concentration from 0 to 20 vol%; **(b)**: Torque increase (ΔS that is $S'_{Max.} - S'_{Min.}$) as a function of filler loading with different concentration of xg M**5**, xg C**750**, UF1 C**98** and CB-N**339** filler.

5.3.2. Rheological Properties through RPA studies

Dependence of storage modulus-G' as a function of strain amplitude for xg C**750** filled compounds, with nanofiller amount from **0** to **20** vol%, is presented in **figure 5.4(a)**. The storage modulus increases with increasing filler loading in NBR matrix. This could be due to high surface area of xg C**750** or improved filler networking in due to polarity of NBR. The storage modulus – G' as a function of filler loading for xg C**750**, xg

M**5**, UF**1** C**98** and CB-N**339** are described in **figure 5.4b**. G' increases with increasing filler loading in the NBR matrix. Among all the filler investigated, xg C**750** shows dominant **G**' at all loading than xg M**5**, CB-N**339** or UF**1** C**98**. Storage modulus decreases from increase in temperature from **60** ^{o}C to **100** ^{o}C as presented in **figure 5.4c**. The filler networking is influenced by several parameters like temperature, pH of matrix for compatibility of polymer-filler, mixing and processing parameters. The temperature affects orientation-disorientation of xGnP platelets which affects polymer-filler microstructures formed during compounding in filler-dispersion phase. The interfacial interactions between organic and inorganic phases play an important role in filler dispersion, reinforcement and other properties and are temperature dependent. The characteristic properties improve with increasing filler concentration and above a certain filler concentration, a sharp increase in these properties was observed. This filler concentration is known as "*filler percolation threshold*" loading concentration. **figure 5.4d** presents percolation threshold calculation for xg C**750** (~**6.5** vol%), xg M5 (~**9** vol%), UF**1** C**98** (**11.4** vol%) and CB-N339 (**14.1** vol%). The percolation threshold was seen to be less dependent on polymer chain regime (entangled or rouse regime) and has direct dependency on filler volume fraction.

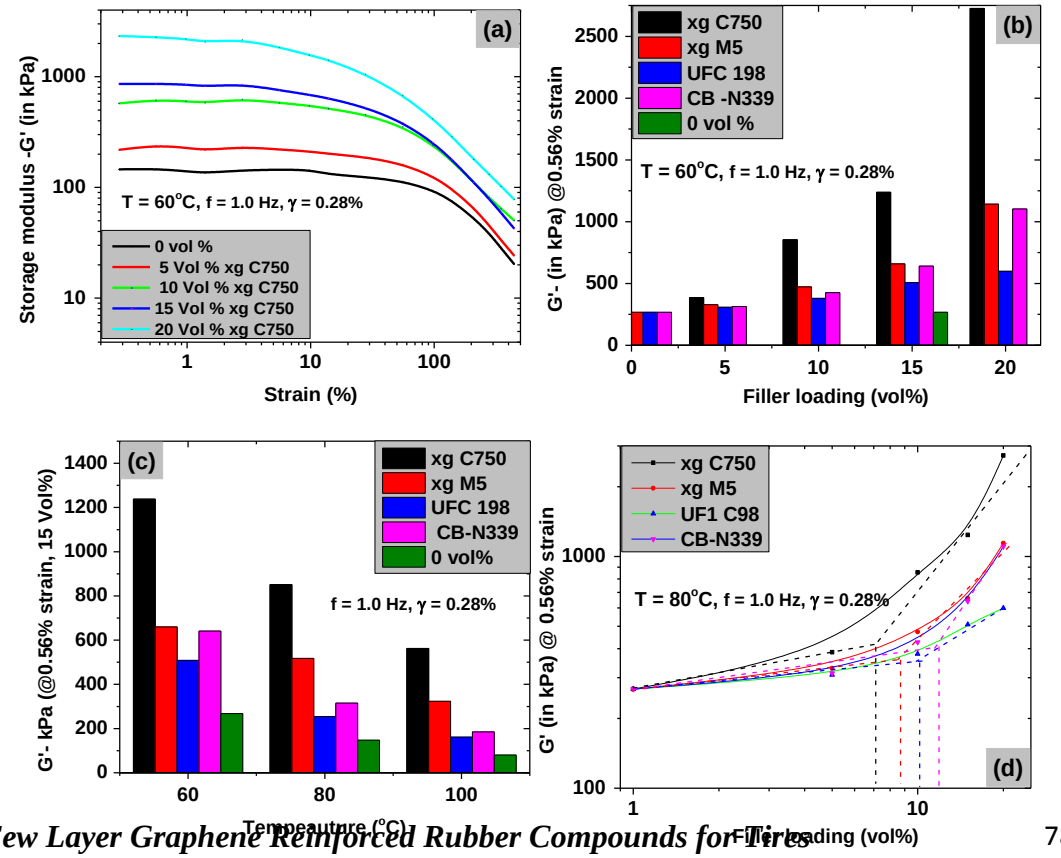

Figure 5.4: Rheological Properties of NBR compounds through RPA studies: (**a**) Storage modulus (G', kPa) as a function of different strains (increasing from 0.28% to 300%) for xg C750 filler with increasing loading from 0 to 20 vol%; Storage modulus at minimum strain for compounds based on xg C750, xg M5, UF1 C98, N339 fillers: **(b)** as a function of filler loading; **(c)** as a function of temperature (60 ^{o}C, 80 ^{o}C and 100 ^{o}C); **(d)** Filler Percolation Threshold: plot of the storage modulus at minimum strain, as a function of the filler volume fraction for xg C750, xg M5, UF1 C98, N339 fillers.

5.3.3. Stress-strain behavior for Tensile strength

The reinforcing factor (σ_F/σ_0) at **50**% strain and elongation at break of rubber compounds is presented in **figure 5.5 (a, b)**. It was found that xg M**5** shows highest reinforcement properties followed by xg C**750**, UF**1** C**98** and CB-N**339** exhibits least reinforcement. It was however found that UF**1** C**98** shows best elongation at break properties where at **20** vol % filler loading, it shows upto **249**% elongation when compared with other fillers such as CB-N**339**, xg C**750** and xg M**5**.

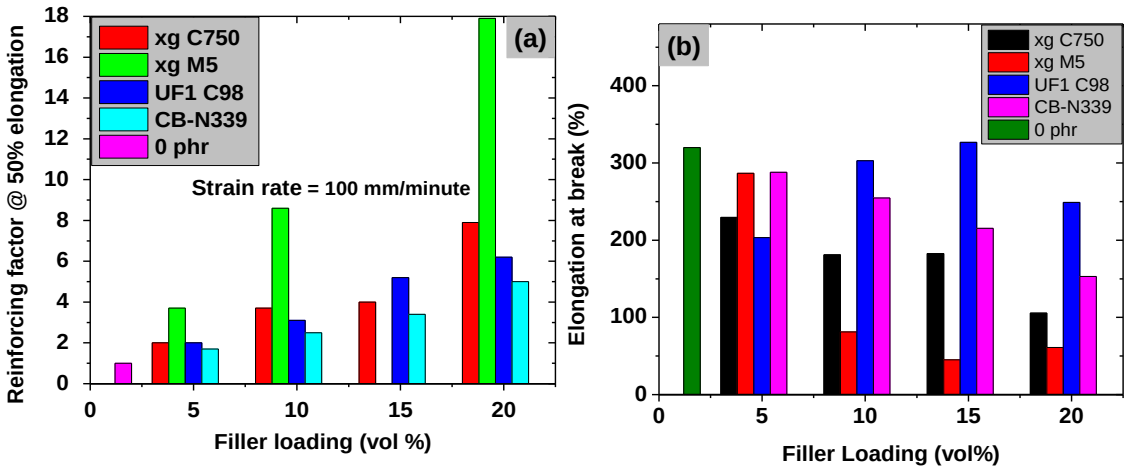

Figure 5.5: Stress-Strain behaviour of xg C**750**, xg M**5**, UF**1** C**98**, CB-N**339** in NBR compounds: **(a)** Reinforcing factor (σ_F/σ_0) at **50** % for content increasing from **0** to **20** vol%; **(b)** Elongation at break on same fillers.

5.3.4. Hardness

Hardness is considered as one of important parameter as it directly affects several characteristics properties of rubber compounds. The softer compounds (<**70** Shore **A** hardness) can be stretched and processed easier for several applications. Harder rubber compounds on other side offers obscure properties like high extrusion resistance or high enthalpy consumption during processing in tire based applications. **figure 5.6** show that

xGnP filled compounds exhibits good hardness properties at very low filler loading as compared with UF**1** C**98** and N**339**. Higher hardness was obtained (~**91** Shore A) for xg M**5** filled compounds at higher loading of **20** Vol%.

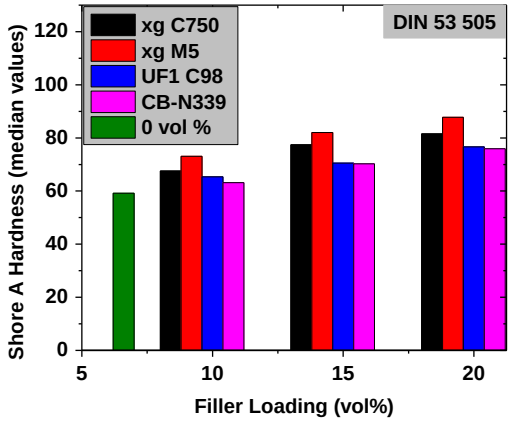

Figure 5.6 – Hardness (Shore **A**) comparative of xg C**750**, xg M**5**, UF**1** C**98**, N**339** filled NBR compounds

5.3.5. Tear Strength

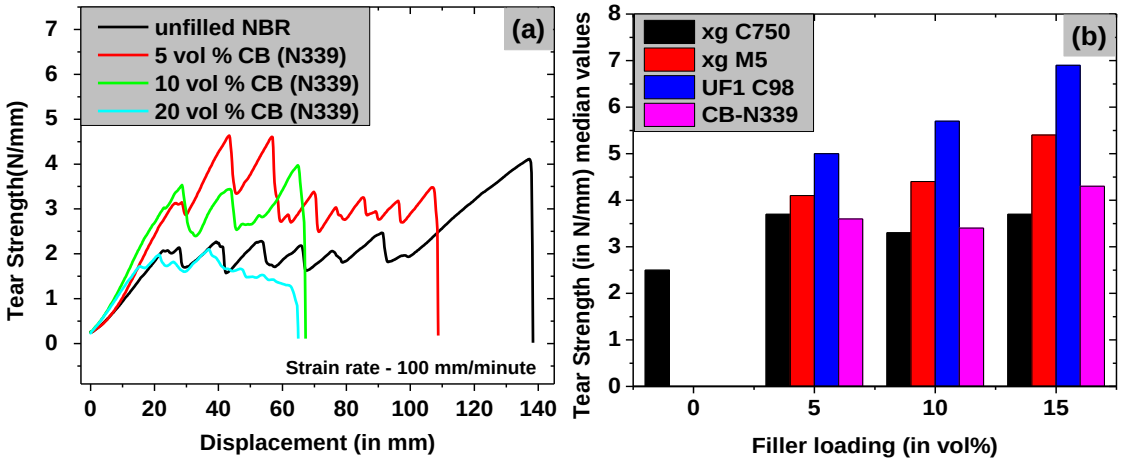

Figure 5.7: Tear Strength for NBR compounds: **(a)** CB-N339 concentration increasing from 0 to 20 vol%; **(b)** tear strength of on xg C750, xg M5, UF1 C98, N339 fillers for loading from 0 to 20 vol%.

The tear strength of fillers (xg C**750**, xg M**5**, CB-N**339** and UF**1** C**98**) are studied comparatively according to **ISO 34** standards as presented in **figure 5.9**. The tear strength

scheme for CB-N**339** filled composite is presented in **figure 5.9(a)**. It can be observed from measurements that neat rubber has very low capacity to bear mechanical. The compounds with low tear resistance normally show poor abrasion resistance or durability of life span. The tear strength of the xg C**750**, xg M**5**, UF**1** C**98** and N**339** are comparatively presented in **figure 5.9(b)**. An UF**1** C**98** filled rubber compound shows highest resistance to tear propagation under load than xg M**5**, xg C**750** and N**339**. It could be proposed due to higher platelet like morphology of the filler which resists crack propagation

5.3.6. Swelling Tests

The swelling tests were performed to study networking density of cured rubber nanocomposites in presence and absence of filler. The amount of solvent uptake as a function of time for filled NBR rubber nanocomposites are shown in **figure 5.8 (a, b)**.

It was observed that the amount of solvent uptake decreases with increasing filler loading from unfilled to **20** vol %. It can be interpreted that the rate of solvent intake in compounds continues until equilibrium between the forces inside polymer chains balances the forces that tend to swell the networks. Least quantity if solvent was observed in **20** vol % filled compound. It could be due to higher filler networking density.

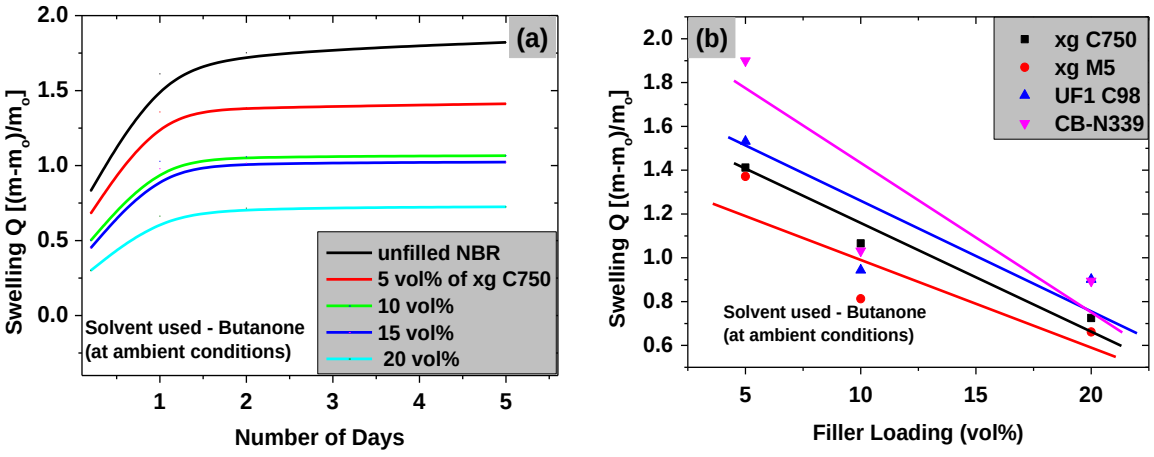

Figure 5.8: Swelling tests for NBR compounds: **(a)** Swelling as a function of number of days for xg C**750** filler; **(b)** Swelling on xg C**750**, xg M**5**, UF**1** C**98**, N**339** as a function of filler loading

5.4. Conclusions

It was demonstrated that xGnP can be a promising alternative of CB-N**339** to improve over-all properties of rubber compounds for tire applications. It can be concluded from adsorption isotherms that the nature of gas infused for BET surface area characterization significantly provide different surface area (xg C**750** shows BET area of **817. 3** m^2/g in N_2 and **573.6** m^2/g in n-butene). The dry mixing method was successfully implemented for dispersing fillers.

From rheometric curves, we have found that torque increases and scorch time decreases with increasing filler concentration in NBR matrix. We have also found that curing time (t'_{90}) decreases with increasing filler loading. DIAS filler dispersion studies shows that CB-N339 was very highly efficient (>**99.5**% dispersion over all) and compatible with NBR matrix than xg C**750** in which filler dispersion increases with increasing filler loading. xg C**750** shows large number of particles whch ranges from a broad range from **30** μm^2 to >**700** μm^2 as compared to N**339**. The hardness of rubber nanocomposites increases with increasing filler loading in NBR matrix where xg M**5** shows highest over all hardness as compared with other comparative fillers.

The RPA study shows an increase in storage modulus with increasing filler loading and decreasing temperature from **100** ^oC to **60** ^oC. The filler percolation threshold (FPT) was achieved at very low filler loading using nanofillers xg C750 (~**6.5** vol%), xg M**5** (~**9** vol%), UF1 C98 (**11.4** vol%) and than other traditional fillers such as CB-N**339** attains FPT at **14.1** vol%.

From stress-strain measurements, it was found that xg M**5** shows higher reinforcing ability for NBR rubber matrix than other filler investigated. Higher strain prior to break was observed for all N**339** filled nanocomposites. The elongation at break was found highest in unfilled rubber which decreases from UF**1** C**98** to xg M**5**. Multi-hysteresis strain-strain experiments show that stress increases with increasing filler loading. From swelling measurements, it was found that amount of solvent intake decreases with increasing filler loading. The dielectric conductivity and permeability measurement shows that xg M**5** as nanofiller can provide higher electric properties than CB-N**339**.

5.5. References

[1] D. Ponnamma, H. J. Maria, A. K. Chandra, S. Thomas, Advan. *Elastomers II Advan. Struct. Mater.*, **12**, 69 (2013).

[2] M. Galimberti, V. Cipolletti, S. Musto, S. Cioppa, G. Peli, M. Mauro, G. Guerra, S. Agnelli, T. Riccò, V. Kumar, *Proceedings of the Fall 184th Technical Meeting of the Rubber Division of the American Chemical Society*, Inc. Cleveland (OH) (8 – 10 october 2013).

[3] M. M. Möwes, F. Fleck, M. Klüppel, *Poster and Proceedings: 10th Fall Rubber Colloquium*, P. 99, Hannover, Germany, (7- 9 November 2012).
ISBN: 978-3-9814076-1-7.

[4] M. Galimberti, V. Cipolletti, V. Kumar, *Natural Rubber Based Composites and Nanocomposites*, S. Thomas, C. H. Chan, L. A. Pothan, Ramanan, J. Maria Eds., *Royal Soc. Chem.*, Chapter **2**, (2014).

[5] M. Klüppel, *Advan.Polym. Sci.*, **164**, 1, (2003).

[6] M. M. Möwes, F. Fleck, M. Klueppel, *Rubber Chem. Technol*. (2013)- in press.

[7] M. Galimberti, V. Kumar, M. Coombs, V. Cipolletti, S. Agnelli, S. Pandini, L. Conzatti, *Rubber Chem. Technol*. (2013)- in press.

[8] L. Bokobza, *Polymer*, **48(17)**, 4907 (2007).

[9] M.M. Möwes, F. Fleck, M. Klüppel, *Proceedings of the Fall 182nd Technical Meeting of the Rubber Division of the American Chemical Society*, Inc. Cincinnati (OH), (12^{th} October 2012).

[10] V. Kumar, U. Giese, T. Hanel, L. Giannini, M. Galimberti, *Kautsch. Gummi Kunstst.* (2014) (accpeted and in press)

[11] J. C.-González, H. Retsos, R. Verdejo, S. Toki, B. S. Hsiao , E. P. Giannelis, M. A. L.-Manchado, *Macromolecules*, **41(18)** 6763 (2008).

[12] V. Kumar, U. Giese, T. Hanel, L. Giannini, M. Galimberti, *Kautsch. Gummi Kunstst.*, (2014) (accepted) – in press.

[13] J. S. Bergström, M. C. Boyce, *Rubber Chem. Technol*., **72(4)** 633 (1999).

[14] A. R. Payne and R. E. Whittaker, *Rubber Chem. Technol.*, **44(2)** 440 (1971).

[15] L. Mullins, N. R. Tobin, *J. Appl. Polym. Sci.,* **9(9)** 2993 (1965).

[16] S. Thomas, R. Stephen, *Rubber Nanocomposites: Prepration, Properties and Applications*, ISBN 978-0-470-82345-3, Wiley, (2010).

Chapter 6

*Compounds based on **high** surface area few layer graphene and **polar** epoxidized diene rubbers*

6.1. Introduction

This work presents the correlation of FLG with **high** surface area, effects of presence of epoxy functional groups along polymer chains on filler networking, polymer-filler interactions, filler dispersion and dynamic mechanical properties of rubber compounds. The rate of epoxidation was quantitatively demonstrated using ^{1}NMR, DSC technique was adopted to study epoxidation effects on $T_{g..}$ Optical microscopy was carried out to examine the filler dispersion index of rubber compounds. Rheological properties were studied through strain sweep measurements and mechanical measurements were studied with stress-strain tests, dynamo-mechanical temperature experiments. The stress-strain multi-hysteresis experiments were carried out to investigate compound stability under cyclic strains determining the energy dissipation.

In present study, xg C**750** and carbon black-N**234** were used as nanofillers as described in section **7.1.1** (Chapter-**7**). The morphological and structural characterizations of these nanfillers are described already in section **4.2.1**, **4.2.2** and **4.2.3** (chapter-**4**). The filler loading in epoxidized-rubber was increased from **0** to **40** phr. SBR and IR were used as rubber matrix as detailed in section **7.1.2** (chapter-**7**). The chemicals used for epoxidation are described in section **7.1.4.** (chapter-**7**).

6.2. Results and discussion

6.2.1. Epoxidation of diene rubber

The epoxidation of polybutadiene rubbers such as SBR was obtained by using peroxide and formic acid that converts the double bonds of polymer chains into epoxy groups (**figure 6.1**). This conversion is based on the reaction of in-situ formed performic acid with **1,4-** and **1,2** poly-butadiene units. In this reaction, a cyclic transition state is formed in which the proton of the peroxy acid is transferred to the carbonyl group of the same molecule. This destabilizes the O-O bond and the nucleophile oxygen can be added to the unsaturated double bond of the alkene. For these experiments, we selected a fixed reagent relation of H_2O_2/C=C/HCOOH (**3**/**2**/**1.5**) at **25**°C and are easily attackable by

nucleophile species. Epoxy rings are only attacked by nucleophile species if side products of the reaction are carbonyl groups or hydroxyl groups due to the opening of the oxirane ring. **1,2**-vinyl units are less reactive than **1,4**-cis and **1,4**-trans units due to due to steric hindrance. [1, 2] It was reported in the literature that the nature of ring-opened structures depends directly on the epoxidation degree. At lower epoxidation degree, the majority of epoxide groups are isolated, simple diols and oftenly hydroxyacetates are formed. However, at high level of epoxidation, blocks of epoxide predominate and majority of products are five-membered cyclic ether. At **100** mole% modification, a white amorphous thermoplastic product was obtained that consist of almost entirely "*furan*" structures [3].

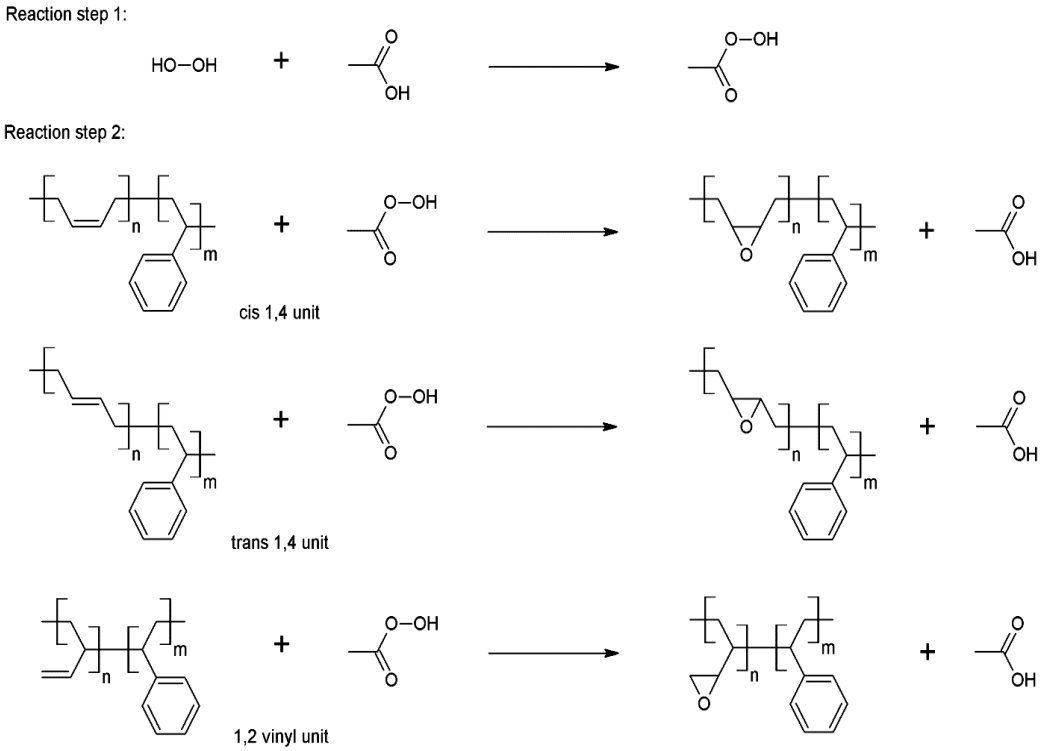

Figure 6.1: Schematic representation of epoxidation in diene rubbers such as SBR.

6.2.2. NMR studies for determining degree of epoxidation

The structural changes of epoxidized rubber can be investigated by ^{1}H-NMR spectroscopy. Particularly, the epoxidation reaction can be followed by the disappearance of peaks of polybutadiene double bonds of *cis* and *trans*-**1,4** units and **1,2** vinyl units and the appearance of the epoxy group peaks (**figure 6.2**). The peaks of the created epoxy groups can be divided also into *cis* and *trans* **1,4**- (δ=**2.7** ppm and δ=**3.0** ppm) and **1,2**-

units (**3.4** ppm). These ^{1}H-NMR corresponding peak are in line with published results [4]. It was reported that with an increase of epoxy groups (~**34**%), signals at **2.45** ppm and **2.70** ppm (*trans* and *cis*-epoxy) increases while **5.2** ppm peak (unsaturated **1,4**-polybutadiene protons) decreased [4]. The rate of epoxidation was maintained low (below **10**%) to preserve the T_g of the epoxidized-SBR and to keep it nearer to unepoxidized-SBR.

The calculation of epoxidation degrees of SBR samples was carried out by the method described by *R.H. Schuster et al* [4] using the following **equation 6.1** -

$$X\% \frac{A_{epox}}{A_{epox} + A_{1,4} + A_{1,2}} \qquad (6.1)$$

where A_{epoxy} is the sum of the integrated proton area intensities by the appearance of the epoxy groups of *cis* and *trans*-**1,4** units and are the proton area intensities for the unsaturated double bonds of **1,4** and **1,2** units. The separation of the epoxy peaks of *trans* **1,4**- and *cis* **1,4**- polybutadiene enables the verification of the preferred double bonds in the polybutadiene structure. **equations 6.2** and **6.3** used for determining *cis* **1,4** or *trans* **1,4** peak is-

$$X\% \frac{A_{epox}(1,4\ trans)}{A_{epox}(1,4\ trans) + A_{epox}(1,4\ cis) + A_{1,4} + A_{1,2}} \qquad (6.2)$$

$$X\% \frac{A_{epox}(1,4\ cis)}{A_{epox}(1,4\ trans) + A_{epox}(1,4\ cis) + A_{1,4} + A_{1,2}} \qquad (6.3)$$

Table 6.1: Summary of epoxidation degrees for epoxidized-SBR against reaction times

Epoxidation time [min]	**Cis 1,4-unit** [%]	**Trans 1,4-unit** [%]	**All over 1,4-unit** [%]
0	0	0	0
60	1.47	2.96	4.44
90	2.81	4.35	7.16
180	6.11	8.2	14.31
Master Batch	3.58	5.21	8.79

The epoxidation degree depends on the microstructure of the used rubber. In polybutadiene rubber, *trans* **1,4** units are more reactive for the epoxidation reaction than

cis-**1,4** units. The epoxidation reaction rate is as well higher for **1,4** units than for **1,2** vinyl units. All samples containing low epoxidation degrees (<**15** %) where the behaviour of epoxidation degree is linear against glass transition temperature. It was reported that that the epoxidation rate is inversely proportional to vinyl content that is increases with decrease of vinyl content under the same epoxidation conditions. It indicates that **1,4** units are more reactive during the epoxidation reaction than the **1,2** units [4,5].

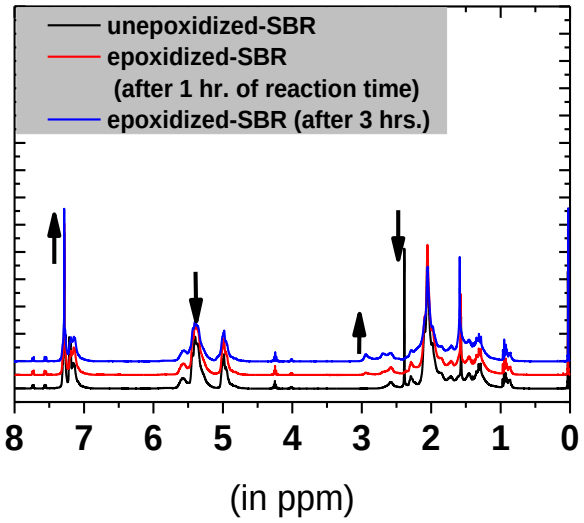

Figure 6.2: ^{1}NMR comparative of SBR with epoxidized-SBR at different conditions

6.2.3. DSC measurements

The insertion of epoxy groups in unsaturated double bonds of polybutadiene rubber increases the stiffness of main backbone polymer chain. The shift of Tg with increase of degree of epoxidation is shown in **figure 6.3a**. The T_g of un-epoxidized rubber SBR changed during the epoxidation reaction (3 h) from **-47.2**°C to **-34**°C. For SBR type **2525** (that is **25**% vinyl and 25% styrene) which was used in the experimental setup, a conversion factor of **0.91** °C/mol% was found. The degree of epoxidation as a function of reaction time (**figure 6.3b**) shows that with increasing reaction time, both T_g and rate of epoxidation was increased. Also, if we consider that the epoxidized segments

are distributed statically alongside the polymer chains, their individual contribution to chain mobility is strongly additive. Recently, *R. H. Schuster* et al reported that DSC measurements can be used to determine the epoxidation content lower than **10** mol% considering that the precision of the measurement is ~**1.8** ^{o}C [5].

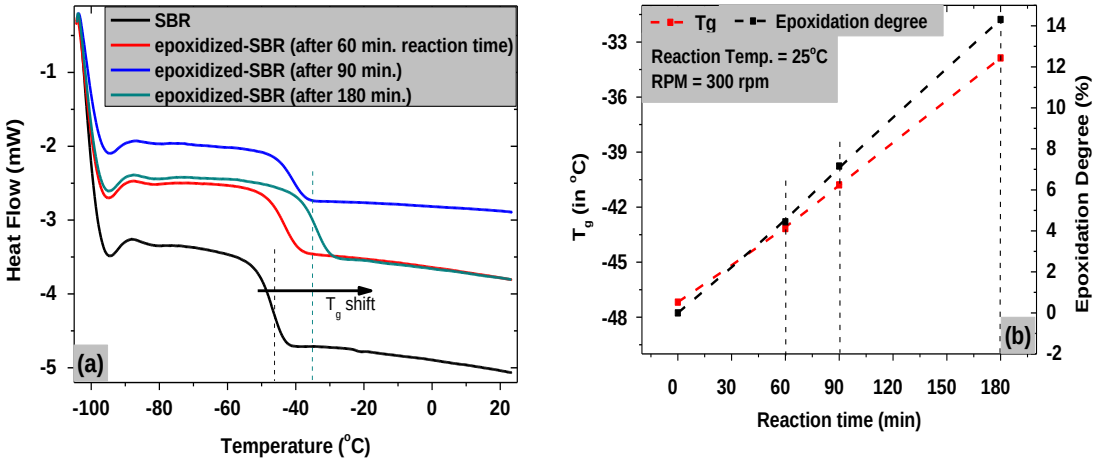

Figure 6.3: (a) DSC curves showing shift of glass transition temperature with increasing rate of epoxidation; **(b)** Comparative figure showing change of degree of epoxidation and T_g as a function of reaction time.

6.2.4. Optical Microscopy for studying filler dispersion

The properties of rubber compounds depend mostly on quality of filler dispersion. An optical microscopy tool was utilized to study filler dispersion. Optical microscopy helps us to investigate influence of filler loading on properties such as filler dispersion, amount of increase in aggregates, agglomerates and number of particles in such aggregating range. Optical image for carbon black-N**234** filled rubber compounds at **20** phr and **40** phr loading is presented in **figure 6.4a, b**. It can be noticed that the filler dispersion increases with increasing loading from **20** to **40** phr but it led to formation of more aggregated and agglomeratic structures. Filler dispersion index (**D_I**) at **85** % grey scale for N**234** filled rubber compounds is presented in **figure 6.4c**. It was found from the **D_I** that N**234** shows increase in filler dispersion from **20** phr **(~65**%) to **40** phr (**~79**%).

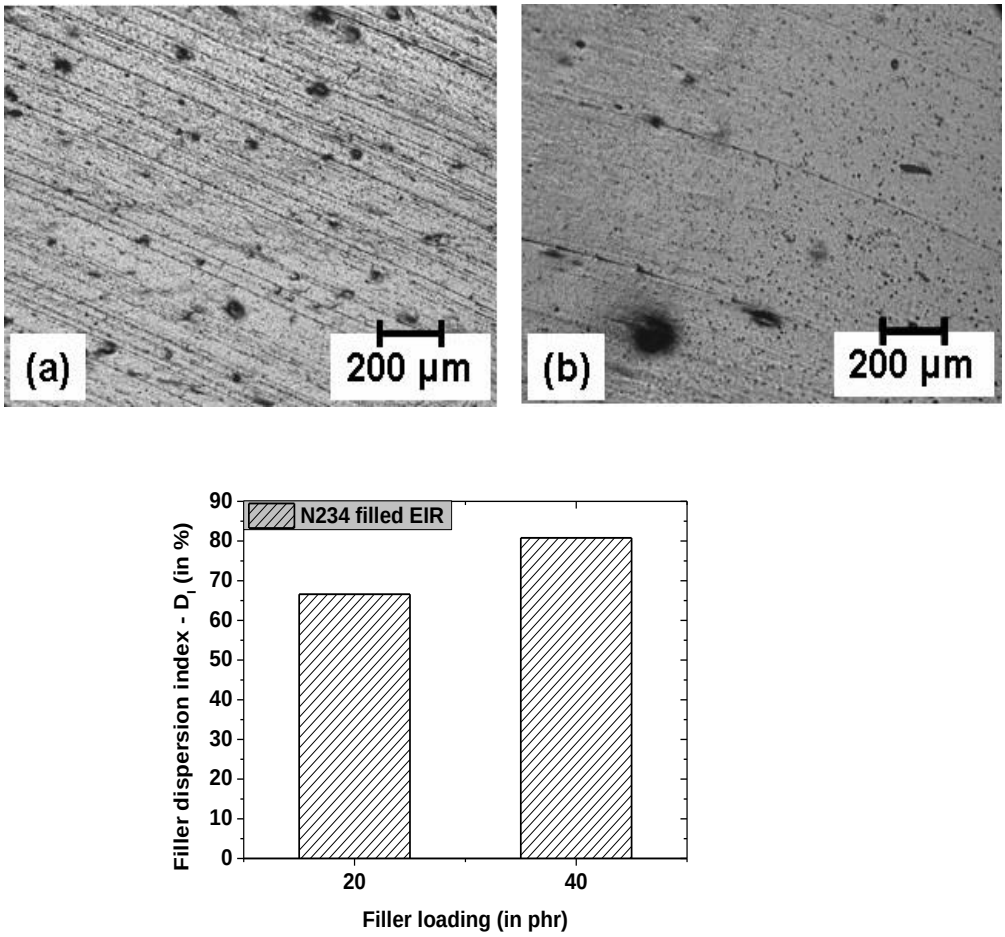

Figure 6.4a: Optical Image of N234/ epoxidized isoprene rubber compounds (EIR) containing (**a**) **20** phr; (**b**) **40** phr of filler; (**c**): $\mathbf{D_I}$ calculated for N**234**/EIR compounds.

6.3. Compounds based on **Styrene butadiene rubber** used as **polar** epoxidized diene rubber

6.3.1. Rheometric curves

Rheometric curves for N**234** filled epoxidized-SBR compounds are presented in **figure 6.5a** and were used for obtaining curing time (t'_{90}) of rubber compounds. It was found that the torque increases and the curing time decreases with increasing filler loading for both N**234** and xg C**750** fillers. Such effects are due to influence of filler networking and epoxidized functional groups in the filled rubber matrix. Our results of decreasing scorch time and increasing torque respectively as a function of filler loading agrees with published data in literature with similar filler or rubber systems [6- 12].

A comparative study of t'$_{05}$ (scorch time) as a function filled loading is presented in **figure 6.5b** for both xg C**750** and N**234** filled epoxidized-SBR compounds. It was found that scorch (t'$_{05}$) time decreases with increasing filler loading and a sharp fall in scorch time for xg C**750** filled epoxidized-SBR composites was observed. Investigations are reported which presents role of change in initial accelerator and sulfur concentration in the rubber during vulcanization or identified and determined the intermediate compounds which appear to be formed during vulcanization [13].

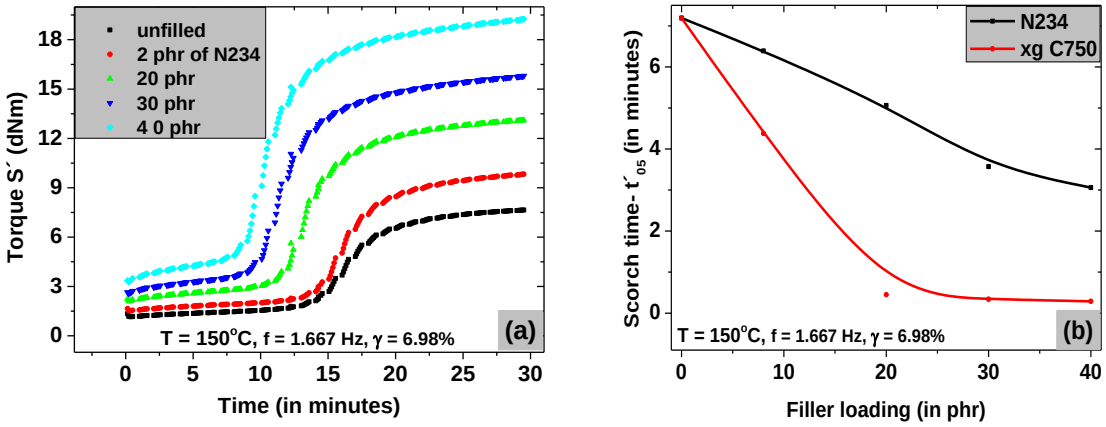

Figure 6.5: **(a)** Rheometric curves for epoxidized-SBR based nanocomposites containing N**234** concentration from **0** to **40** phr; **(b)** The t'$_{05}$ (scorch time) decreasing behaviour in epoxidized-SBR nanocomposites containing different filler concentration of xg C**750** and N**234**.

6.3.2. Rheological Properties through RPA studies

The viscoelastic behavior of xg C**750** and carbon black-N**234** filled epoxidized-SBR compounds was investigated through strain sweep tests. The behavior of storage modulus - G' (in kPa) as a function of strain sweep for xg C**750** filled epoxidized-SBR compounds, with increasing loading from **0** to **40** phr, is presented in **figure 6.6a**. It was observed that with an increase in filler loading in epoxidized-SBR matrix, the main characteristic plateau of G' at low strain (**~0.56%**) reaches lower strain amplitudes. A substantial decrease in G' values were observed at relatively large strain amplitudes (>**100%** strain). It could be due to break-down of secondary in-rubber interactions at this

strain. It was reported in the literature that the values of G'_0 and G' enhances in modified systems due to improved filler networking in rubber matrix [14]. We have also observed increase G'_0 and G' values that could be due to presence of epoxy groups which influence improved filler networking in xg C**750** filled epoxidized compounds.

A comparative study for carbon black N**234** and xg C**750** filled epoxidized-SBR rubber compounds as a function of filler loading is presented in **figure 6.6b**. It can be noticed that an exponential increase in modulus was seen for the loading above **20** phr for both xg C**750** and N**234** filled compounds. Such increase in modulus could be due to improved interactions in filler networking. The relatively improved interaction in filler networking between epodixized-SBR (than un-epoxidized SBR) with xg C**750** or N**234** fillers can be interpreted due to presence of reactive species such as functional groups like OH or COOH (which possibly exist due to acidic treatment in xg C**750**) or due to other reactive species from epoxidized-SBR such as a proton catalysed opening of oxirane ring favors interactions. Similar hypothesis for precipitated silica/epodixized-SBR was reported in literature [14]. The improved stiffness therefore results an enhanced filler networking and thus higher modulus.

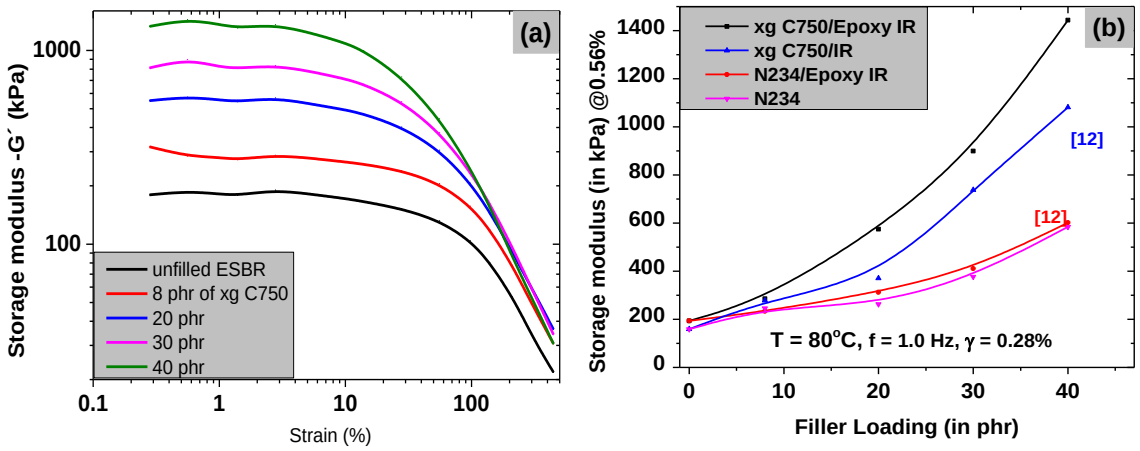

Figure 6.6: **(a)** Storage modulus (G', kPa) as a function of different strains (increasing from 0.28% to 300%) for xg C**750** filled uncured epoxidized-SBR nanocomposites; **(b)** comparative description of storage modulus with different filler loadings of xg C**750** and N234 filled epoxidized-SBR and SBR [12] nanocomposites.

6.3.3. Stress-strain behavior for Tensile strength

Stress-strain measurements were carried out at **200** mm/minute on **2** mm thick cured samples and the behavior of xg C**750** filled rubber nanocomposites is shown in **figure 6.7a**. It was observed that with an increasing concentration of xg C**750** in epoxidized-SBR matrix, the stress values increases with increasing strain amplitude which goes to maximum before elongation at break. It was due to influence of improved filler networking in xg C**750** that cause such effects. The stress-strain behavior for xg C**750** and N**234** filled epoxidized-SBR composites at **8** phr loading were presented in **figure 6.7b**. The stress–strain curves initially increase relatively flatly, upto approximately **100**% strain. It was observed that the xg C**750** shows a behavior almost similar to the N**234**-filled sample at **100**% strain, irrespective of the fact that the BET surface area of xg C**750** is about ~**8** times more than N**234**. The similar findings for xg C**750** and CB systems are reported recently in NBR matrix. [9]

Multi-hysteresis experiments were carried out at **40** mm/minute to study the effect of filler loading on energy dissipation. The increase in N**234** concentration in epoxidized-SBR matrix increases stress and decreasing the elongation at break (**figure 6.7c).** Under stress, the filler clusters can break and become softer, leading to a decreasing strain amplification factor. It could be further attributed due to cyclic breakdown of new clusters and re-aggregation or re-formation of damaged clusters. A comparative multi-hysteresis stress-strain at **8** phr for N**234** and xg C**750**/epoxidized-SBR nanocomposites is presented in **figure 6.7d**. It was observed that xg C**750** based composites shows higher stress while N**234**/epoxidized-SBR shows higher stress values at higher elongations. When the sample is stretched beyond elasticity range, irreversible deformations happens that led to permanent changes in filler networking structure. Recently, such experimental findings are theoretical modeled for three-dimensional stress states using the concept of representative directions [15-17].

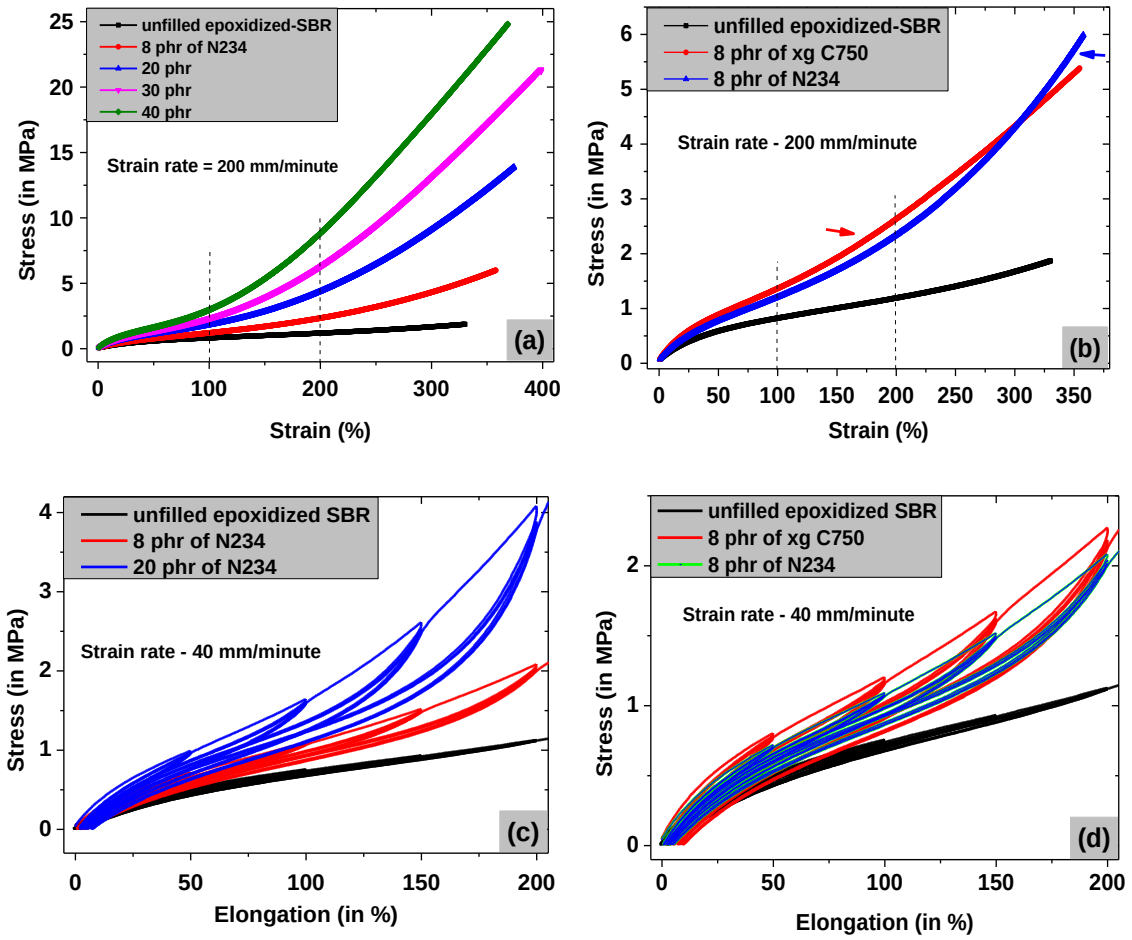

Figure 6.7: **(a)** Stress-Strain curves obtained from N**234**/epoxidized SBR nanocomposites with varying strain; **(b)** Stress-Strain comparative curves at 8 phr loading from N**234** and xg C**750**/epoxidized-SBR nanocomposites; **(c)** Multi-Hysteresis Stress-Strain curves comparatives for N**234**/epoxidized-SBR Nanocomposites; **(d)** Multi-hysteresis Stress-Strain comparative for **8** phr of N**234** and xg C**750**/ epoxidized-SBR nanocomposites.

6.3.4. Dynamic Mechanical Temperature Analysis (DMTA)

The mechanical performance can be further evaluated through DMTA test. It was performed to analyze the effects of epoxy functional groups on filler networking and thus reinforcement [18]. In DMTA, we study the behavior of complex modulus (G*) as a function of temperature sweep increasing from **-60** ^{o}C to **80** ^{o}C. The low cryogenic temperature was achieved by continuous supply of nitrogen during measurements. A comparative behaviour of G* (in Pa) for both fillers, in epoxidized-SBR matrix at **30** phr loading, are presented in **figure 6.8a**. It can be seen that the modulus falls sharply after glass transition region. As compared with unfilled rubber, a small shift in T_g was

observed for both xg C**750** and N**234**/epoxidized-SBR composites which is due to influence of fillers. Similar extent of shift in tan δ (**figure 6.8b**) peak near glass transition temperature was also found. Filler's networking results smaller T_g shifts by influencing polymer chain mobility. The area under tan δ curve under different temperatures indicates the total amount of energy that can be absorbed by a material [18-19]. Such characteristics are exciting, because most reinforcement will inevitably lead to a higher rigidity. Similar hypothesis is reported for such behavior in the literature [18-19].

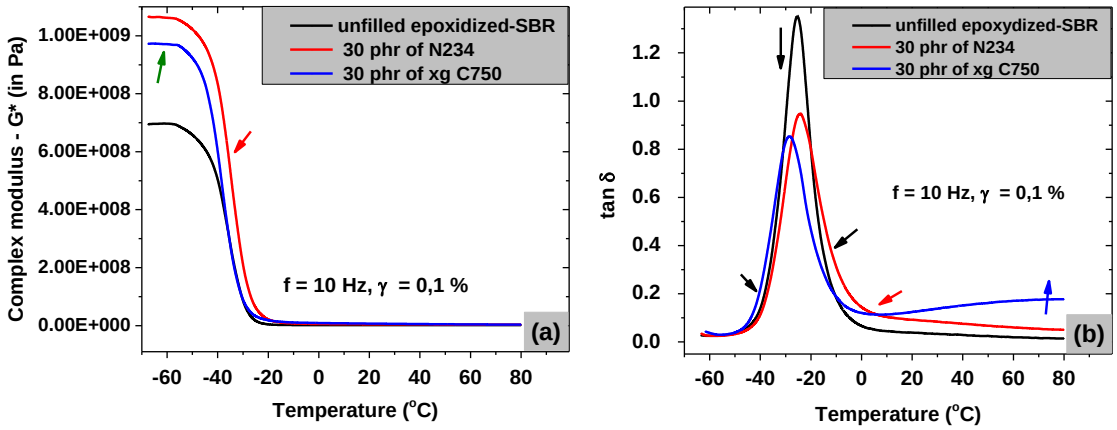

Figure 6.8: **(a)** DMA comparative of N**234** and xg C750/ epoxidized-SBR nanocomposite containing **30** phr of filler; **(b)** tan δ comparative of N**234** and xg C**750**/ epoxidized-SBR nanocomposite containing **30** phr of filler.

6.4. Synthetic isoprene rubber used as **polar** epoxidized diene rubber

6.4.1. Rheometric curves

The sulphur based rheometric curves of N**234**/ epoxidized-isoprene rubber (EIR) compounds are shown in **figure 6.9**. The cross-linking reversion was found very low (less than **5**%) for both fillers. Rheometric curve shows that with increasing concentration of N**234** in the EIR matrix, torque increases and scorch time decreases from **0** to **40** phr of N**234** in EIR. Such increase in torque is enhanced by improved filler networking due to presence of epoxidized functional groups in the filled rubber matrix. These findings are in line with literature on similar filler or rubber systems [6-12].

A comparative study of t'_{05} as a function of filled loading is shown in **figure 6.9b** for both xg C**750** and N**234** filled EIR compounds. It was found that t'_{05} (scorch time) decreases with increasing filler loading. The xg C**750** shows lowest t'_{05} as compared to N**234**/EIR compounds at all filler loadings. The decrease in scorch time is influenced either by epoxy functional groups or improved interactions between filler and rubber. The high surface area also promotes sharp improvement in scorch time as found in xg C750 filled epoxidized rubber compounds. The thermal conductivity of the filler also plays a significant role in decreasing activation time and it could be proposed to be another reason for sharp fall of scorch time for xg C**750** filled compounds.

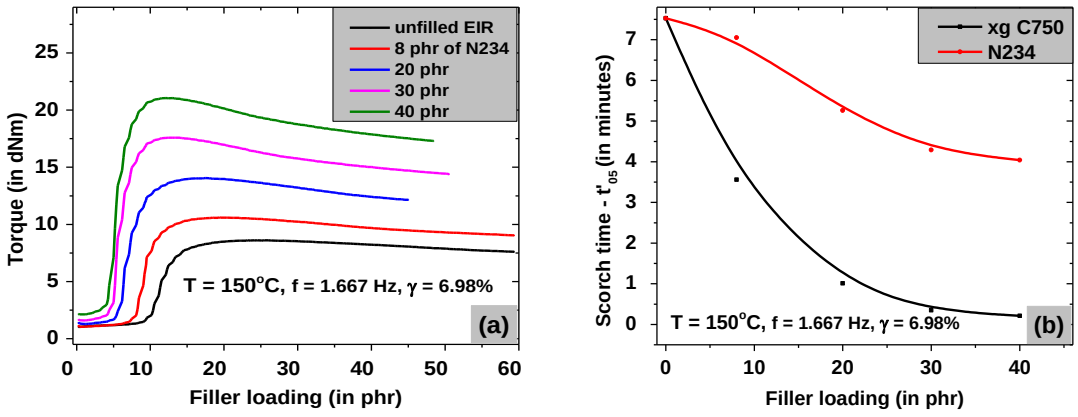

Figure 6.9: (a) Rheometric curves for N234/EIR compounds; (**b)** Comparative study of scorch time for N**234** and xg C**750**/EIR compounds.

6.4.2. Rheological Properties through RPA studies

The strain-sweep behavior of storage modulus - G' (in kPa) for xg C**750** filled EIR composites are shown in **figure 6.10a**. We found a non-linear dependence (Payne effect) of G' with an increase in strain amplitude upto **100**% strain. It could be due to polymer-filler networking in this region. A comparative study of G' for N**234** and xg C**750** filled EIR rubber compounds (epoxidized and un-epoxidized) as a function of filler loading is shown in **figure 6.10b**. The improvement in storage modulus values are due to enhancement filler networking and presence of reactive functional groups. The

increase in G' in EIR was more pronounced due to presence of reactive species as described previously in section **6.3.2** of same chapter.

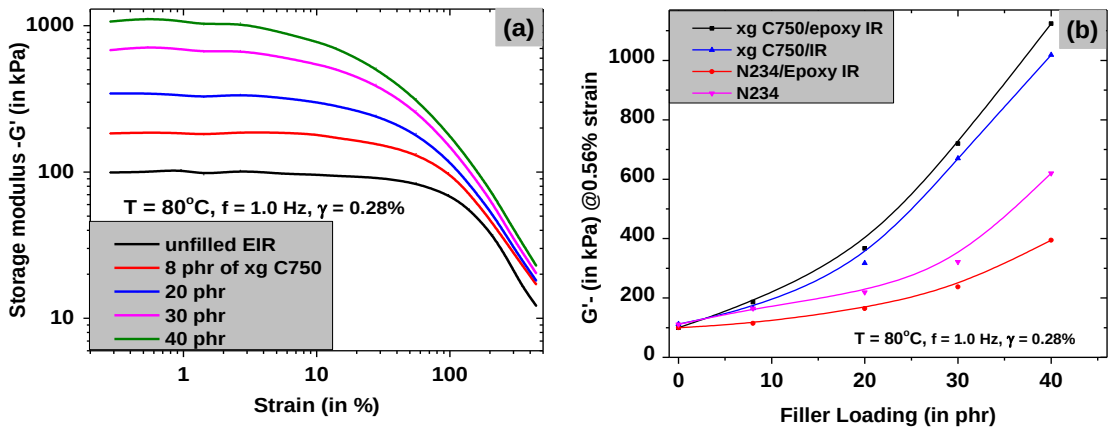

Figure 6.10: **(a)** RPA strain-sweep study for xg C**750**/EIR compounds; **(b)** Comparative study of Storage modulus for N**234** and xg C**750**/EIR compounds. The results were compared with un-epoxidized nanocomposites.

6.4.3. Stress-strain behavior for Tensile strength

The Stress-Strain behavior of N**234**/EIR rubber nanocomposites is shown in **figure 6.11a**. It was observed that with increasing N**234** concentrations from **8** to **40** phr in EIR, the stress value increases before elongation at break. The stress-strain behavior for xg C**750** and N**234** filled epoxidized-SBR composites at **8** phr and **30** phr loading were presented in **figure 6.11b**. It was found that with an increase in concentration of xg C**750** and N**234** into EIR matrix, stress values increases with increasing strain amplitude. At **30** phr loading, N**234** shows dominant stress and elongation at break as compared to xg C**750**. Such effects are due to influence of increasing aggregates and agglomerates in xg C**750** as compared with low surface area and spherical filler that is N**234** filled EIR compounds.

Multi-hysteresis experiments were carried out at **40** mm/minute to study the effect of filler loading on energy dissipation (**figure 6.11c)**. When the sample is stretched beyond elasticity range, irreversible deformations occurring and leading to a permanent

change in the filler network structure. A multi-hysteresis stress-strain at **8** phr and **30** phr for xg C**750**/EIR nanocomposites is presented in **figure 6.11d**. It was found that the amount of energy dissipation increases with increasing filler concentration. Higher energy dissipation was noticed in composites of both filler at **30** phr loading.

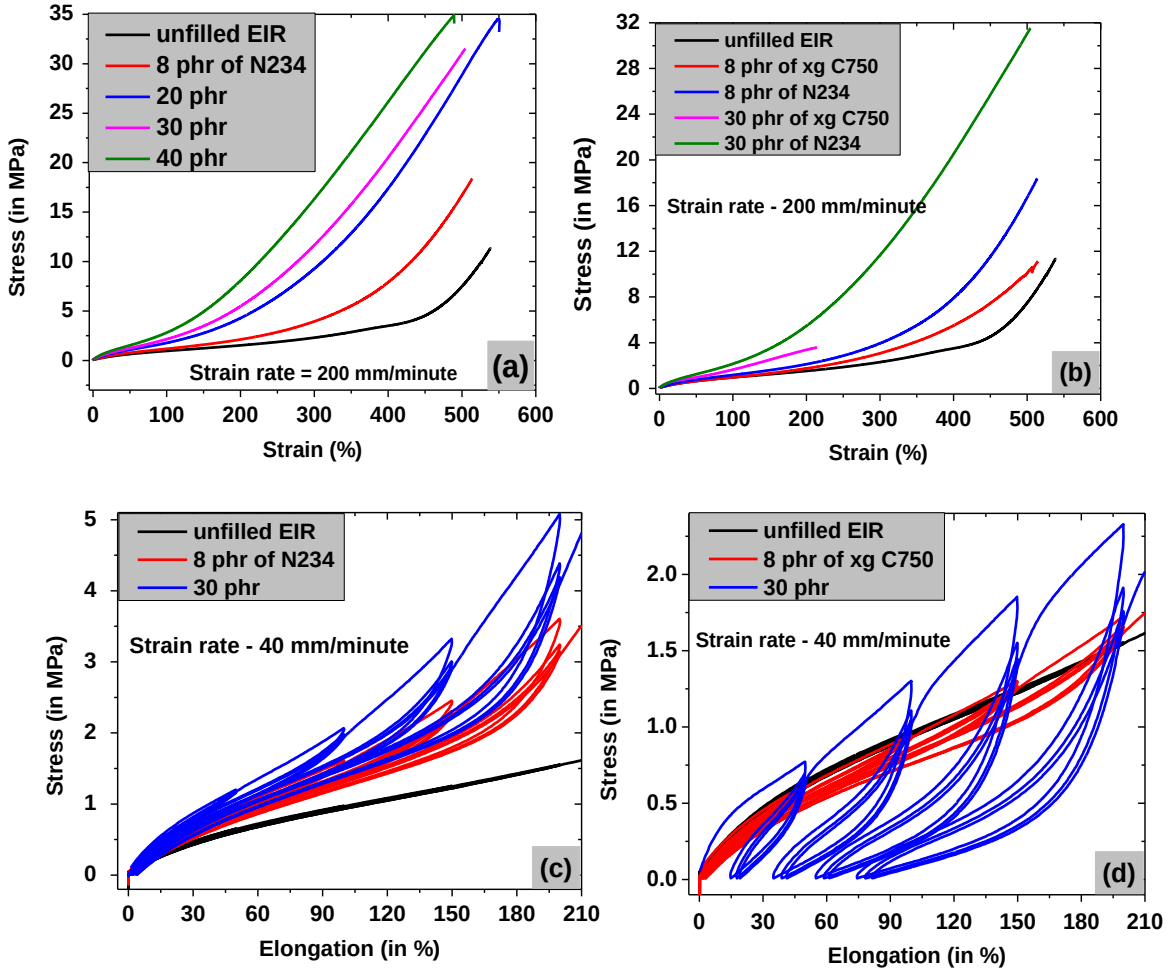

Figure 6.11: (a) Stress-Strain study for N234/EIR nanocomposites; (**b)** Stress-Strain study for comparative at **8** phr and **30** phr N234 and xg C750/EIR nanocomposites; **(c)** Stress-Strain multi-hysteresis study for comparative at **8** phr and **30** phr N234/EIR nanocomposites; **(d)** Stress-Strain multi-hysteresis study for comparative at **8** phr and **30** phr xg C750/EIR nanocomposites.

6.4.4. Dynamic Mechanical Thermal Analysis (DMTA)

Behaviour of complex modulus G* (in Pa) as a function of temperature, for N**234** and xg C**750** filled EIR matrix at **30** phr loading, is presented in **figure 6.12a**. The results were compared with unfilled EIR. It was found that the modulus falls sharply below glass

transition region. At **30** phr, a small shift of T_g was observed for both xg C**750** and N**234**/EIR compounds. The tan δ (**figure 6.12b**) peak shifts slightly near the glass transition temperature due to the influence of the used filler and higher tan δ can be evidenced at higher temperature for xg C**750**/EIR compounds.

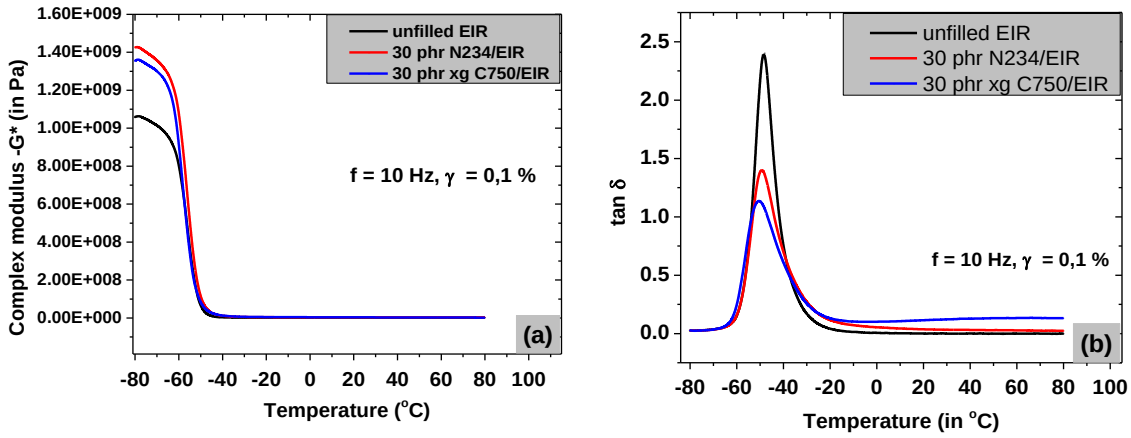

Figure 6.12: **(a)** DMA study for comparative at **30** phr for xg C**750** and N**234**/EIR nanocomposites; **(b)** tan δ study for comparative at **30** phr for xg C**750** and N**234**/EIR

6.5. Conclusions

All epoxidation reactions were successfully prepared in a **5** L Büchi reactor with mounted thermostat at **25**°C. The epoxidation reaction rate is as well higher for **1,4** units than for **1,2** vinyl units, because of the not determinable **1,2** epoxy groups. NMR study shows that the rate of epoxidation increases with increasing reaction time in both epoxidized-SBR and IR. All samples containing low epoxidation degrees below **15** % where epoxidation degree is in linear reaction range of the epoxidation in both rubbers studied.

The filled epoxidized-SBR and EIR compounds were prepared successfully by dry melt mixing method suing small Haake Rheomix 600®. Optical microscopy shows that the dispersion index (D_I) that N234 shows increase in filler dispersion from **20** phr (**~65**%) to **40** phr (**~79**%). It was demonstrated that the functionalization of IR with epoxy groups improves polymer-filler interaction and over-all properties especially "mechanical reinforcement" for the epoxidized-SBR and EIR compounds. It has been

demonstrated from our present work that the "high" surface area nanofillers such as xg C**750** shows an improvement in rheological properties (such as scorch time, storage modulus etc) in both epoxidized-SBR and EIR compounds as compared with traditional filler such as CB- N**234**. A significant improvement in scotch time was found for xg C**750** than N**234**/epoxidized-SBR and EIR compounds. From RPA strain sweep experiments, we found a non-linear dependence of G' with an increase in strain amplitude from 0.**28**% to **300** % and it decreases sharply after **100**% strain. Stress-Strain measurements shows a significant improvement in stress with increasing filler loading where xg C750 filled nanocomposites shows higher reinforcement at lower strain ranges while N**234**/epoxidized-SBR shows higher at higher strains. Multi-hysteresis shows higher stability of filler networking and increase of dissipation energy with increasing filler loadings. From DMTA measurements, it was concluded that the modulus falls sharply below glass transition region. A small shift (< **2** ^{o}C) in T_g was observed even at higher loading of **30** phr for both xg C**750** and N**234**/epoxidized-SBR composites. The Rheological studies show that the xg C**750** filled epoxidized-SBR compounds shows higher storage modulus than SBR [12] and N**234** filled compounds.

DSC studies show that the glass transition tempearutre of the master batch of epoxidized-**SBR** did not shift significantly (less than -**8** ^{o}C). The T_g of un-epoxidized rubber SBR was changed during the epoxidation reaction of 3h from -**47.2**°C to -**34**°C at an epoxidation degree of ~ **13**%. For this **SBR** type **2525** (that is **25**% vinyl and **25**% styrene) which was used in the experimental setup, a conversion factor as **0.91** °C/mol% was found.

6.6. References

[1] M. Hesse, H. meier, B. Zeeh, *Spektropische Methoden in der organischen Chemie*, Georg Theieme Verlag, 200, (2005).

[2] D. Zuchowska, *Polymer*, **21**, 514 (1980).

[3] I. R. Gelling, *Rubber Chem. Technol*., **58(1)** 86 (1985).

[4] M. M. Jacobi, C. P. Neto, C. G. Schneider, T. L. C. Rocha, R.H. Schuster, *Kautschuk Gummi Kunstst.*, **55**, 1 (2002).

[5] M. M. Jacobi, C. P. Neto, C. G. Schneider, T. L. A. C. Rocha, Porto Alegre-RS and R. H. Schuster, *Kautsch. Gummi Kunstst.*, **55(11)** 590 (2002).

[6] M. Klüppel, *Adv. Polym. Sci.*, **164**, 1 (2003).

[7] V. Kumar, U. Giese, T. Hanel, L. Giannini, Proceedings of the 1st ISN2A, 1st International Symposium on Nanoparticles/ Nanomaterials and Applications, Caparica - Almada, Portugal, (20-22 January, 2014) ISBN 978-9-8998415-9-8

[8] V. Kumar, U. Giese, T. Hanel, L. Giannini, M. Galimberti, *Kautschuk Gummi Kunstst.* (submitted and accepted) (2014) - in press.

[9] M. M. Moewes, F. Fleck, M. Klueppel, *Rubber Chem. Technol.*, (2013) -in press.

[10] M. M. Möwes, F. Fleck, M. Klüppel, Poster and Proceedings: 10th Fall Rubber Colloquium, Hannover, Germany, (7-9. November 2012), ISBN: 978-3-9814076-1-7.

[11] M. Galimberti, V. Kumar, M. Coombs, V. Cipolletti, S. Agnelli, S. Pandini, L. Conzatti, *Rubber Chem. Technol*., (2013) - in press.

DOI: http://dx.doi.org/10.5254/rct.13.87903

[12] V. Kumar, U. Giese, T. Hanel, M. Galimberti, *Kautschuk Gummi Kunstst.* (submitted and accepted) (2014).

[13] R. H. Campbell and R. W. Wise, *Rubber Chem. Technol.*, **37(3)** 635 (1964).

[14] T. L. A. C. Rocha, R. H. Schuster, M. M. Jacobi and D. Samios, Porto Alegre, *Kautschuk Gummi Kunstst.*, **57(12)** 82 (2004).

[15] H. Lorenz, M. Klüppel, G. Heinrich, ZAMM – *J. Appl. Mathematics Mech*., / Zeitschrift für Angewandte Mathematik und Mechanik, **92(8)** 608 (2012).

[16] H. Lorenz, J. Meier, M. Klüppel, Elastomere Friction Lecture Notes in *Appl. Computational Mech.*, **51**, 27 (2010).

[17] U. Lange, T. Hirsch, V.M. Mirsky, and O.S. Wolfbeis, *Electrochim. Acta*., **56**, 3707 (2011).

[18] Z. Peng, C.F. Feng, Y.Y. Luo, Y.Z. Li, and L.X. Kong, *Carbon*, **48**, 4497 (2010).

[19] S.A. Paul, C. Sinturel, K. Joseph, G.D.G. Mathew, L.A. Pothan, and S. Thomas, *Polym. Eng. Sci.*, **50**, 384 (2009).

Chapter 7

Materials, Chemicals, Preparation and Details of Characterization Techniques

7.1. Materials used

7.1.1. NanoFillers

Commercially available "*few layer graphene*" nanofillers utilized were: an exfoliated graphene nanoplatelets (xGnPs) of type xg C**750** and xg M**5** - purchased from XG Sciences, nanoG (Synthetic Graphite **8427**®, named as nanoG in present work) - purchased from Asbury Graphite Mills Inc., UF**1** C**98** and EXG **9840** – bought from Kropfmühl AMG.

Carbon Black - N**339** and N**234** were purchased from Cobot®, Carbon Black-Printex xe**2** was obtained from Orion Engineered Carbons.

Carbon nanoTubes with trade name NANOCYL NC **7000**™ obtained from Nanocyl S.A, Belgium.

7.1.2. Rubbers

Synthetic poly(**1,4**-*cis*-isoprene) (IR) was from Nizhnekamskneftechim Export, with trade name ***SKI3*** and **70** M.U. as mooney viscosity (ML_{1+4} at **100** ^{o}C). Similar IR grade was used in epoxidation.

Styrene Butadiene Rubber (SBR) with trade name Buna VSL **2525-0** M (having **25**% styrene and **25**% vinyl content) with mooney viscosity (ML_{1+4}) of **54** and Tg of **-49** ^{o}C) and synthetic nitrile butadiene rubber (NBR, acryl-nitrile content was **39**%, and ML_{1+4} at **100**°C was **45** and density of **0.99** g/cm^3) with trade name - *Perbunan*® ***3945 F*** were purchased from Lanxess AG. Similar SBR rubber was used for epoxidation.

7.1.3. Crosslinking Ingredients

Zinc oxide and Stearic acid were used as activators for sulphur based crosslinking system. Cyclohexyl benzothiazol-**2**-sulfenamide (CBS) was used as an accelerating agent.

7.1.4. Chemicals used in epoxidation experiments

Hydrogen Peroxide (H_2O_2, **30**%wt, Merk) Formic acid (**98**%, Fluka), Tween **20**, Toluene (CG Chemikalien) and Ethanol (CG Chemikalien).

7.2. Preparation Procedures

7.2.1. Compounds were prepared by melt mixing as

A. Using Small Haake Rheomix 600®

The rubber compounds characterized in chapter **3** (part-**1** and part-**2**), Chapter **4** and chapter **6** were prepared using lab mixer (Haake Rheomix **600**® at **60** rpm and at an initial temperature of **50** ^{o}C.

In **step 1**, rubber (IR or SBR) was masticated in the mixing chamber for the first minute. The filler was introduced in **step 2** and mixed for **4**-**5** minutes until a stable torque was achieved. The maximum temperature of nearly **90** °C was reached during mixing at **50** phr loading in xg C**750** -filled rubber compounds. Zinc oxide and stearic acid were fed into mixing chamber for **2** minutes in **step 3**. In **step 4**, curatives were added by introducing **2** phr of sulphur at starting temperature of **50** °C and mixed for **2** minutes. CBS was added alongside with the sulphur. Master batches were passed through a two roll-mill **5**-**6** times for homogenizing ingredients.

Following roll milling, rubber compounds were kept for upto **24** hours at least under ambient temperature before monitoring vulcanization time through rheometric curves. The vulcanization conditions (temperature at **150** °C, strain at **6.67**% and frequency at **1.67** Hz) for obtaining rheometric curves were kept constant for all filler loading. The vulcanization time (t'_{90}) is defined as the time where **90**% of the maximum torque was reached and this duration was used for crosslinked compounds. The raw rubber compounds were cured in a hot rubber press under **150** bar pressure at **150** °C to t'_{90}. The two minutes were added to the final t'_{90} curing time to compensate **2** mm plate thickness which counted as delayed heat transfer across sample. The tensile tests and dielectric measurements were conducted on these crosslinked samples.

B. Using Big Haake Rheomix 3000®

The rubber compounds characterized in Chapter **5** were prepared using lab mixer (Big Haake Rheomix **3000®** at **50** rpm and at an initial temperature of **50** ^{o}C. The Haake Rheomix **3000®**. The mixing was initiated as step-**1** by introducing rubber in mixing chamber and mastication upto **2** minutes. In step-**2**, nanofillers were added step by step and mixed thoroughly. The ZnO and Stearic acid were added at **11**th minute and total mixing last for **20** minutes before discharging master batches from mixing chamber for adding curing systems. The sulphur curatives were added on open-mill for additional **5** minutes and finally homogenized **5-6** times under nip size of **1** cm.

7.2.2. Procedure for epoxidation

All epoxidation reactions were performed in a **5** L Büchi reactor with mounted thermostat at **25** °C (**figure 7.1**). The SBR rubber (~**175** g; **2.91** mol) was dissolved in toluene (~**2.62** L; **24.7** mol) at ambient temperature conditions by stirring at **300** rpm overnight. The solution was then heated and maintained at **25** °C before adding Tween **20** solution (~**8.7** ml) with a concentration of ~**0.075** g/ml. After **15** minutes till solution attains equilibration under continuous stirring; hydrogen peroxide (**446** ml) was added.

After adding H_2O_2, the solution was stirred for **15** minutes before formic acid (~**55** ml; **1.45** mol) was added. The reaction was finally aborted through neutralizing acidic solution with a **5**% w/V sodium carbonate solution (~**1.54** L). For a complete reaction, the reaction was stirred for additional **30** minutes. Lastly, from separating phases, the aqueous phase was removed. Finally, the rubber solution was washed with water two times and then precipitated with ethanol. The precipitated polymer was lastly dried in a vacuum oven at **40** °C under low pressure for **24** h. The epoxidization of rubbers were performed through cooperation with Mr. Uwe Schneider and Mr. Viktor Jose at DIK eV, Germany.

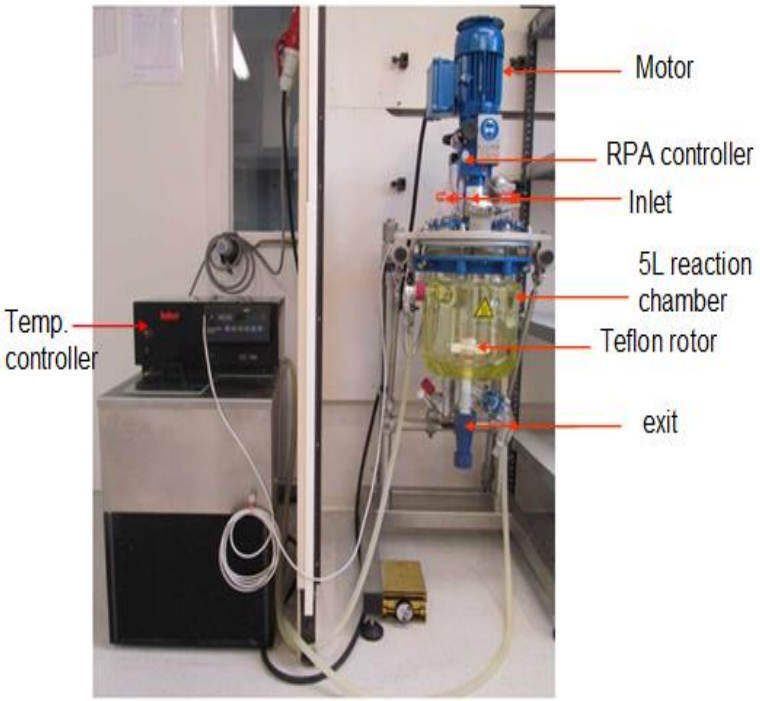

Figure 7.1: Experimental set-up for epoxidising rubber.

7.3. Characterization Techniques

7.3.1. Optical Microscopy for studying filler dispersion

The Janovert Olympus DP**72** **12.5**x**0.25** ∞/-A, GF - Plamachromont was employed for imaging and samples were imaged, processed in program "*analysis pro*" for getting filler dispersion index (D_I) on **70%** grey scale for NBR compounds and **85%** grey scale for epoxidized- rubber compounds. The filler dispersion can be studied using optical microscopy.

7.3.2. Transmission Electron Microscopy (TEM)

TEM micrograph on rubber compounds were obtained by using Zeiss EM **900** microscope incorporated with an accelerating voltage of **80** kV. Ultra-thin sections (~ **40-50** nm in thickness) were obtained by using a Leica EM FCS cryo-ultramicrotome with a diamond knife (sample temperature: ~**120** °C). The low cryogenic temperature condition was maintained with continues nitrogen supply in the sample chamber. The TEM samples were than deposited on copper grids coated with carbon film and analyzed.

7.3.3. Scanning Electron Microscopy (SEM)

Surface morphology of nanofillers were observed using scanning electron microscope (SEM, Zeiss EVO MA **10**) equipped with tungsten filament and carried out at a controlled voltage of **8** kV. The conductivity of the specimen surface can be improved by sputtering a thin coating of a conductive metal such as gold.

7.3.4. Static adsorption isotherms

The static gas adsorption isotherms were carried out using a volumetric adsorption tool BELSORP-max (BEL, Japan Inc.). The adsorption isotherms were obtained at a relative pressure (p/p_o) range of **10^{-6}-10^{1}** and a surface coverage (V/V_m) from **10^{-2}-10^{1}**, where V_m is the monolayer volume. The nanofiller samples were characterized in N_2 and *n-butene* with isotherms to obtain their surface characteristics such as BET area, surface activity, porosity and surface roughness.

7.3.5. Wide angle X-ray diffraction (WAXD)

The investigations were obtained using automated Bruker D**8** advanced diffractometer which was operated at an accelerating voltage of **35** kV using Ni filtered Cu-K_α radiation of λ = **1.5418** Å. The important features of a filler such as shape anisotropy, number of graphene layers in a stack, can be calculated through WXRD technique. The correlated stack dimensions can be calculated using Scherrer's equation and d-spacings can be obtained from well known Bragg's equation.

7.3.6. Dynamic Scanning Calorimetry (DSC)

The DSC on freshly epoxidized-SBR samples was carried our using TA-instruments DSC **2920** CE. The heating rate was kept constant at the rate of **10** ^{o}C/ minute. The epoxidized-SBR samples were infused in sample holder before placing them in sample chamber of the instrument. Liquid nitrogen was used to maintain cryogenic conditions during the experiment.

7.3.7. Nuclear Magnetic Resonance (NMR)

The protonated NMR (^{1}H-NMR) on epoxidized-SBR samples were carried out using Bruker DPX **400** MHz spectrometer. The epoxidized-SBR suspensions were made in **$CDCl_3$** solvent and homogenized on a shaker overnight before pouring the solution (**20** mg/ml) inside NMR tubes for characterization and investigations were utilized to calculate the degree of epoxidation in SBR. The NMR studies were performed through cooperation of DIK eV and Leibniz Universität Hannover, Germany

7.3.8. Hardness

The hardness of rubber compounds was investigated using **6** mm thick cured sample using Shore **A** durometer Zwick **5109.01** according to DIN **53 505** standards at ambient conditions and **70-80** durometer hardness offers good processing and favorable properties most often for applications like tires.

7.3.9. Rheological Properties through RPA studies (strain sweep)

Rheological measurements were carried out on rubber compounds using a Rubber Process Analyzer (RPA **2000**) at **80** °C and **1** Hz frequency in a strain sweep range from **0.28** % to **300** %.

7.3.10. RPA Frequency sweep experiments

Rheological strain sweep investigations were carried out on rubber compounds using Rubber Process Analyzer (RPA **2000**) at **80** °C from **0.1** Hz to **30** Hz.

7.3.11. Stress-strain behavior for Tensile strength

The tensile strength of cured samples were investigated according to DIN **53 504** standards using universal tensile testing machine (*Zwick/Roell **Z010***) with a preload of **0.5** N. The measurements were carried out by simply stretching strips of dumbbell shape sample between two clamps as a sequence of increasing weights attached to lower clamp. The gauge length was measured with cathetometer.

Multi-hysteresis measurements were obtained from **2** mm thick cured compounds carried out using an universal tensile testing machine (*Zwick/Roell **Z010***) with a preload

of **0.5** N at strain rate of **40** mm/minute and were utilized to calculate energy dissipation during stress-strain cycles.

7.3.12. Tear Strength

The tear resistance test of filled rubber compounds were investigated using **2** mm thick cured sample using universal *Zwick/Roell **Z010*** under ambient conditions. The experiments were carried out at strain rate of **100** mm/minute. The measurement was carried out according to ISO **34** standards. The *trouser-shape* sample was hold between two clumps like in stress-strain measurements.

7.3.13. Dynamic Mechanical Thermal Analysis

The dynamic mechanical analysis of filled rubber compounds was investigated using **2** mm thick cured sample using Rheometer (ARES, Rheometric scientific) at temperature range from **-40** ^{o}C to **80** ^{o}C at **10** Hz and **0.1** % strain. The low cryogenic temperature was achieved and maintained with continuous N_2 supply. The modulus peak shift in tan **δ** plot can be observed carefully from findings.

7.3.14. Dielectric AC Conductivity Properties

Dielectric properties of rubber compounds samples (d=**2** mm, and diameter of **20** mm) were studied using a Dielectric Broadband Analyzer (BDA, Novaconctrol GmbH) from $\mathbf{10^{-2}}$ Hz to $\mathbf{10^{6}}$ Hz. The samples were first ultrasonically rinsed for **10** minutes in ethanol to clean the surface. The surface of rubber compounds was then sputtered with gold for **10** minutes to form thin film to decrease the surface contact resistance of rubber compounds.

Conclusions

In this thesis, rubber compounds based new class innovative carbon nanofillers made by few layers of graphene (**FLG**) were analyzed. Research activity on FLG was initiated by selecting FLG nanofillers mainly on basis of surface area and shape anisotropy. The number of graphene layers in a stack and shape anisotropy of nanofiller were successfully calculated using Scherrer's equation and Bragg's equation from WAXD characterizations. The investigations for calculating surface area, surface activity and porosity were obtained through adsorption isotherms tests.

It has been demonstrated that the use of nanofillers brings a significant improvement in over-all properties of compounds in both apolar and polar diene rubbers as compared with traditional filler such as CB- N**234** and CB-N**339**. Generally, scorch time (t'_{05}) for both **high** and **low** surface area FLG filled rubber compounds, decreases with increasing filler concentration in all diene rubbers. A strong correlation of surface area with scorch time was obtained in both single and hybrid filler systems. A high surface area xg C**750** - FLG nanofiller shows shortest scorch time as compared with all other nanofillers investigated. The characteristic plateau of storage modulus- G' at low strain reaches lower strain amplitudes with an increase of filler concentration for all diene rubbers investigated. A particular enhancement of the G' plateau value is obtained for values passing nearer to filler percolation threshold of nanofillers. A correlation of surface area with values of G' at low strain amplitude were noticed in all diene rubbers investigated. A high surface area xg C**750** - FLG nanofiller shows dominant values of G' at low strain against all FLG fillers investigated.

Filler networking was studied quantitatively with Huber–Vilgis double logarithmic plot in the neat and filled rubber matrix through dynamic-mechanical and in some studies with electrical measurements. Filler with high surface area shows attainment of filler percolation at lower concentration in all diene rubbers. Nanofiller with higher shape anisotropy but lower surface area (nanoG, **21.9** phr in SBR matrix) stills found to attain filler percolation threshold at higher concentration than a filler with high surface area (xg C**750, 16.6** phr in SBR matrix) in apolar diene rubbers. As compared with

traditional fillers like CB-N234 and CB-N339, higer filler flocculation was observed for nanofillers at higer concetration in both diene rubbers. For filler-networking in hybrid filler systems in IR, a synergistic effect was observed after xg C**750** loading of **3** phr in IR rubber. For all FLG, Stresses at all the elongations remarkably increase with the filler content in both diene rubbers. However, no direct evidence of FLG with high surface area (xg C**750**) for enhancing tensile strength was observed in both diene rubbers. Multi-hysteresis stress-strain investigations show the first cycle exhibits higher energy dissipation than the third cycle and it was demonstrated that a stable filler networking can reduce hysteresis losses.

Finally, epoxidation of diene rubbers (IR and SBR) was successfully carried out in a **5** L Büchi reactor. Rubber master batches were prepared and their X% and T_g was investigated quantatively using ^{1}NMR and DSC technique respectively. A direct correlation between **X%** and $\mathbf{T_g}$ was found. In last part of thesis, it was demonstrated that presence of epoxy finctional gropus along polymer chains enhances filler networking, polymer-filler interactions, filler dispersion and dynamic mechanical properties of rubber compounds. A direct evidence of such enhancement was observed and was demonstrated in **figure 6.6b** and **figure 6.10b** of chapter **6** of thesis.

Annex

A. Publications

Journal Manuscript (s) **(****corresponding author(s) underlined***)**

1. *M. Galimberti**, **V. Kumar**, M. Coombs, V. Cipolletti, S. Agnelli, S. Pandini, L. Conzatti, "*Nano-Graphite with a High Shape Anisotropy for an Efficient Filler Networking in a Hydrocarbon Polymer and Synergism with Carbon Black",* Rubber Chem. Technol., ACS, **2013**, - in press

DOI: http://dx.doi.org/10.5254/rct.13.87903

2. *M. Galimberti**, V. Cipolletti, S. Musto, S. Cioppa, G. Peli, M. Mauro, G. Guerra, S. Agnelli, T. Riccò, **V. Kumar**, "*Recent Advancements in Rubber Nanocomposites*" Manuscript **submitted** to Rubber Chem. Technol., ACS, **2013**.

3. *V. Kumar**, *U. Giese**, T. Hanel, L. Giannini, M. Galimberti "*Graphene Reinforced Synthetic Isoprene Rubber based Nanocomposites",* Manuscript **accepted** in Kautschuk Gummi Kunstoffe, **2014**. – in press

4. *V. Kumar**, *U. Giese**, T. Hanel, M. Galimberti, L. Giannini, "*Graphene Reinforced Styrene Butadiene Rubber Nanocomposites",* Manuscript **accepted** in Kautschuk Gummi Kunstoffe journal, **2014**. – in press

Journal Manuscript (s) completed and to be submitted

5. V. Kumar, U. Giese *et al* "*Graphene/epoxidized Styrene Butadiene Rubber Nanocomposites",* Manuscript **completed** and under revision, **2014**.

6. V. Kumar, U. Giese et al. "*Few Layer Graphene Reinforced Styrene Rubber Nanocomposites",* Manuscript **completed** and under revision, **2014**.

7. V. Kumar, U. Giese et al "*Graphene/Nitrile butadiene rubber nanocomposites",* Manuscript **completed** and under revision, **2014**.

8. V. Kumar, U. Giese et al "*Interactive effects between Graphene-CNT-CB fillers on reinforcing and dielectric conductivity properties of synthetic poly-isoprene based nanocomposites",* Manuscript **completed** and under revision, **2014**.

Chapter (s) in a Book (**corresponding author(s) underlined***)**

1. *M. Galimberti**, V. Cipolletti,**V. Kumar**, *Natural Rubber Based Composites and Nanocomposites* S. Thomas, C. H. Chan, L. A. Pothan, Ramanan, J. Maria Eds., Royal Society of Chemistry, Chapter **2**, **2014**. Print ISBN**:** 978-1-84973-631-2,

PDF eISBN**:** 978-1-84973-765-4, *DOI***:***10.1039/9781849737654-00034*.

Proceeding (s) **(**presenting author underlined*)**

1. *M. Galimberti**, V. Cipolletti, M. Coombs, **V. Kumar**, M. Mauro, G. Guerra, L. Conzatti and L. Giannini, "*Layered Nanofillers for Rubber*" Proceedings of the fall 182nd Technical Meeting & Educational Symposium Rubber Division, ACS, October 9-11, **2012**, Cincinnati - OH, USA. **(Oral presentation)**

2. *M. Galimberti**, V. Cipolletti, S. Musto, S. Cioppa, G. Peli, M. Mauro, G. Guerra, S. Agnelli, T. Ricco, **V. Kumar**, "*Recent Advancements in Rubber Nanocomposites*" Proceedings of the fall 184th Technical Meeting & Educational Symposium Rubber Division, ACS, October 8-10, **2013**, Cleveland - OH, USA. **(Oral presentation)**

3. *V. Kumar**, U. Giese, T. Hanel, L. Giannini, "*Graphene nanoplatlets (GNPs) Reinforced Rubber Nanocomposites*" Proceedings of the 1st ISN2A, *1*st International Symposium on Nanoparticles/ Nanomaterials and Applications, 20-22 January, **2014.** Caparica - Almada, Portugal, ISBN *978-9-8998415-9-8*. **(Poster)**

4. *V. Kumar**, U. Giese, T. Hanel, L. Giannini, M. Galimberti, Proceeding of 11th KHK Technical colloquium, **2014**, Hannover, Germany. (**Poster**)/**Accepted**

Conferences - *(*Presenting author underlined)*

1. *V. Kumar**, M. Galimberti, "*Filler Networking of Graphite with High Shape Anisotropy in Poly (1,4- cis-isoprene)*", AIM Macrogiovani Congress at Department of CMIC 'Giulio Natta', Politecnico di Milano (Italy), 11 February, **2013**. **(Poster)**

2. *V. Kumar**, V. Cipolletti , M. Mauro, M. Galimberti, G. Guerra, R. Scotti, L. Conzatti, "*Graphite and graphite derivatives with high shape anisotropy for polymer nanocomposites*" *T*hird International Symposium: Frontiers in Polymer Science, Melia-Sitges (Spain), 21-23 May, **2013**. **(Poster)**

3**. V. Kumar**, V. Cipolletti, M. Mauro*, G. Guerra, M. Galimberti, "*Exfoliation of Graphite with High Shape Anisotropy in Poly(1,4-cis-isoprene)*" European Polymer Congress (EPF), Pisa (Italy), 16 -21 June, **2013**. **(Poster)**

4. M. Galimberti, V. Cipolletti , *V. Kumar**, M. Mauro, L. Conzatti,"*Graphite oxide intercalation compounds in hydrocarbon polymer*" Eurofiller-2013, Bratislava (Slovakia), 25-29 August, **2013**. **(Poster)**

5. *V. Kumar**, U. Giese, T. Hanel, *International Seminar on Elastomers*. Bratislava, Slovakia. August 24 - 28, **2014**. **(Oral presentation)**/Accepted

B. Acknowledgements

First thanks go to Italia for giving me opportunity of serving for more than 3 years as a PhD student. It was a pleasing experience for doing PhD in Italy.

From UNIMIB, Prof. R. Scotti is thanked for accepting as my thesis supervisor, permitting me to go to DIK eV for six months and many academic assignments. Thanks also to L. Tadiello, A. Susanna and L. Wahba. Thanks also to Prof. G.P. Brivio for providing this Ph.D. position with financial support. Thanks to Dr. M.I. Trioni, Dr. S. Achilli, Dr. G. Fratesi and Dr. C. Motta for guiding me for various academic helps. Dr. M.C. Fassina is thanked for cooperating in all academic assignments.

From POLIMI, Prof. M. Galimberti is thanked for guiding me as tutor of thesis and many academic helps. Dr. V. Cipolletti and Dr. S. Musto thanked for useful discussions and many helps at PoliMi and Pirelli. Special thanks to colleagues Dr. G. Peli, Dr. S. Shoshidia, Ms. S. Cioppa, Dr. V. Barbera, for many helps during my stay at PoliMi, Dr. Mirvana thanked or lab security courses.

From Pirelli Tire, Dr. V. Boffa, Dr. T. Hanel, Dr. Giannini, Dr. L. Castellani are thanked for making arrangements to send to DIK eV and many academic helps. Dr. D. Garbelli is thanked for academic lessons inspite of being so busy. Egr. M. Coombs is thanked for many useful discussions. Dr. R. Donetti is thanked for academic helps. Pirelli-CORIMAV is acknowledged for financial support.

From DIK eV, first thanks goes to Prof. Dr. U. Giese for accepting to guide me as a thesis tutor. Thanks to Ms. T. Rodriguez for many academic and other helps. Thanks to Prof. Dr. H. Geisler (Permission for mechanical tests), Prof. Dr. M. Klueppel (Permission for Dielectric measurements), Ms. A. Geisler (for Dielectric measurements), Mr. J. Hamann and Mr. J. Heier, Ms. G. Pandey (for introducing technical facilities at DIK), Mr. M. Moewes (for introducing xGnP nanofillers), Mr. F. Fleck for helps in Adsorption Isotherms, Ms. T. Dilmann for helps in demonstrating many mechanical measurements, Mr. P. Wagnor for helps in TEM imaging. Dr. A. Diekmann (for SEM), Mr. U. Schneider and Mr. V. Jose for help in epoxidation experiments, Dr. J. McIntyre for helps in paper revisions, Mr. Harish, Mr. Anuj (for several technical helps).

From UNISA, Prof. G. Guerra thanked in allowing us to use his lab facilities. Dr. M. Mauro thanked for demonstrating XRD tests.

From CNR-Genova, Dr. L. Conzatti thanked in allowing us to use her TEM lab facilities.

From UNIBS, Dr. S. Pandini, Dr. S. Agnelli thanked for many useful discussions.